RRD5329-AN-01

EMI 2

2 / 91

INVESTIGATION OF HIGHLY PRESSURIZED TWO-PHASE, REACTING FLOW

G. Klingenberg

Fraunhofer-Gesellschaft

Fraunhofer-Institut für Kurzzeitdynamik
• Ernst-Mach-Institut •
Institutsteil Weil am Rhein

2 / 91

INVESTIGATION OF HIGHLY PRESSURIZED TWO-PHASE, REACTING FLOW

G. Klingenberg

Weil am Rhein, March 1991

86 Pages
71 Figures
29 References

Ernst-Mach-Institut, Eckerstraße 4, D-7800 Freiburg, Telefon (0761) 2714-0
Institutsteil Weil am Rhein,
Hauptstraße 18, D-7858 Weil am Rhein, Telefon (07621) 71067
Institutsteil Wintersweiler,
Am Klingelberg 1, D-7859 Efringen-Kirchen 6, Telefon (07628) 805-0

REPORT DOCUMENTATION PAGE

REPORT SECURITY CLASSIFICATION Unclassified	1b. RESTRICTIVE MARKINGS
SECURITY CLASSIFICATION AUTHORITY	3 DISTRIBUTION / AVAILABILITY OF REPORT Approved for public release; distribution unlimited
DECLASSIFICATION / DOWNGRADING SCHEDULE	
PERFORMING ORGANIZATION REPORT NUMBER(S)	5. MONITORING ORGANIZATION REPORT NUMBER(S) R&D 5329-AN-01
NAME OF PERFORMING ORGANIZATION Fraunhofer-Institut für Kurzzeitdynamik, Ernst-Mach-Institut (EMI)	6b. OFFICE SYMBOL 7a NAME OF MONITORING ORGANIZATION USARDSG-UK EUROPEAN RESEARCH OFFICE
ADDRESS (City, State, and ZIP Code) Hauptstrasse 18 D-7858 Weil am Rhein, FRG	7b ADDRESS (City, State, and ZIP Code) Box 65 FPO New York 09510-1500
NAME OF FUNDING / SPONSORING ORGANIZATION USARDSG-UK ARO E EUROPEAN RESEARCH OFFICE	8b OFFICE SYMBOL (If applicable) 9 PROCUREMENT INSTRUMENT IDENTIFICATION NUMBER DAJA 45-88-C-0004
ADDRESS (City, State, and ZIP Code) Box 65 FPO New York 09510-1500	10 SOURCE OF FUNDING NUMBERS PROGRAM ELEMENT NO: 61102A PROJECT NO: 1L161102BH57 TASK NO: 07 OG WORK UNIT ACCESSION NO: AR

TITLE (Include Security Classification)

(U) - Investigation of Highly Pressurized Two-Phase, Reacting Flow

PERSONAL AUTHOR(S)
G. Klingenberg (Principal Investigator)

13a TYPE OF REPORT	13b TIME COVERED	14 DATE OF REPORT (Year Month Day)	15 PAGE COUNT
Final Technical	FROM Oct. 87 TO	1991, Mar	

SUPPLEMENTARY NOTATION

COSATI CODES		
FIELD	GROUP	SUB GROUP

18 SUBJECT TERMS (Continue on reverse if necessary and identify by block number)
(U) Guns; (U) Gas Propellant, Two-Phase Flow
(U) Hydrogen/Oxygen Combustion

A single-stage gas gun is used for simulating gun tube flows. The gas gun is driven by the combustion of gas mixtures consisting of $H_2/O_2/He$, $H_2/He/CO/O_2$, and CO/O_2. Thus, the two main combustion reactions occurring in chemical gun propulsion are simulated. Experiments had the goal to improve the knowledge of reacting two-phase (gas/solid) gun tube flows providing a data bank applicable for interior ballistic model validation. Parameters measured include pressure and temperature as well as velocity gradient at various positions along the gun tube. Multi-channel near-infrared spectroscopy measurements for recording the transient gas phase species were also performed.

20 DISTRIBUTION / AVAILABILITY OF ABSTRACT ☒ UNCLASSIFIED/UNLIMITED ☒ SAME AS RPT ☒ DTIC USERS	21 ABSTRACT SECURITY CLASSIFICATION Unclassified
22a NAME OF RESPONSIBLE INDIVIDUAL Dr. R. Reichenbach	22b TELEPHONE (Include Area Code) 071-409-4485 22c. OFFICE SYMBOL AMXSN-UK-RA

DD FORM 1473, 84 MAR 83 APR edition may be used until exhausted. All other editions are obsolete.

INVESTIGATION OF HIGHLY PRESSURIZED TWO-PHASE, REACTING FLOW

G. Klingenberg

FINAL TECHNICAL REPORT

Contract Number DAJA 45-88-C-0004

CONTRACTING OFFICE:

United States Army Research, Development and Standardization Group (UK)
London, United Kingdom

CONTRACTOR:

Fraunhofer-Gesellschaft zur Förderung der Angewandten Forschung e. V.
Leonrodstrasse 54, D-8000 München 19, Germany

March 1991

TABLE OF CONTENTS

TABLE OF CONTENTS (continued)

TABLE OF CONTENTS (continued)

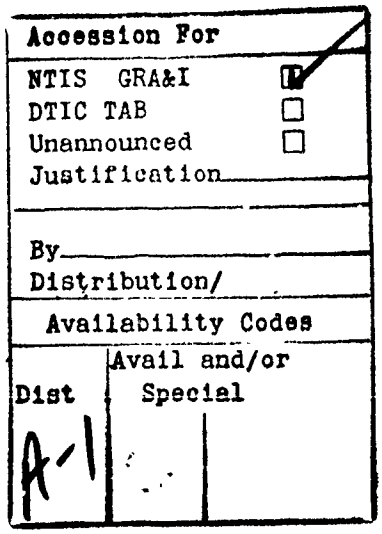

1. INTRODUCTION

1.1 General

This Final Technical Report concludes the three-year contract research work performed by the Principal Investigator, Guenter Klingenberg, at the Fraunhofer-Institut für Kurzzeitdynamik, Ernst-Mach-Institut, Institutsteil Weil am Rhein, under Contract Number DAJA 45-88-C-0004. On October 30, 1987, the non-personal research and development work entitled: "Investigation of Highly Pressurized Two-Phase, Reacting Flow" had been contracted to the Fraunhofer-Gesellschaft, Munich, Germany, by the United States Army Research, Development and Standardization Group (UK), London, England, under the Requisition/-Purchase Request Number R&D 5708 AN-01. Contracting Officer Technical Representatives of USARDSG (UK) in London were Dr. Fritz Oertel and Dr. Roy Reichenbach. The funds had been provided by the United States Army Ballistic Research Laboratory (BRL), Aberdeen Proving Ground, Maryland, USA. The Scientific Liaison at BRL was Dr. Thomas Minor of the Interior Ballistic Division.

1.2 Ultimate Goal

The ultimate goal of the three-year contract work was to provide new insight into and detailed information on ballistic flow processes that occur in realistic, simulated gun environments in order to assist in the development of combustion submodels. The work conducted over a three-year period therefore comprised the study of the behavior of gas/solid (two-phase), reacting gun tube flow under actual gun pressures and temperatures.

1.3 Research Strategy

The research objective of the experiments was to promote the understanding of unsteady, two-phase (gas/solid) reacting flows. The existing numerical two-phase gasdynamic models need improvement by incorporating, in a realistic fashion, processes such as turbulent mixing, friction, and heat transfer between flowing media. Furthermore, if one wants to explain the complex reacting flow phenomena within the unsteady expanding gun tube flow, one will have to know:

a) the important flow characteristics such as pressure, temperature, and gas velocity histories at several locations along the barrel,

b) the identities of kinetically important chemical species,

c) the chain reaction network describing their mutual interactions, and

d) the values of the corresponding reaction rate coefficients.

Due to the harsh conditions encountered in actual gun firings, the gathering of experimental data is quite difficult. As a result, the existing models for predicting the interior and transitional ballistics of gun firings are based on idealized flow conditions and lack an effective data base. To overcome these difficulties, Klingenberg and Banks [1] recommended using a realistic simulator for the empirical verification of the models in question. This simulator generates well-defined, well-controlled, simplified flows. The strategy calls for initial experiments beginning with single-phase inert flows and followed by experiments that progress in a stepwise manner towards more complex two-phase reacting flows.

1.4 Test Fixture or Gas Gun Simulator

The proposal of reference 1 stimulated interest in several simulation experiments conducted in Europe [1-4]. At some laboratories such detailed interior ballistic research is still under way [5-7].

The Ernst-Mach-Institut has built a single-stage gas gun to conduct simulation experiments. These simulation experiments are conducted with **reacting** interior ballistic flows [8-10]. The three-year research work described in this report addresses the interior ballistic flow problem. In a preceding contract research work, the transient muzzle flow had been investigated with the gas gun simulator [10]. The single-stage gas gun is driven by the combustion of gas mixtures. Here oxygen mixed either with hydrogen or carbon monoxide and mixtures of hydrogen and carbon monoxide were used as gaseous propellants. The diluent was helium pre-mixed with hydrogen or pure helium. Particles could be added to the mixture, if required.

The in-bore motion of the round was produced by the combustion of these propelling charges which, initially, are confined in the gun chamber. A hot wire igniter system is used to ignite the propellant charge. It is important that propellant charges should be ignited consistently and effectively along the gun chamber axis, since irregular ignition may lead to undesired pressure fluctuations or even to a misfire. Following ignition, sustained combustion is established with the combustion characterized by the rapid conversion of the propellant into various reaction products and the simultaneous evolution of pressure and heat. The pressure initiates in-bore acceleration of the projectile. As the projectile accelerates down the gun tube, the increasing tube volume is filled by a mixture of burning gases and particles, if mixed in the flow. The in-bore flow parameters then determine the muzzle exit flow properties.

2. STATEMENT OF WORK

2.1 Scope

In the detailed three-year program various research tasks have been proposed. Some of the items were later narrowed and reformulated to meet the requirements of the experiment. In general, the conduct of the research followed the stated research objectives within the limits of contract terms and conditions. The best available applicable experimental technique was utilized to extend knowledge in the field of interior ballistics and prepare a data bank for the use of the ballistic modeling community.

2.2 Proposed Research Task

2.2.1 First-Year Program

In the first year it was proposed to study the feasibility of simulating reacting flows under real ballistic conditions by extending the H_2/O_2/He mixture charges to include CO combustion. Also, a new gun chamber had to be designed and built with multiple measuring ports.

In summary, the research task during the first year was:

a) Extend the H_2/O_2/He mixture charges to include CO and establish suitable operating ranges for the experiments below;

b) In parallel, design and built an improved gas gun chamber with multiple diagnostic ports;

c) Begin studies of $H_2/CO/O_2$/He mixtures laden with inert particles of known composition and size;

d) Write progress report.

2.2.2 Second-Year Program

In the second year the improved gas gun chamber had to be tested. Also, different gas compositions, laden with inert and reacting particles, were investigated.

In summary, the research task during the second year was:

a) Test the newly fabricated chamber;

b) Perform a survey of different gas compositions that are laden with inert and reacting particles of known sizes and chemical composition;

c) Write progress report.

2.2.3 Third-Year Program

In the third year a more detailed investigation of the interplay between the combustion reactions and the flow was performed.

In summary, the research task during the third year included:

a) Perform a detailed investigation of the various processes that were found to have a significant influence on the flow characteristics;

b) Provide a detailed experimental data base for comparison with interior ballistic models;

c) Write final progress report.

2.3 Experiments

In order to account for the above proposed research tasks a series of sophisticated experiments had to be conducted. Experiments were performed on the gas phase parameter during the gas gun discharge applying spectroscopic techniques for measuring gas pressures, temperature and velocity gradients and particle or species concentrations.

3. BACKGROUND

3.1 Difficulties Encountered

Various numerical and analytical simulations have achieved much progress in the prediction of the interior ballistic cycle. However, to include the salient features of the realistic chemically reacting, turbulent, and multiphase in-bore and muzzle flows of guns is still far outside the scope of existing models. Because of limitations and constraints inherent in current mathematical methods and computer techniques, theoretical predictions are only capable of treating a less complex, idealized interior and transitional ballistic cycle. Further, these predictions suffer due to a severe lack of accurate input data [1,11-13].

Contrary to these theoretical approaches, which rely on idealized flow features in order to obtain solutions, the experimental community usually performs modern flow measurements in real gun firings. This different approach has the advantage of recognizing real flow features and the disadvantage of constraints

inherent in the experimental capabilities. However, other difficulties are encountered in probing the realistic ballistic cycle. Concurrent advances in experimental research, a necessary prerequisite to achieve progress in modeling, are also impeded by the harsh environments of the realistic flow of guns. Further, this approach makes it difficult to

a) establish equivalence between the data obtained from various sources,

b) isolate the effect of a single variable,

c) identify the governing process, and

d) establish a data base applicable for current model validation [1].

3.2 Innovative Experiments

Innovative experiments performed in close interaction with the computational efforts are sorely needed, because existing gasdynamic models of interior ballistics rely on idealization of the flow, and their solutions and underlying assumptions are often inadequately verified, if at all [12]. Topics still to be addressed are, for instance,

a) the role of exothermic gas-phase and solid-phase reactions that occur inside the gun,

b) complexities involved in the burning mechanism of propellants and of flow-borne particulates and unburnt fuels, and

c) mechanisms of ignition that occur in the gun [1,12].

Experiments thus are needed that provide relevant information for proving or disproving model predictions, and on difficulties introduced by the processes occurring in real gun firings which, if recognized, can lead to necessary advancements in interior ballistics.

The ballistic research in the field of conventional guns, though generally considered a mature technology, has been altered over the past decade by refinements in mathematical methods and computer techniques. These have led to an increasing variety of analytical and numerical models that offer solutions in gasdynamics. The advancements in all areas ranging from computational and numerical analysis, stability analysis of numerical algorithms, combustion chemistry, and turbulence through the manifold increases in computer speed and mass storage, permit the investigation of complex phenomena [1]. Conversely, such computer models may entice the researcher to accept computed results in place of experimental information, in spite of the lack of the necessary physical and chemical information on which the underlying assumptions and individual equations should be based [12]. Unfortunately, there are some tendencies to place a much greater belief in the validity of computations than the few known facts would justify. Adjustable parameters, sometimes included in large numbers in gasdynamic models or hydrodynamic codes, can be manipulated to produce better agreement among the results or a better matching of the few available experimental data. Again, more and better-designed laboratory measurements are required to discover and identify the underlying physical and chemical facts in a controlled environment [1]. The present work reported herein takes a step towards this goal.

4. RETROSPECTIVE

4.1 Earlier Experience

The single-stage gas gun built at the Ernst-Mach-Institut [10] is based upon earlier developments of Lord [14] and Wilkins and Carros [15]. A detailed review of simulation experiments is given in refs. 4, 10, and 11.

The feasibility of a gas gun driven by the combustion of a prepressurized mixture of hydrogen and oxygen was demonstrated by studies conducted in the early 1960's. For example, Lord [14] investigated the performance of a 40-mm combustion-heated, light gas gun launcher. His objective was the attainment of a high projectile launch velocity through the use of low molecular weight propellant gas. Controlled combustion was achieved with a gas mixture of hydrogen and oxygen with helium added as a diluent in order to prevent detonation.

The combination that Lord used was ($3H_2 + O_2 + 8He$). The maximum pressure attained in these experiments was 350 MPa indicating that conditions approaching those of real guns are within reach of such gas guns [14].

In 1963, Wilkins and Carros [15] reported on combustion tests performed with stochiometric $H_2/O_2/He$, as well as H_2/O_2 gas mixtures. Their experiments were performed in closed chambers of 0.5 liter and 242 liter volume. Charge pressures, p_1, up to 55 MPa (8250 psi) in the small chamber and 5 MPa (750 psi) in the large chamber were tested. The following parameters were varied:

a) mixing procedure
b) mixing time
c) ignition method
d) flame path-length
e) gas composition
f) charge pressure.

It was found that the order of gas introduction into the pressure chamber is critical. Smooth combustion resulted either with a loading order of: hydrogen, helium, oxygen, or from the addition of premixed oxygen and helium to oxygen. When the gases were filled in the sequence of oxygen, helium, and hydrogen, combustion proceeded in an irregular fashion, sometimes resulting in a detonation.

4.2 Thermodynamic Calculations

Figure 1 shows the BLAKE computations [16] for the realistic virial equation of state together with the data of Lord [14] and of Klingenberg [17]. The two sets of experimental data indicate a straight line dependence, reminiscent of the BLAKE computations for an ideal equation of state (see Fig. 1). The coincidence that Lord's data track the noble gas, ideal equation of state, and BLAKE computations, and that Klingenberg's data track the nitrogen gas, is fortuitous. Both Lord and Klingenberg used helium; and the use of the ideal equation of state is not appropriate at these high pressures. This coincidence misled Lord into concluding that thermal losses had not played much of a role in his

experiment [14], It is now assumed that heat loss is the source of the discrepancies between the BLAKE computations and both experimental sets of data displayed in Figure 1. Also, it shows that relatively large gun chamber pressures or final pressures are obtained when the prepressurization of the fill gases is high enough.

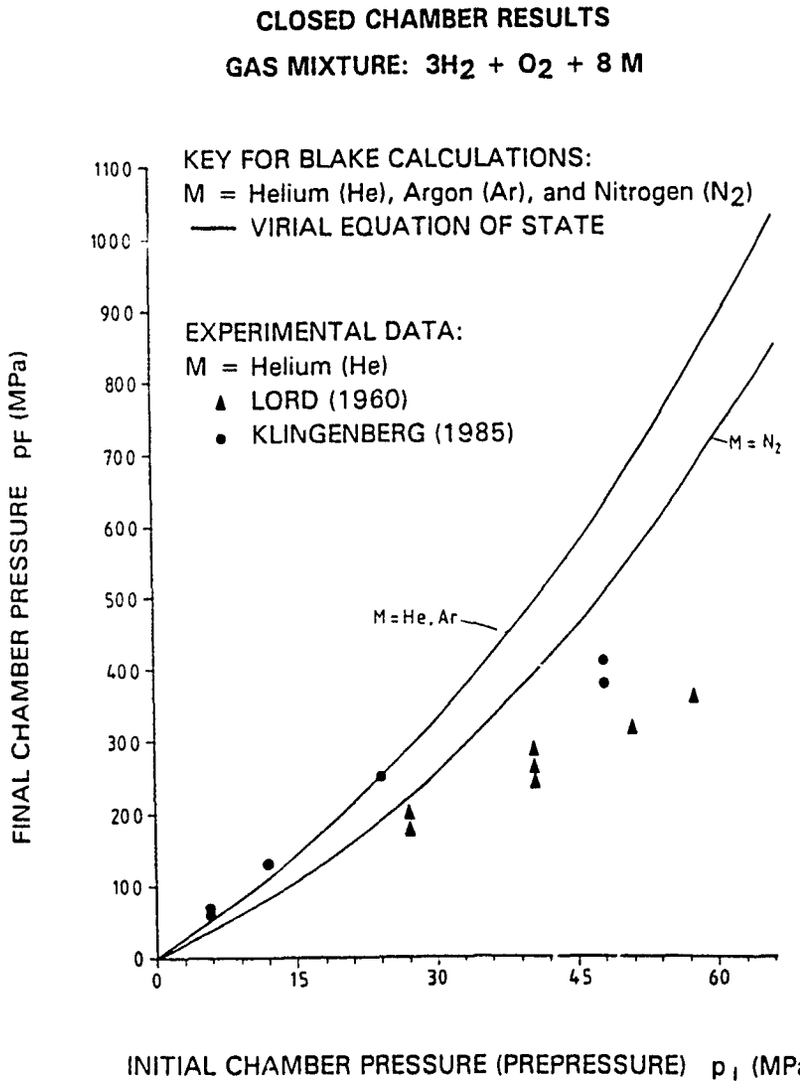

Fig. 1. Final chamber pressure p_F versus initial charge pressure p_I (BLAKE calculation and experimental data) [17].

5. EXPERIMENTAL EQUIPMENT

5.1 Gas Gun

The single-stage gun or gas gun simulator was built with a removable gun tube so that it could be deployed equally well as a stand alone combustion chamber working in the closed bomb mode and as a 20-mm caliber gun simulator.

The photograph in Figure 2 shows the single-stage gas gun with the 20-mm caliber gun tube that vents into an evacuable blast reducing vessel.

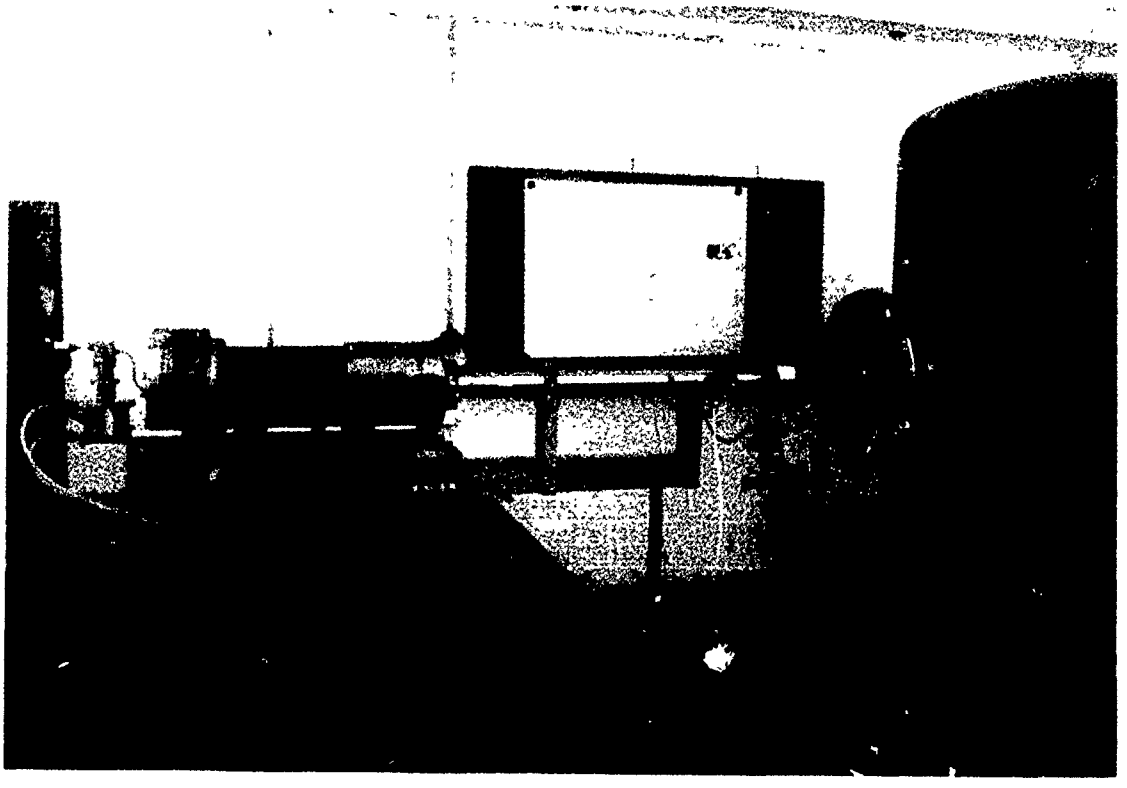

Fig. 2. Single-stage gas gun with blast damping device.

Figure 3 shows the schematic of the single-stage gas gun with the openings for pressure measurements and optical diagnostic instrumentation (M1 to M6). The power cables connecting to the ignition device and the gas-inlet valve are mounted on the breech block (Fig. 2).

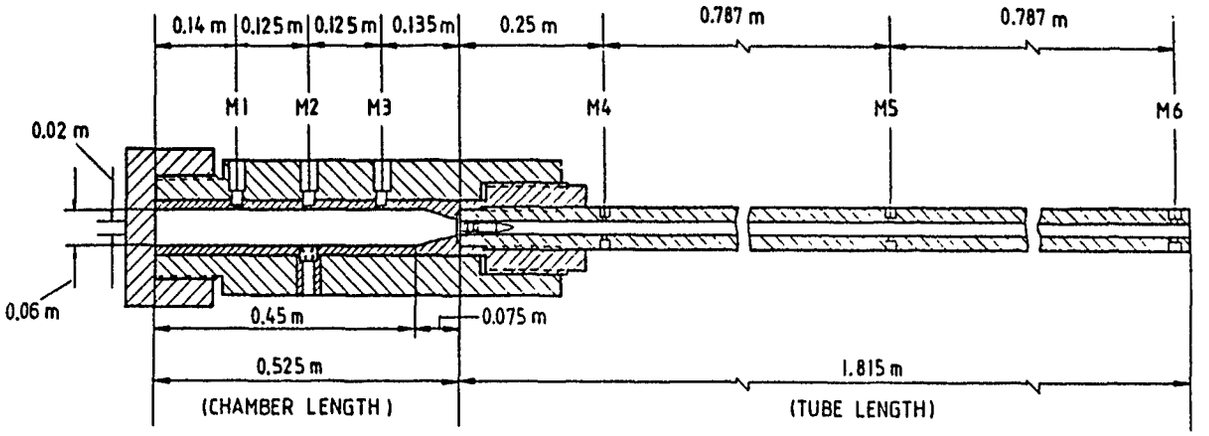

Fig. 3. Schematic of single-stage gas gun.

The gas gun chamber of length l = 550 mm and mean diameter d = 70 mm has a volume of 2 liters. It was designed to be expandable to a 40-mm caliber test fixture [10].

The combustion chamber was sealed initially by a blow-out disk, scored to rupture at a predetermined pressure, in order to simulate the projectile extraction force, which, for conventional 20-mm cased ammunition, is of the order of 90 MPa. If necessary, engraving forces can also be taken into account. A conventional 20-mm projectile and a smooth bore gun tube 1.8 m in length were used for these experiments. The diameter of the projectile rotating band was reduced to 20.1 mm so that it still exceeds the in-bore diameter by 0.1 mm. Then blow-by of the propellant gases is minimized. All of the pressure ports used (M1 through M6) are shown in Figure 5. Temperature measurements, with a specially designed gauge, a thermocouple device and other spectroscopic techniques as well as velocity measurements were conducted through M2, M4, M5, and M6.

5.2 Ignition

For ignition, a current pulse is discharged through a centrally placed single tungsten wire, as shown in the photograph of Figure 4.

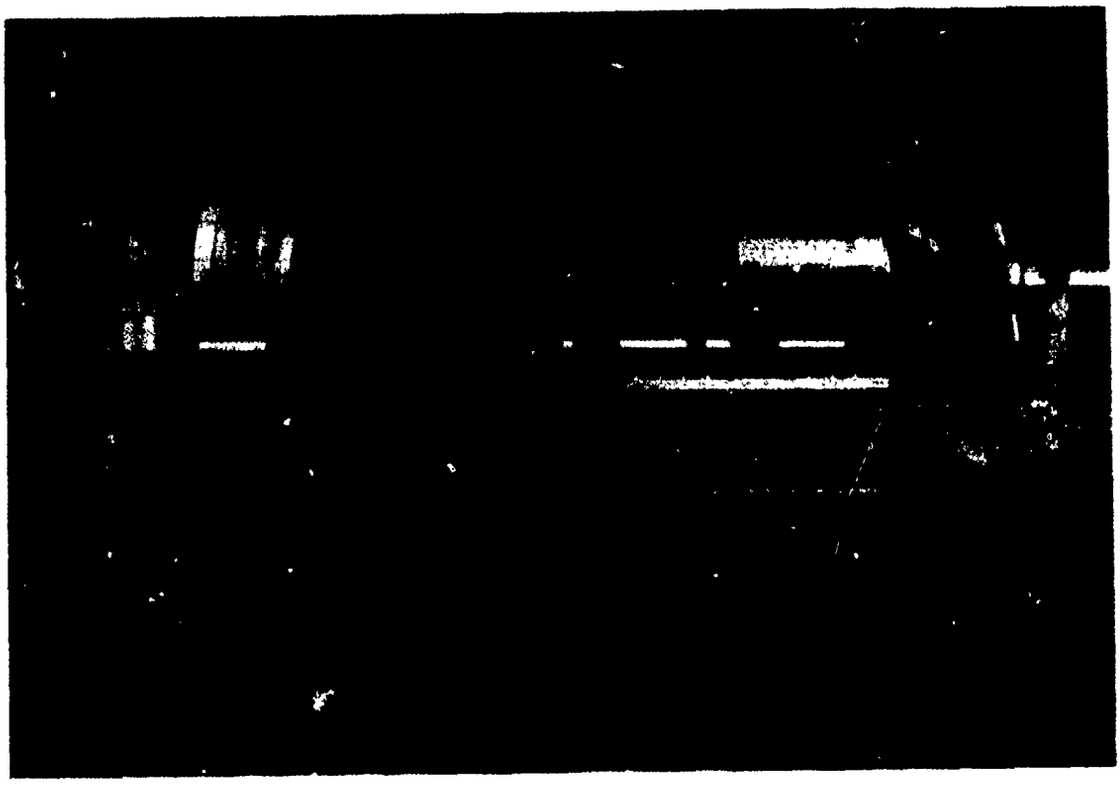

Fig. 4. Combustion chamber with axially placed tungsten wire (breech block removed).

Ignition is achieved through ohmic heating of the centrally placed tungsten wire by the discharge of a capacitor bank. The "soft" hot wire ignition yielded reliable results without deflagration or detonation of the gas mixture. Also, contamination by undefined particles encountered, for example, by the exploding wire ignition technique [10] is prevented.

5.3 Filling Procedure

A specially designed gas compressor is needed to prepressurize the propellant gases. Since prepressurization determines the final pressure p_F in the gas gun chamber, the level of prepressure given by the compressor is monitored during the filling procedure. Before filling the chamber, the feed lines are purged by pumping dry nitrogen through the device. In order to control the mole fraction, the temperature in the feed lines is also monitored by thermocouples [10].

For safety reasons, the possible leakage of hydrogen or carbon monoxide into the test room is monitored by warning devices. These indicators are activated when the gas leakage into the test room amounts to a concentration which exceeds the safety limits, e.g., 4 % of hydrogen in the surrounding air. Then, this device automatically stops the filling procedure, nitrogen is pumped into the feed lines, and a room fan is turned on to remove the gases from the room.

To circumvent the difficulty of initiating combustion instabilities in the gas gun chamber during the combustion of hydrogen, the oxygen is first filled into the chamber followed by a pre-mix of hydrogen/helium gases. A filling order of oxygen and unmixed hydrogen and hydrogen resulted in severe pressure oscillations or even detonation corroborating the findings of Wilkins and Carros [15]. It should be mentioned that the addition of oxygen as the final component also resulted in smooth combustion. What is more, the amount of diluent can then be varied as desired. However, this requires a suitable gas compressor for oxygen. Administering the oxygen directly from the reservoir, which in our case was pressurized to 30 MPa, allows for a simpler apparatus. It is pointed out that difficulties were encountered for mixtures with carbon monoxide because pressure oscillations occurred occasionally during the combustion.

6. EXPERIMENT

6.1 Introductory Remarks

During the initial stage of the three-year program the single-stage gas gun was redesigned and transferred to a new laboratory building at the test site of the Ernst-Mach-Institut. The necessary installation of the feed lines and safety experiment and the construction of an improved gas gun chamber then provided the means for carrying out the experiments.

Fresh research grounds were entered with attempts to use various gas mixtures in the gas gun deviating from the gas composition $O_2/3H_2/8He$ investigated by Lord [14] and Wilkins and Carros [15]. Gas mixtures ranging from hydrogen/-oxygen/helium, formulated to be deficient in oxygen as conventional solid gun propellants, through CO/O_2 or $H_2/CO/O_2/He$ gas propellants were tested. Sometimes deflagration or even detonation occurred in the gun chamber causing damage of the mechanical equipment.

Most severe difficulties were encountered in probing the interior ballistic or gun tube flow. Technological barriers were to overcome in the simulation of reacting in-bore flows and in measuring the important flow characteristics. For example, the combustion of hydrogen produces gases of low molecular weight. The pressure waves that develop in such environments are characterized by a steep pressure rise, dp/dt, so that damage of the optical windows may occur.

A new research area not previously investigated was the approach to determine radial temperature and velocity gradients in the gun tube flow. A typical difficulty in velocity measurements is caused by backscattering of incident laser light. Scattering occurs at the flow-borne particles in two-phase flows and, with a high noise level, at the inner tube wall. New window designs were evolved to overcome this problem. The radial temperature profiles were extended to the tube wall, where interface temperature was measured simultaneously with gas temperature in the core flow by using fast-response thermocouples in addition to emission/absorption spectroscopy.

Most severe limitations were encountered with the methods applied for measuring species concentrations. A novel multichannel infrared spectrometer with a spectral range of 1.4 to 5 μm and a time resolution of 1 ms per spectrum yielded at least some promising results.

In order to generate flow-borne particles for the investigation of two-phase flow inert particles, i.e., titanium dioxide (TiO_2) particles were incorporated in the flow. In other cases reacting particles like soot were formed during the combustion of carbon monoxide in the gas gun chamber. Inert particles can reduce the gas temperature especially near the wall of the gun tube by up to 50 %. However, the incorporation of particles, whether inert or reacting, results in a dramatic, nearly exponential increase of the absorptance of the flow. As a consequence, sophisticated spectroscopic measurements were restricted to clean (single-phase) flows or to flows of relatively low particle concentrations.

6.2 Closed Chamber and Gun Tests

More than 200 tests had been carried out during the three-year program including experiments conducted in the closed bomb mode and in the single-stage gas gun. The gas gun assembly was shown in Figures 2 and 3. The closed bomb mode experiments used the same assembly. However, the blow-out disk mounted at the end of the conical part of the gas gun chamber was replaced by a solid retainer that closed the chamber and contained the reacting gases until the combustion was completed, see Figure 5.

The closed chamber tests were necessary to control and monitor the combustion reactions, especially for unknown gas mixtures.

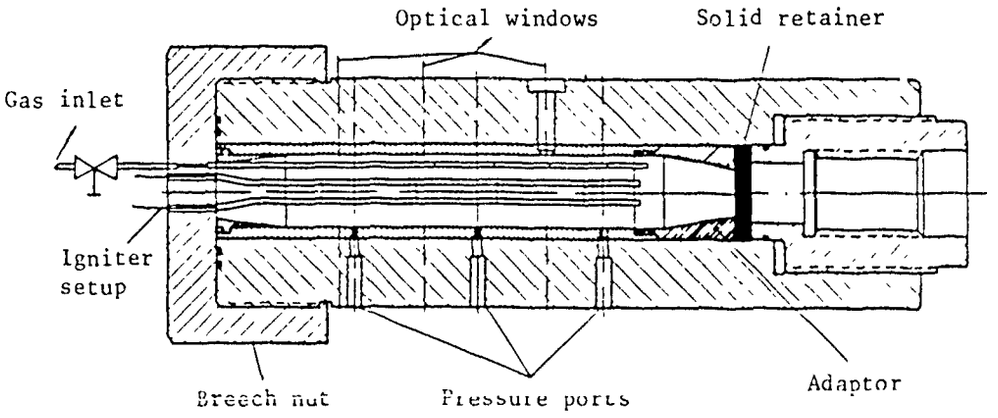

Fig. 5. Gun chamber with solid retainer and igniter setup

6.3 Gas Composition

The advantage of the single-stage gas gun or the gas gun simulator is the potential to generate in-bore flows driven either by one or by both of the two main combustion reactions

$$H_2 + \tfrac{1}{2}\, O_2 \longleftrightarrow H_2O \qquad (1)$$

$$CO + \tfrac{1}{2}\, O_2 \longleftrightarrow CO_2 \qquad (2)$$

which form the basis of chemical propulsion devices be it (a) conventional solid propellant driven gun, (b) liquid propellant (LP) driven gun, or (c) electrothermal-chemical (ETC) driven gun systems [11,18,19]. A further advantage is that the

gas gun firings yield optically transparent gun tube flows. For example, in the visible wavelength (λ) region $0.4 \leq \lambda \leq 0.8\ \mu m$ the absorptance, a, of the gas gun in-bore flow is of the order of a = 0.2. Comparatively, conventional solid propellant or liquid propellant driven gun tube flows are characterized by optically thick in-bore flows with absorptances of a > 0.9 [20-22]. The extremely high absorptance of such gun tube flows is due to the presence of either large concentrations of flow-borne particles [20,21] or of opaque liquid droplet/gas mixtures [22]. Thus, the optical probing of the core flow in such systems is nearly impossible. The gas gun overcomes the difficulty, because suitably diluted mixtures of hydrogen and oxygen and hydrogen, carbon monoxide and oxygen were chosen as the propellant. This selection keeps the chemistry as simple as possible and avoids complications in the interior ballistic and in-bore flow dynamics. On the other hand, the selection of hydrogen as the propelling agent involves the formation of the aforementioned steep pressure gradients inside the bore of the gas gun causing window damage. To avoid mechanical failure of the optical measuring ports the chamber and in-bore pressures had to be reduced. Generally, the preferred fill or prepressures, p_I, were of the order of 12 MPa or 24 MPa yielding maximum chamber pressures of p_F = 100 - 110 MPa or 150 MPa. However, a few tests were also made at chamber pressures of p_F = 400 MPa. Thus, pressures and temperatures typical of an actual gun had been generated.

6.4 "Standard" Gas Mixtures

The first series of tests used the "standard" gas mixture ($O_2 + 3H_2 + 8He$) known from the earlier work of Lord [14] and Wilkins and Carros [15] and the recent studies of Klingenberg and Heimerl [10,11,17]. This mixture is formulated to be deficient in oxygen comparable to those solid propellants fired in conventional gun systems [18,19]. The fill or prepressures ranged from 6 MPa through 45 MPa resulting in maximum chamber pressures of 50 - 400 MPa. The bulk of data were taken at fill pressures of 12 MPa and 24 MPa. The pressure histories that develop along the gun tube are shown in Figures 6 and 7. Figure 6 presents the pressure versus time curves obtained at a prepressure of p_I = 12 MPa at locations M1, M3, M4, M5 and M6. The location of the pressure port is seen in Figure 3.

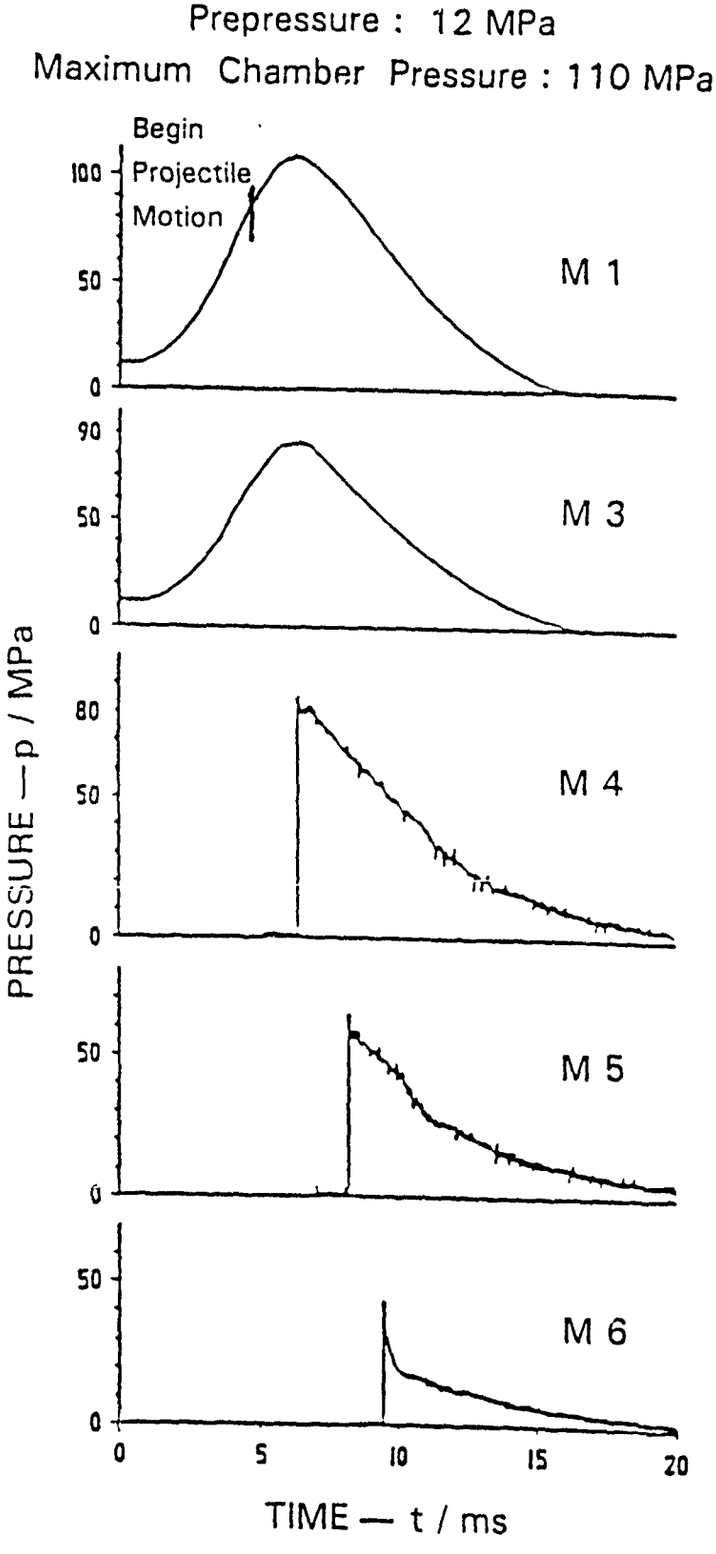

Fig. 6. Pressure vs time at locations M1 to M6

The projectile starts its motion at about p = 90 MPa as the blow-out disk bursts, i.e., 4 ms after the current pulse had been applied to the igniter wire in the gun chamber. The maximum chamber pressure of p_F = 110 MPa is reached at about 7 ms after ignition just before the base of the projectile passes measurement location M4. A steep pressure gradient develops as the projectile passes locations M4, M5, and M6 in the gun tube.

Figure 7 presents the pressure versus time curves at locations M1, M3, M5, and M6 obtained for a prepressure of 24 MPa.

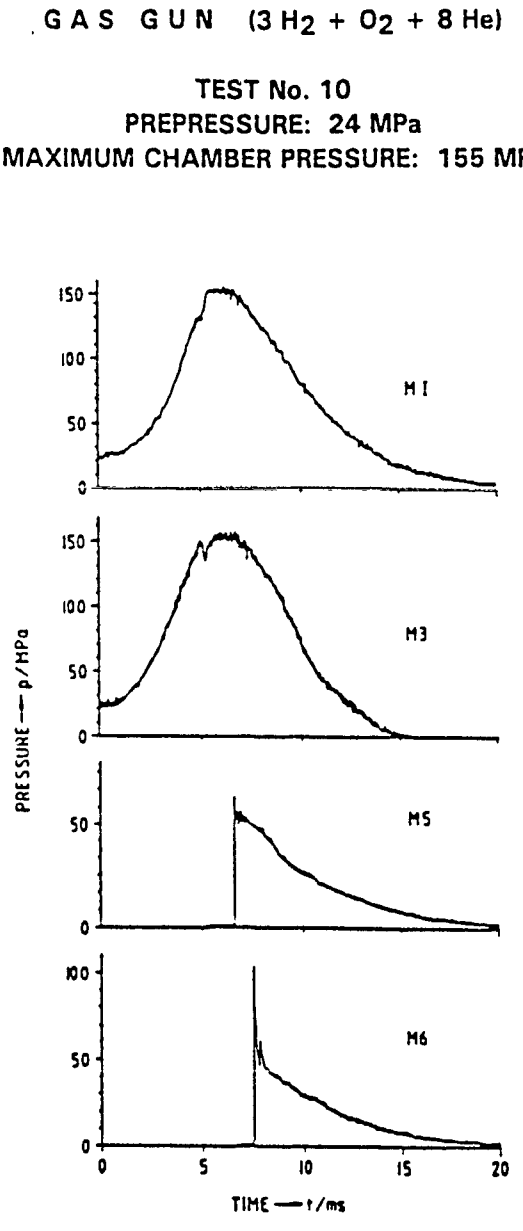

Fig. 7. Pressure vs time at locations M1, M3, M5 and M6

Accordingly, higher in-bore pressures are recorded in this test. While the projectile launch velocity at fill or prepressures of p_l = 12 MPa is $v_0 \approx$ 750 m/s, here a higher velocity of $v_0 \approx$ 950 m/s is obtained. Again steep dp/dt rises are measured at locations M5 and M6 after the base of the projectile has passed the pressure ports. For example, Figure 8 shows a portion of the M6 p vs t curve of Figure 7 on an extended time scale.

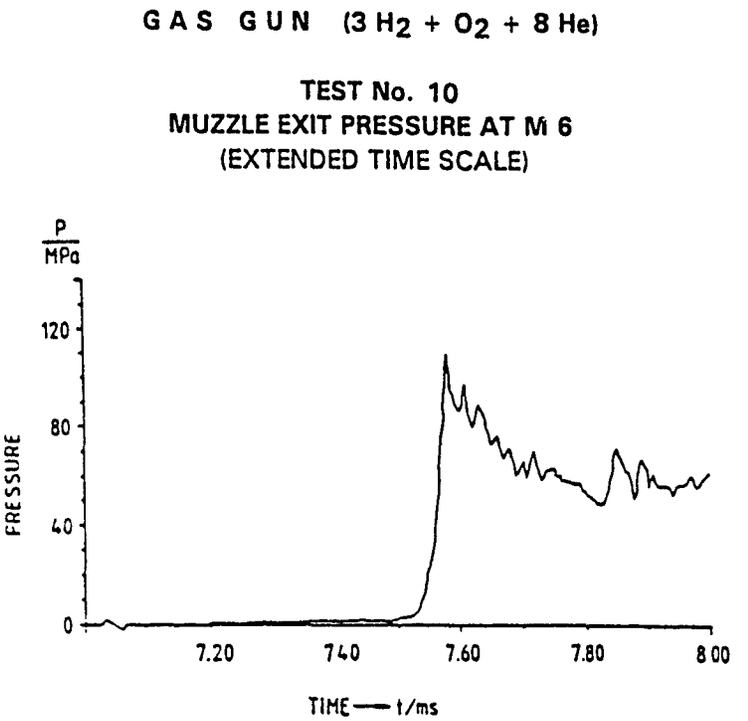

Fig. 8. Muzzle pressure vs time at M6

It demonstrates that the Kistler gauge used responds to the steep increase of p by generating oscillations.

6.5 Hydrogen/Oxygen Gas Mixtures with Different O/F Ratios

The oxygen/hydrogen/helium gas mixture was varied so that O/F ratios of 0.5, 1.0, and 3/4 could be investigated. The gas mixtures were composed of

a) $1.5\ O_2 + 3\ H_2 + 8$ He; (O/F = 0.5)

b) $3\ O_2 + 3\ H_2 + 8$ He; (O/F = 1.0)

c) $4\ O_2 + 3\ H_2 + 8$ He; (O/F = 4/3)

For example, Figures 9, 10 and 11 show the p vs t curves recorded in the gas gun chamber at location M3 for fill or prepressures of p_I = 12 MPa when conducting closed chamber mode experiments.

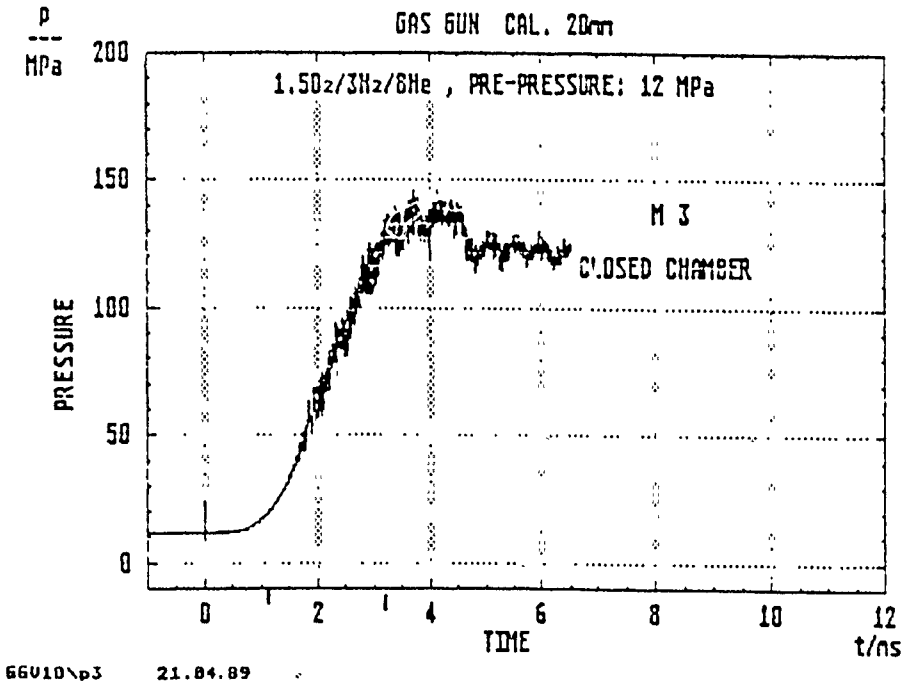

Fig. 9. Pressure vs time (1.5 O_2 + 3 H_2 + 8 He)

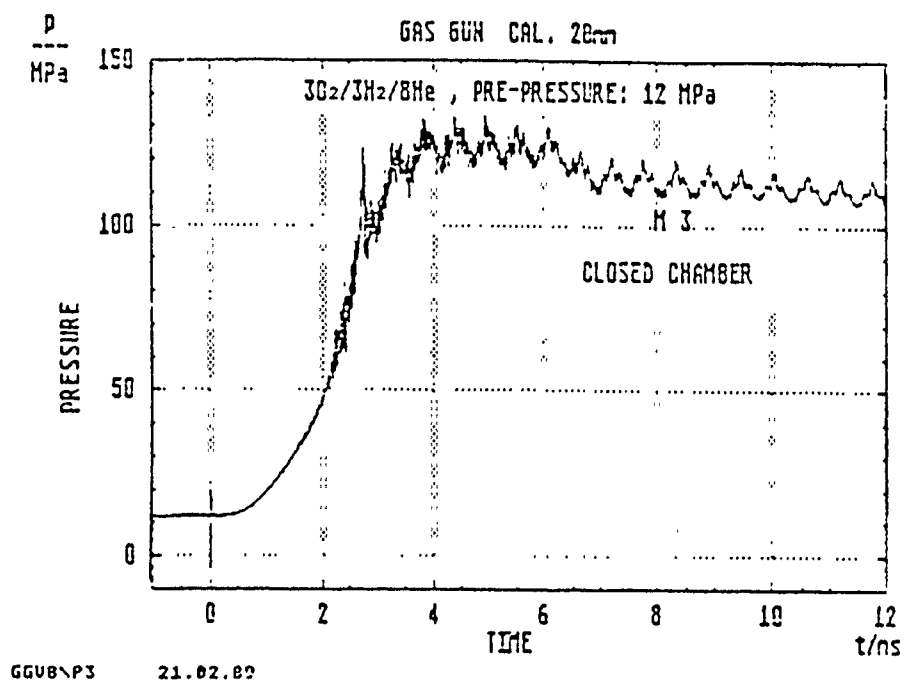

Fig. 10. Pressure vs time (3 O_2 + 3 H_2 + 8 He)

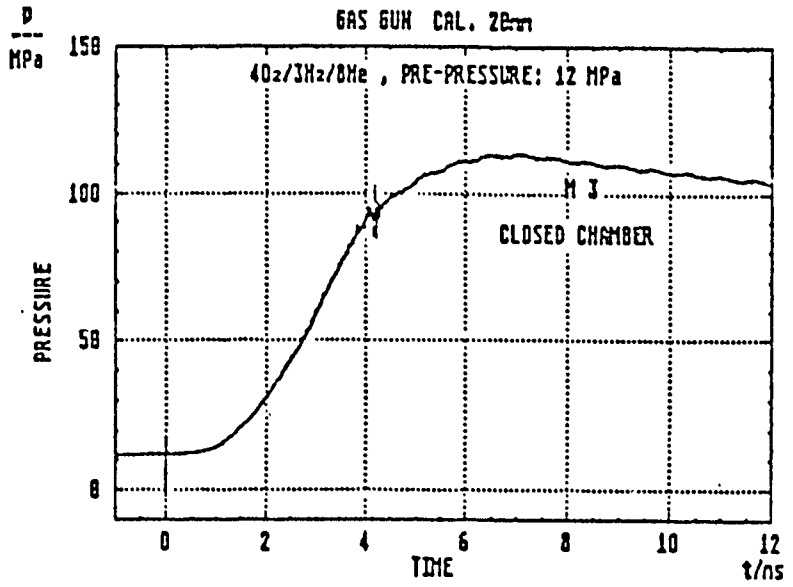

Fig. 11. Pressure vs time (4 O_2 + 3 H_2 + 8 He)

In these tests small pressure oscillations were recorded whose amplitude decreased with the increase of the O/F ratio of the propelling gas mixture used. The pressure oscillations are attributed to irregular ignition causing unstable or abnormal combustion in the gun chamber. The maximum chamber pressure and the rise time of the pressure curve between 10 % and 90 % of the dp/dt rise, Δt, are also dependent upon the O/F ratio, see Table 1.

Table 1. Closed bomb results

Gas Composition	O/F Ratio	Maximum chamber pressure p_F (MPa)	Rise time Δt (ms)
O_2 + 3 H_2 + 8 He	1/3	120	1.0
1.5 O_2 + 3 H_2 + 8 He	1/2	135	0.9
3 O_2 + 3 H_2 + 8 He	1	125	1.2
4 O_2 + 3 H_2 + 8 He	4/3	115	1.8

Obviously, the highest chamber pressure and shortest rise time was obtained when firing the (1.5 O + 3 H_2 + 8 He) gas mixture having a fuel to oxidizer ratio of O/F = 1/2. For the "standard" gas mixture (O/F = 1/3) the maximum chamber pressure is slightly higher (120 MPa) than predicted (110 MPa) and the rate of pressure rise is relatively steep, Δt = 1.0 ms.

6.6 Oxygen/Carbon Monoxide Gas Mixtures

In addition to the above pure oxygen/hydrogen/helium gas mixtures various compositions with carbon monoxide have been tested including pure CO/O_2 compositions. The objective was to investigate the applicability of such gas mixtures, because there were no informations available that could predict the behavior of such gas compositions during the combustion at high pressures and temperatures inside the gun. The gas mixtures with pure CO/O_2 investigated included compositions such as (O_2 + 2 CO_2) and (O_2 + 3 CO_2). However, in some cases, the reactions during the combustion of such gas mixtures resulted in a detonation causing severe damage to the hardware. The reasons are not yet understood. There may be an effect of the mixing time and/or of debris or water droplets remaining in the reaction chamber from the previous firing. A systematic study is not easily carried out, as there was considerable damage including the destroyment of Kistler pressure gauges in each firing. The pressure gauges stopped the recordings above 70 MPa due to gauge failure. Also, the oxygen "rich" mixture $2CO/O_2$ reacted strongly with the iron in the chamber wall. Compounds of Fe^{3+} were deposited on the tungsten wire. The mixture $3CO/O_2$ showed violet metallic deposits on the tungsten wire. These originate from compounds with mixed lower oxidation states of iron. (In these cases the apparatus had acted rather like an oversize halogen light bulb: volatile Fe/CO compounds pyrolized on the tungsten wire.)

6.7 Oxygen/Hydrogen/Helium/Carbon Monoxide Gas Mixtures

Further tests were conducted using compositions with the two fuel components hydrogen and carbon monoxide. For example, the following mixtures were fired at prepressures ranging from 6 through 12 MPa so that maximum chamber pressures of 70 to 110 MPa could be obtained:

a) $(O_2 + 1.5\ H_2 + 4\ He + 1.5\ CO)$

b) $(1.3\ O_2 + 3.1\ H_2 + 8.4\ He + 0.5\ CO)$

c) $(O_2 + 3\ H_2 + 8\ He + 0.2\ CO)$

d) $(0.6\ O_2 + 1.5\ H_2 + 4\ He + 0.3\ CO)$

Again, severe damage to the hardware and pressure transducers occurred in the firing a) with 1.5 CO. Considerable time was spent on repair work replacing the parts in the aftermath of such detonations. Therefore, the CO content was reduced and most of the measurements were performed at a prepressure of 12 MPa using the gas mixture d) with 0.3 CO. However, even for mixtures with 0. sometimes dramatic pressure oscillations occurred caused by undesired ignition delays, see Figure 12.

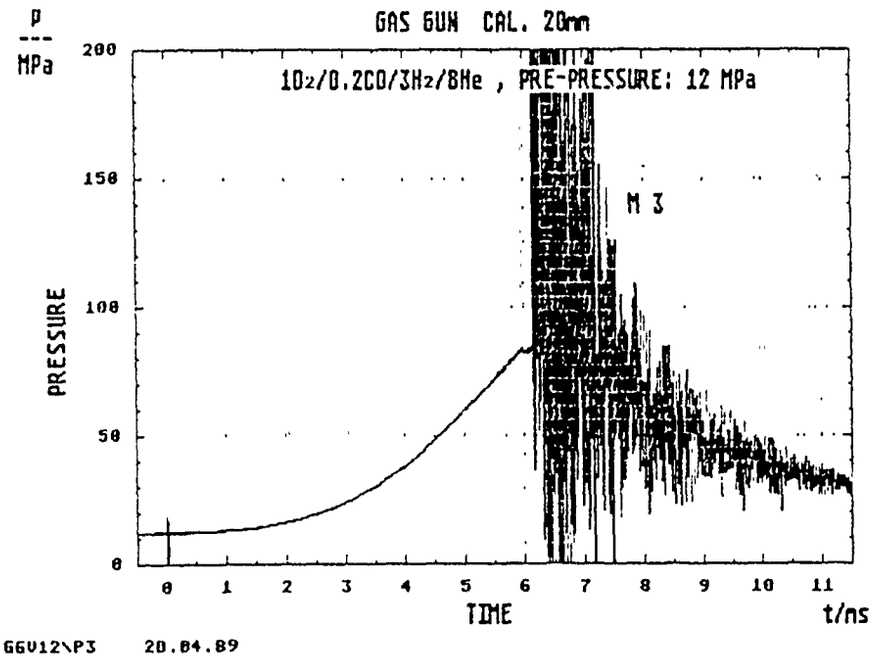

Fig. 12. Pressure vs time at location M3 $(O_2 + 3\ H_2 + 8\ He + 0.2\ CO)$

6.8 Reacting and Nonreacting Particles

The addition of CO to the gas mixture offers the potential to generate reacting soot particles and lessen the steep in-bore dp/dt rise encountered in the pure H_2/O_2 firings. For example, the benign gas mixture d) with 0.3 CO produces varying amounts of soot which is swept along the gun tube and increases the absorptance of the flow as well as the emission in the continuous region of the spectrum, because the soot particle radiate.

6.9 Gun Chamber Pressures and Temperatures

In addition to pressures p(t) temperature histories, T(t), were measured inside the gun chamber using emission and/or emission/absorption methods. In some cases, determination by means of the emission gauge technique designed by Klingenberg [23] was inaccurate, due to nonequilibrium emission from the reacting gases. For example, IR spectroscopy has shown that, in general, there is a strong emission from H_2O bands between 1.4 μm and 2.5 μm during the initial phase of the combustion. This emission may be responsible for the high reading from the gauge. Since the rate processes involved are very fast these bands are not in thermal equilibrium. Therefore, emission/absorption methods or modified reversal methods were used to measure T(t) at different wavelengths.

Another difficulty encountered during the temperature measurements was the occlusion of the sapphire windows by condensed water vapor and, with CO part of the reaction mixture, soot formation. Therefore, the surface quality of the windows were monitored during the experiments in order to account for this effect. Also, damage of window material occurred when steep pressure gradients were encountered. Table 2 lists some of the data measured for the various gas compositions and fill pressures.

Table 2. Maximum gun chamber gas pressures and temperatures

Gas composition	Pre-pressure p(MPa)	Maximum Gas Pressure p(MPa)	Maximum Gas Temperature T(K)
O_2 + 3$H_2$6 + 8He	6	50	1870
	12	110	2150
	24	150	2300
0.6O_2 + 1.5H_2 + 4He + 0.3CO	6	50	1900
	12	110	2200

7. HIGH SPEED INFRARED SPECTROSCOPY

7.1 Overview

Multichannel infrared (IR) spectroscopy was used to investigate the gas gun in-bore flow. The spectral range was 1.2 μm to 5.3 μm. The infrared (IR) emission produced by the combustion of prepressurized gas mixtures consisting of hydrogen/oxygen/helium and carbon monoxide/oxygen was recorded by linear, 96 element, InSb diode arrays. Maximum time resolution was 1 ms for a full spectrum. The method has the potential to measure time resolved species concentrations in instationary combustion reactions at high pressures [24].

7.2 Background

The reactions of hydrogen and carbon monoxide with oxygen under high pressure were studied. The parameters measured included not only pressure, temperature, and gas velocity, but also species concentrations. Nonintrusive methods were preferred to avoid disturbances of the flow. Here, a novel multichannel infrared spectrometer was used to monitor species concentrations. The 96 channel high speed infrared (IR) spectrometer was designed according to the specification given by the Forschungsinstitut für Optik (FfO) der Forschungsgesellschaft für Angewandte Naturwissenschaften e. V., Tübingen, and by the Fraunhofer-Institut für Kurzzeitdynamik, Ernst-Mach-Institut (EMI), Weil am Rhein. It was manufactured by the Sira, Ltd., South Hill, Chislehurst, Kent, England, and funded by the German Ministry of Defence (MOD). The German MOD gave the permission to use the instrument in both the FfO and EMI institutes. The current owner is the FfO, Tübingen, though the spectrometer is still located and used at the EMI in Weil am Rhein.

Recent years have seen rapid advances in spectroscopic analysis of flames and reacting flows. Progress has been notable with laser methods such as Laser Induced Fluorescence (LIF) and Coherent Anti Stokes Raman (CARS) spectroscopy. These and most of the other known spectroscopic techniques, however, are not well suited for application in either highly instationary or optically thick, particle-laden flows. At higher pressures, possible line broadening and/or signal quenching result in loss of information. Further, the complete description of even simple flames, such as that of H_2/O_2, must account for a sizable number

of elementary reaction steps; namely, 19 for H_2/O_2 [25]. Hence, combustion research has focussed mainly on clean, stationary, low pressure flames with low numbers of reactants. The IR technique applied here is a suitable diagnostics tool for the analysis of highly instationary, particle laden, high pressure reacting flows. It is basically insensitive to scattering from particulates, and a number of species relevant for combustion show absorption bands in the near infrared.

7.3 Multi-channel High Speed Spectroradiometer

The spectroradiometer consists of the

detector head
local box
computer.

The detector head contains the optics and the line drivers for the analog outputs from the detectors. The analog signals are relayed via cable to the local box, where signal amplification and digitization take place. Finally, the digitized information is sent to the system controling computer for processing and storage.

The optical imaging is shown in Figure 13. Light enters the system through two apertures of 10 mm diameter. Low pass filters with cut-off frequencies at 1.4 μm and 2.6 μm sort out the visible and UV regions. Subsequently, the two beams are enlarged fourfold by an afocal system of a pair of mirrors for each beam and one jointly used field lens. Frequency dispersion is achieved by the gratings, one per beam. Light coming from the gratings is then focussed onto two nitrogen cooled, linear, 48 element diode arrays for a total of 96 channels. The detectors are of InSb, manufactured by EGG Judson, Cincinnatti. The operating range of the spectrometer is, nominally, 0.64 to 5.32 μm, divided into subregions of 0.64 to 2.67 μm and 2.42 to 5.32 μm. Resolution is 0.042 μm respective 0.06 μm per channel. In practice, the low wavelength limit is 1.3 μm due to the entrance filters. Higher resolution, at the expense of total spectral range, is achievable depending on the gratings.

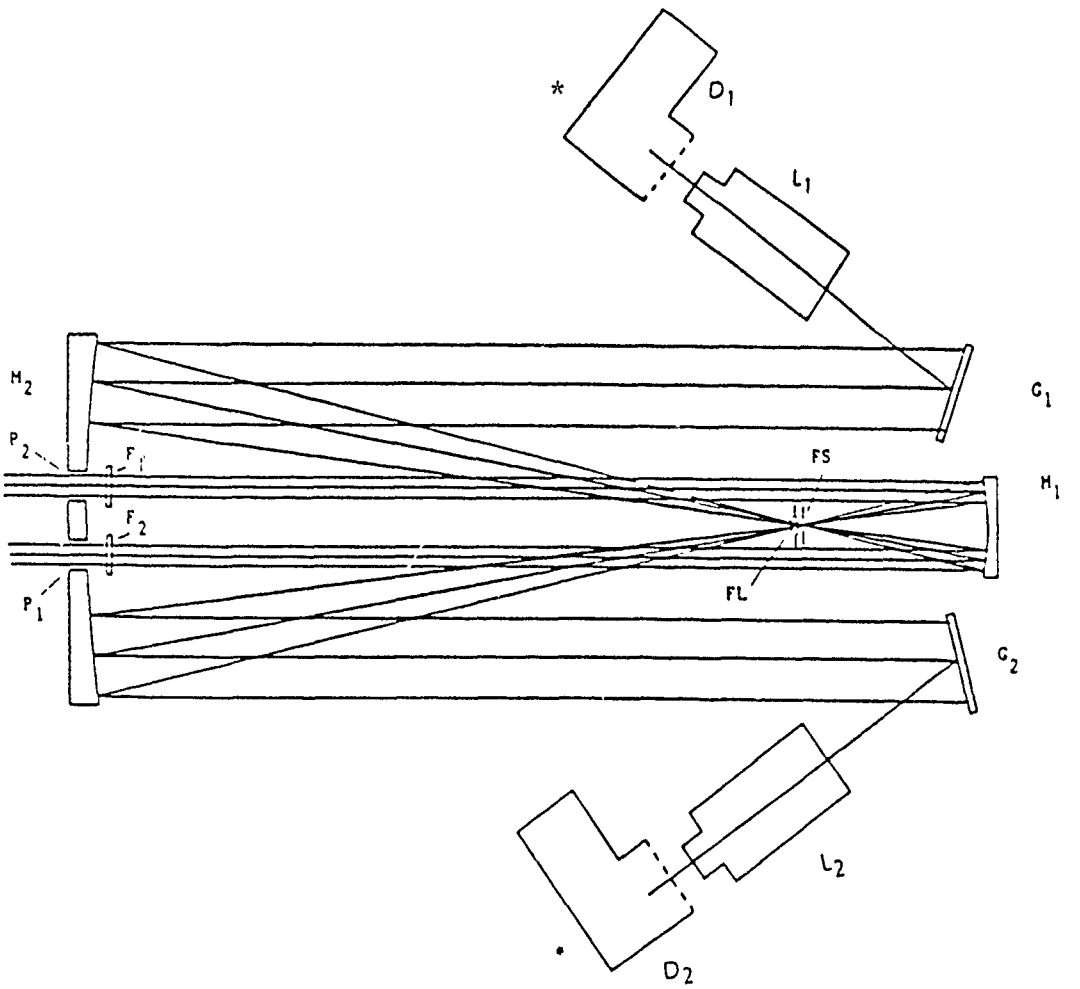

Fig. 13. Schematic of imaging optics

7.4 Calibration

Of the various possible calibration modes, calibration against a black body was chosen, in order to minimize systematic errors induced by the optics. The spectrum was recorded and subsequently compared channel by channel with a theoretical, computer stored reference, see equation (3). The true spectral intensity value, E_i, then, is the produt of the measured value, M_i, and the calibration factor, C_i.

$$E_i = C_i \cdot M_i \qquad (3)$$

Calibration is necessary, because spectral sensitivity varies between different channels. For example, the grating efficiency being rather low at the edges of the spectral range reduces the amount of light transmitted.

For reference purposes, the spectrum of a well known stationary flame, Hefner's Candle, is drawn in Figure 14. The single most conspicuous signal is the strong carbon dioxide band at 4.3 μm. A weak signal at 2.7 μm is also caused by CO_2. The continuum between 1.2 and 3.6 μm is due to the black body emission from soot particles present in the flame. The entrance filter's transmissivity cutoff at 1.2 μm causes a corresponding cut in the spectrum.

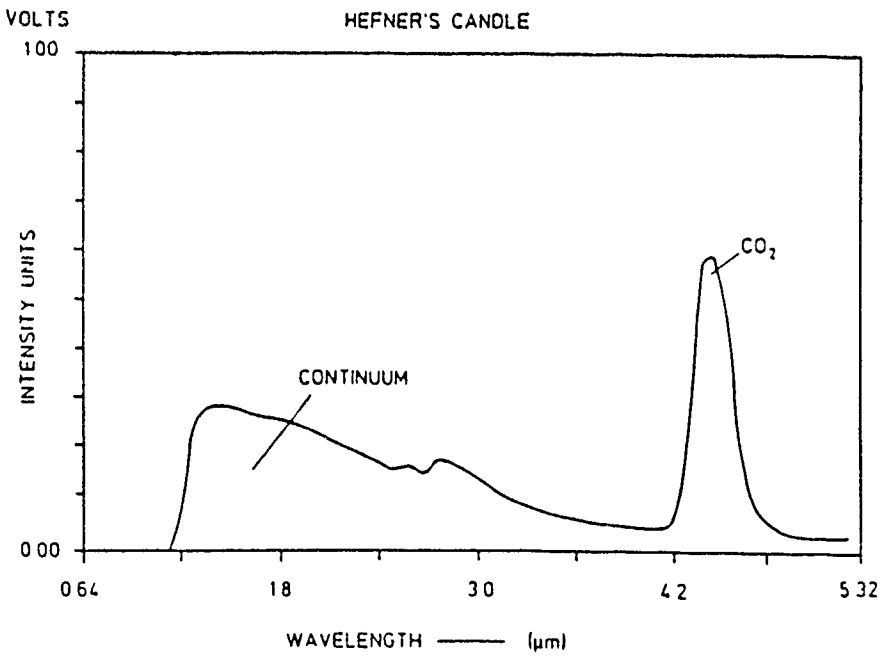

Fig. 14. IR emission spectrum of Hefner's candle

7.5 Sample Results

A sequence of spectra recorded during the combustion of hydrogen and oxygen in the gun chamber is shown in Figure 15. Helium was present as a diluent in order to prevent premature detonation. The mixture was 30 % deficient in oxygen; higher, stoichiometric amounts of oxygen gave excessive formation of iron oxides from reactions with the steel chamber wall. For this test the pre-pressure (fill pressure), p_i, was 7.2 MPa. Here, the burst disk was set to open at 60 MPa.

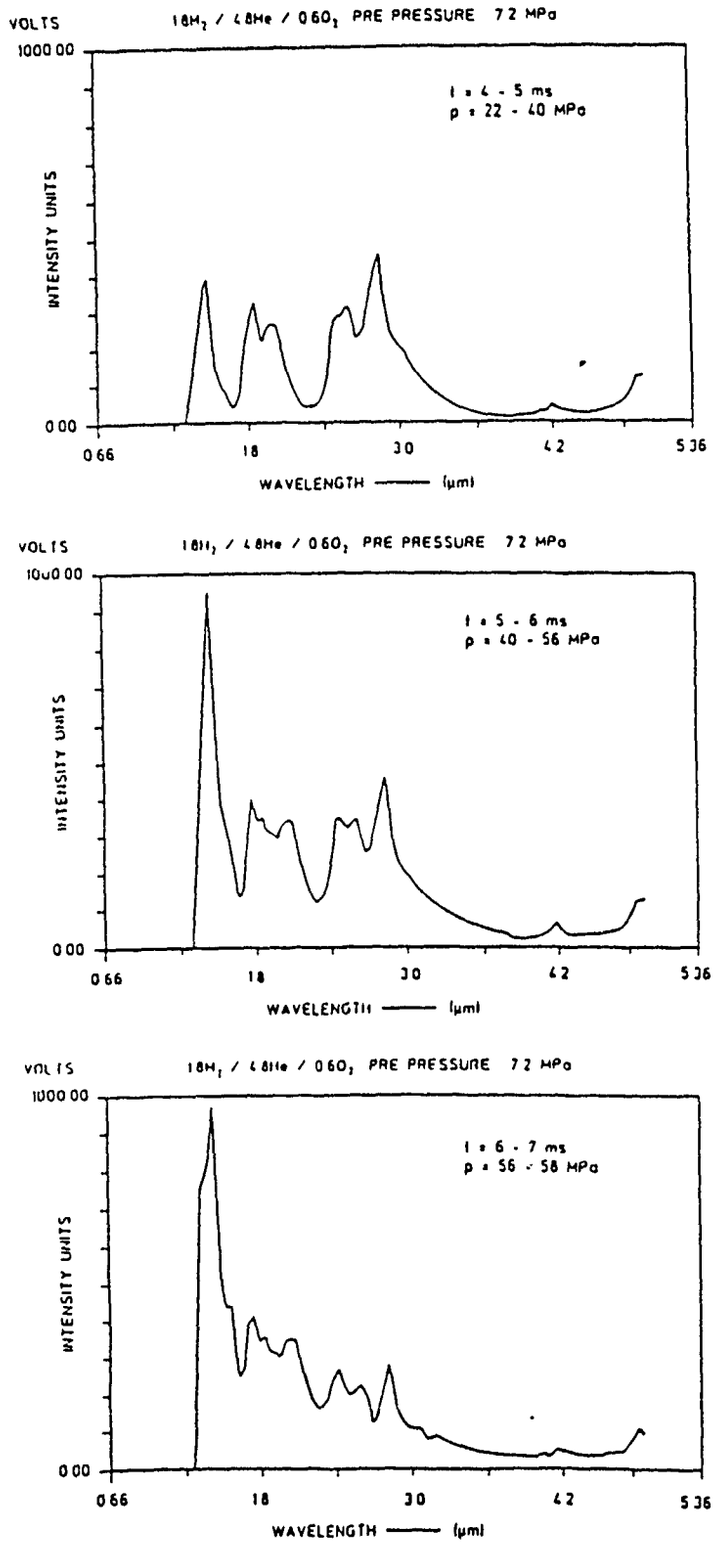

Fig. 15. Series of IR spectra from H_2/O_2 combustion; helium diluent

The three consecutive spectra presented in Figure 15 were recorded at the following time intervals and pressures: establishing in the gun chamber:

a) t = 4 - 5 ms; p = 22 - 40 MPa

b) t = 5 - 6 ms; p = 40 - 56 MPa

c) t = 6 - 7 ms; p = 56 - 58 MPa

The reaction starts at t > 2 ms after triggering of the electrical ignition circuit. The maximum pressure is attained at t = 6.4 ms. At this point the blow out disk ruptured, limiting the maximum pressure to 58 MPa.

Generally, there is a paucity of spectral data in the literature for high pressure, high temperature environments, especially in the infrared region of interest. Therefore, measurements are sorely needed. At present, quantitative determination of species is limited.

Qualitatively, the variations in relative peak intensities with time (Fig. 15) are indicative of changes in species mole fractions during hydrogen combustion. The bands at about 1.4, 1.9, and 2.5 μm coincide with water emission bands as described in the literature [26]. The signal at 2.5 μm is possibly a superposition of H_2O and OH modes. The 2.7 μm signal decreases in relative intensity during the course of the reaction. Comparatively, the 2.5 μm emission remains more or less unchanged. This supports a peak assignment of the 2.7 μm signal as the OH stretching mode. OH is found primarily in flame fronts, that is in the early stages of combustion. The very prominent signal at 1.4 μm, on the other hand, increases during combustion. Here, the peak intensity ratio of the 1.4/1.9 μm H_2O (overtone) bands is of the order of 2/1, whereas data taken from rocket exhaust at normal pressure display a ratio of 1/1 [26]. Note, however, that the signal is distorted by the filter cut-off already mentined above and is thus difficult to interpret. The variations in signal intensities with time observed above appear plausible.

Figure 16 shows a sequence of spectra recorded from a carbon monoxide/-oxygen combustion. Again, the mixture was 30 % deficient in oxygen. Unfortunately, the presence of carbon monoxide as fuel component results in extensive reaction with iron from the chamber wall. After the experiment, the tungsten ignition wire was found to have been clad with an iron oxide of violet, metallic appearance. Further, a certain amount of soot is deposited on the chamber walls, as expected for oxygen deficient combustion. The initial (fill) pressure

was 4 MPa, the maximum pressure was 60 MPa with pressure fluctuations of ± 20 MPa at a frequency of 100 Hz, which indicates unstable combustion. The reaction begins about 1 ms after circuit closure, the maximum pressure of 60 MPa is reached after 1.8 ms. The spectra were recorded at the following times and pressures establishing in the gun chamber:

a) t = 1 - 2 ms; p = 4 - 60 MPa

b) t = 3 - 4 ms; p = 55 MPa (average pressure)

c) t = 5 - 6 ms; p = 50 MPa (average pressure)

The variations in the spectra from the carbon monoxide reaction are discussed qualitatively. During the early combustion phase (Fig. 16a) an emission band at 2.7 μm is the single most prominent feature. This band coincides with a CO_2 overtone mode. Smaller peaks are visible at 2, 2.4, and 4.3 μm. The latter is also ascribed to CO_2. Surprisingly, the stretching vibration of CO centered at 4.7 μm is not recorded. It cannot be excluded, that the limited transmissivity of the optical windows prevents its detection. The cut-off wavelength of sapphire is of the order of 4.5 μm.

In the next time frame (Fig. 16b) the 2.7 μm peak has nearly doubled. Also, the bands at 2 and 2.4 μm, and a new signal at 1.4 μm have more than doubled. The 4.3 μm absorption, by contrast, has virtually disappeared under the base line, which would indicate that its appearance in the first frame (Fig. 16a) is not combustion related, but is caused by ambient carbon dioxide within the optics system.

In the final spectrum (Fig. 16c) the 1.4 μm peak has lost most of its strength. The 2, 2.4, and 2.7 μm peaks have slightly increased, approximately retaining their relative intensities. For the reasons stated above, the identification of the emissions at 1.4, 2, and 2.4 μm was not possible. The best estimate is that these bands originate from carbon-carbon bonds which emit between 1.1 and 2.7 μm. A further possibility is that iron containing species also participate in the emissions. Soot generated black body emission, if present, has been swamped out.

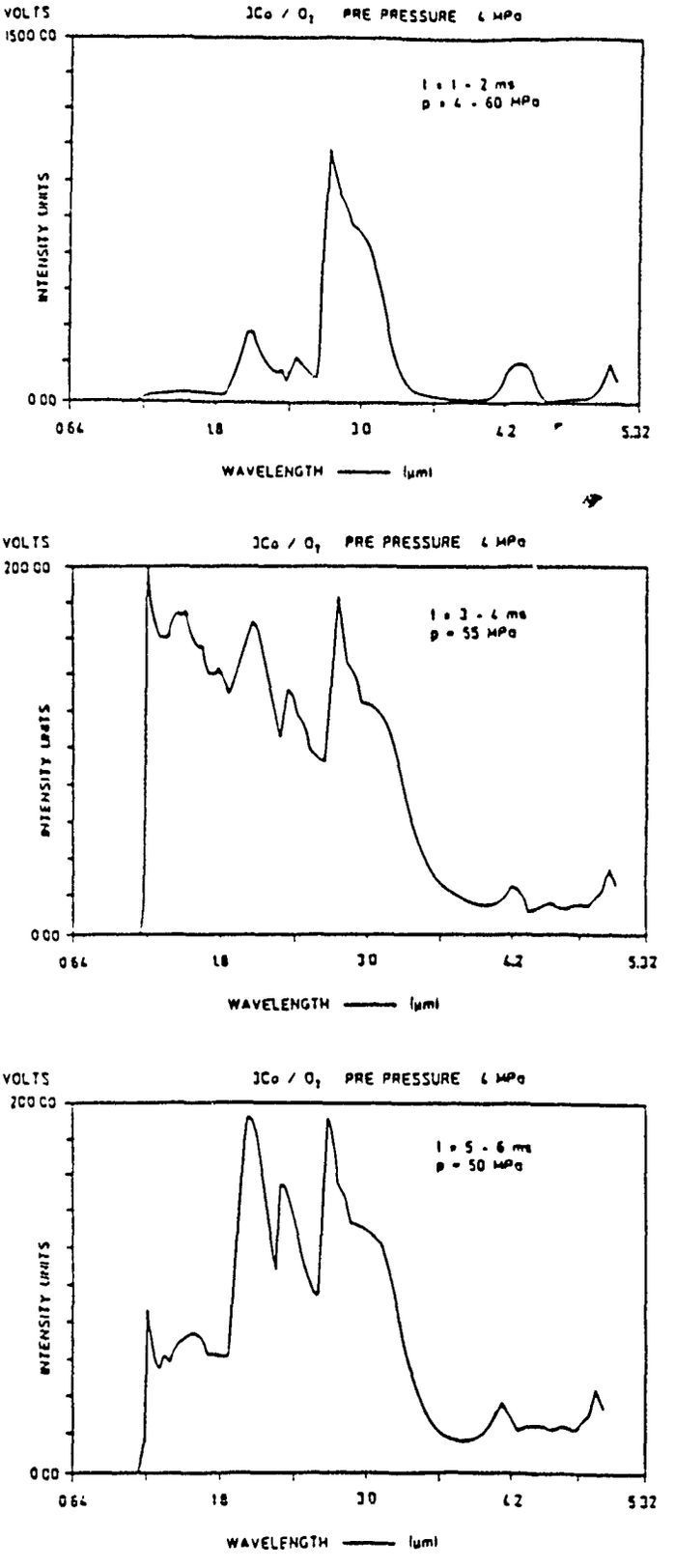

Fig. 16. Series of IR spectra from CO/O_2 combustion

No further measurements could be carried out, since the apparatus fell down accidentially and the diode arrays were damaged. No replacement was possible during the course of this work. It takes about 14 months to get the order processed through the channels, due to export licence restrictions in the USA. And so more detailed species concentration measurements await the repairment of the instrument.

7.6 Discussion

The potential of an infrared spectrometer with a spectral range of 1.4 to 5 μm and a time resolution of 1 ms per spectrum for analysing high pressure, instationary combustion reactions has been demonstrated for the simple cases of hydrogen/oxygen and carbon monoxide/oxygen reactions.

The initial results presented here, have shown that the major reaction species are resolvable with the multi-channel IR apparatus. However, identification of the emission bands at high pressures and temperatures is still limited. Further studies could unravel the fundamental combustion processes of H_2, CO, and CH containing gases in mode detail.

Improvement of the required spectral and temporal resolution of the spectrometer has been projected. Attainment of a temporal resolution of 1 μs per spectrum is feasible using straightforward the present state-of-the-art technology. Moreover, an extension of the spectral range from the visible to the 10 μm infrared region is envisaged. The improvement will be based upon modularized detector units with interchangeable submodules containing different detector arrays and it would afford an investment of about 200.000 $.

8. TEMPERATURE MEASUREMENTS

8.1 Overview

As mentioned previously, temperature distributions were measured using the a) temperature gauge technique, b) emission/absorption methods, and c) a fast thermocouple mounted in the gun tube wall. Complete profiles of T(t) are presented in the Section 10. Here the limitations of the methods used are described presenting sample results.

8.2 Emission or Temperature Gauge Technique

Two different types of emission gauges have been designed and applied for intrusive temperature measurements in the combustion gases of solid and liquid gun propellants [23]. The first high-pressure emission gauge design consists of a steel tube which contains on its axis a bundle of 25 individual optical fibers arranged in parallel (Figure 17). The bundle of optical fibers is glued into the steel tube with epoxy. The diameter of a single fiber is 0.1 mm, and the diameter of the bundle is 0.5 mm. The surface area of the optical fiber bundle is 0.19 mm^2, and its opening angle at the end surface or flow facing side is 25 degrees. To be able to screw the emission gauge into conventional pressure ports, both the diameter and the thread of the outer steel tube are adapted to the dimension of commercial pressure transducers, as, for example, to the dimensions of Kistler or PCB pressure gauges. The design with the bundle of 25 fibers was selected from a trial-and-error approach. The goal was to achieve an optimum transfer of radiant energy in a high-pressure environment. The design shown in Figure 17 withstands a maximum gas pressure of p = 400 MPa. The second type contains a specially designed IR transparent light pipe and serves to measure the contamination of the window surface by soot or other deposits [23].

The emission gauge or temperature gauge shown in Figure 17 measures, however, the brightness temperature of flow, $T_S(\lambda)$, which approaches the true gas temperature, T, only when the absorption of the flow is relatively high ($a > 0.7$), see Ref. 11. This is demonstrated in Figure 18 showing temperature histories (T vs t) measured simultaneously at locations M1 and M2 in the gas gun chamber using both the emission or temperature gauge and the modified

reversal methods. Obviously, the emission gauge indicates much lower temperatures than the reversal method, because the absorptance of the gas mixture (O_2 + 3 H_2 + 8 He) is of the order of a = 0.2 and thus $T_S(\lambda) < T$.

Better agreement was achieved when firing mixtures with higher particles concentrations (TiO_2 or soot). For concentrations of the order of 0.5 g/cm^3 $T_S(\lambda)$ approaches T.

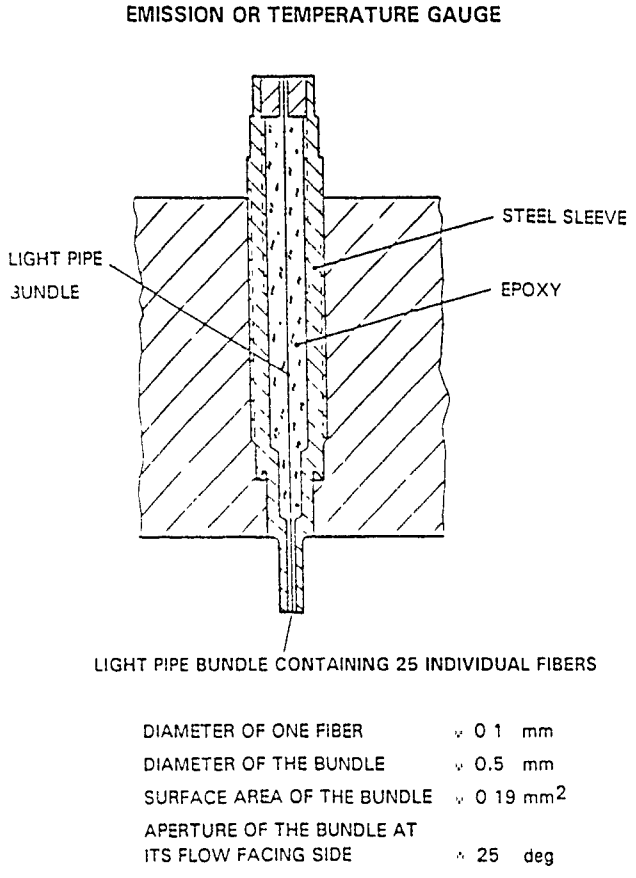

Fig. 17. Intrusive temperature gauge for probing optically thick flows [23]

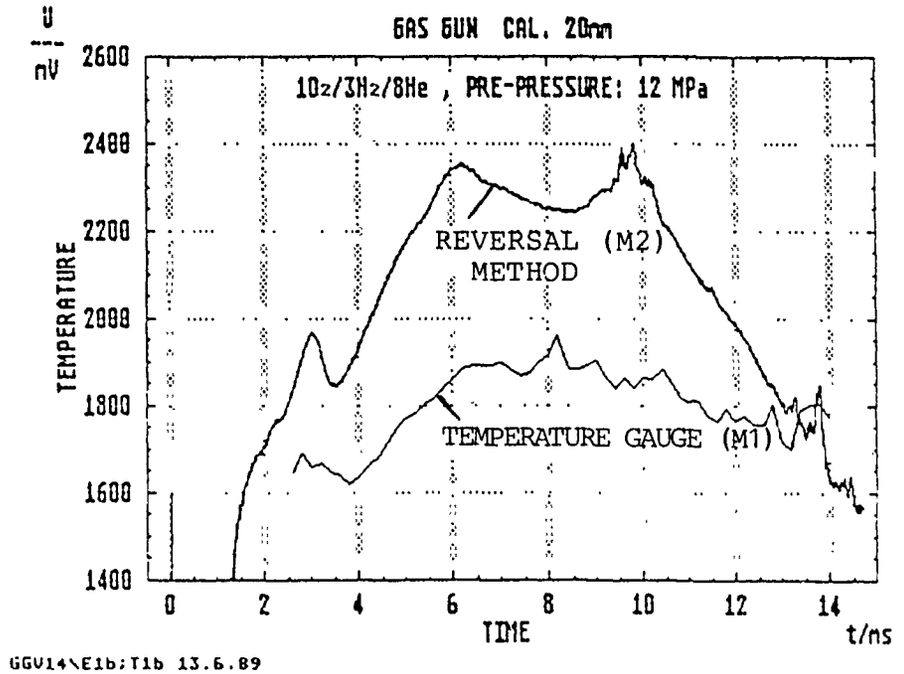

Fig. 18. Temperature vs time measured simultaneously at locations M1 and M2 by using the emission gauge technique and the reversal method (Gas mixture: O_2 + 3 H_2 + 8 He; prepressure: 12 MPa)

8.3 Modified Reversal Method

The reversal method is well known [11] and widely used. It determines T(t) from the emission L_λ and absorption a_λ measured along an optical path through the flow [11]. In transient flows, a modified reversal technique is applied which permits an approximate determination of the reversal point [11]. In this technique, the radiation flux with and without superimposed radiation of the background source is recorded photoelectrically, and the spectral radiances L_λ^2 and L_λ^3 are measured either simultaneously along parallel or vertical optical paths or alternately by chopping the beam of the backlight source, Figures 19 and 20. The spectral radiance of the comparison source L_λ^1 is determined before or after the flow occurs. Then, we obtain from the radiation equations [11],

$$\frac{L_\lambda^3}{L_\lambda^1 - L_\lambda^2} = \frac{L_\lambda^b(T)}{L_\lambda^b[T_S(\lambda)]} = e^{-(c_2/\lambda)[1/T - 1/T_S(\lambda)]} \quad . \tag{4}$$

where L_λ denotes the spectral radiance and L_λ^b the spectral radiance of a blackbody.

By taking the natural logarithm and regrouping, it follows that

$$\frac{1}{T} = \frac{1}{T_s(\lambda)} + \frac{\lambda}{C_2} \ln\left(\frac{L_\lambda^1 - L_\lambda^2}{L_\lambda^3} \right) . \qquad (5)$$

The spectral absorptance is given by the absorbed fraction of the incident beam, i.e.,

$$a_\lambda(T) = \left(1 - \frac{L_\lambda^2}{L_\lambda^1} \right) . \qquad (6)$$

The error of the modified reversal measurement is dependent upon the difference between T and $T_S(\lambda)$ and upon the emitter concentration expressed in terms of $a_\lambda(T)$:

$$\left| \frac{\Delta T}{T} \right| \sim \frac{[1/T - 1/T_s(\lambda)]^{1/2}}{a_\lambda(T)} . \qquad (7)$$

The error is small if the brightness temperature of the background source is well adjusted to the flame temperature and high emitter concentrations are present in the flow. The difficulties involved in the line reversal method are discussed in Reference [11].

The modified method with chopped reference beam emitting L_λ^1 is shown in Figure 20 together with the calibration setup and the typical signal recorded at the detector displaying L_λ^1, L_λ^2, and L_λ^3. The calibration is made by means of a tungsten ribbon lamp of known spectral emittance and temperature. In Figure 20 the temperature 1/T is related to the transmittance τ_λ, where τ_λ = 1-a_λ.

Sample results of emission/absorption measurement through the gas gun tube flow at location M5 are shown in Figure 21. An interesting feature is revealed in the emission/absorption measurement at a), b), and c). After the projectile has passed the window located at position M5, at time t = 7.0 ms the absorption falls suddenly down to a value of 0.4 at t = 7.3 ms only to rise once more to 0.78 at time t = 7.8 ms (Figure 21a). The absorption history recorded (Fig. 21b) behaves in the opposite manner, i.e., it rises in the time interval $7 \leq t \leq 7.4$ ms, and then it decreases until t = 8 ms. The explanation is given in the final section of this report.

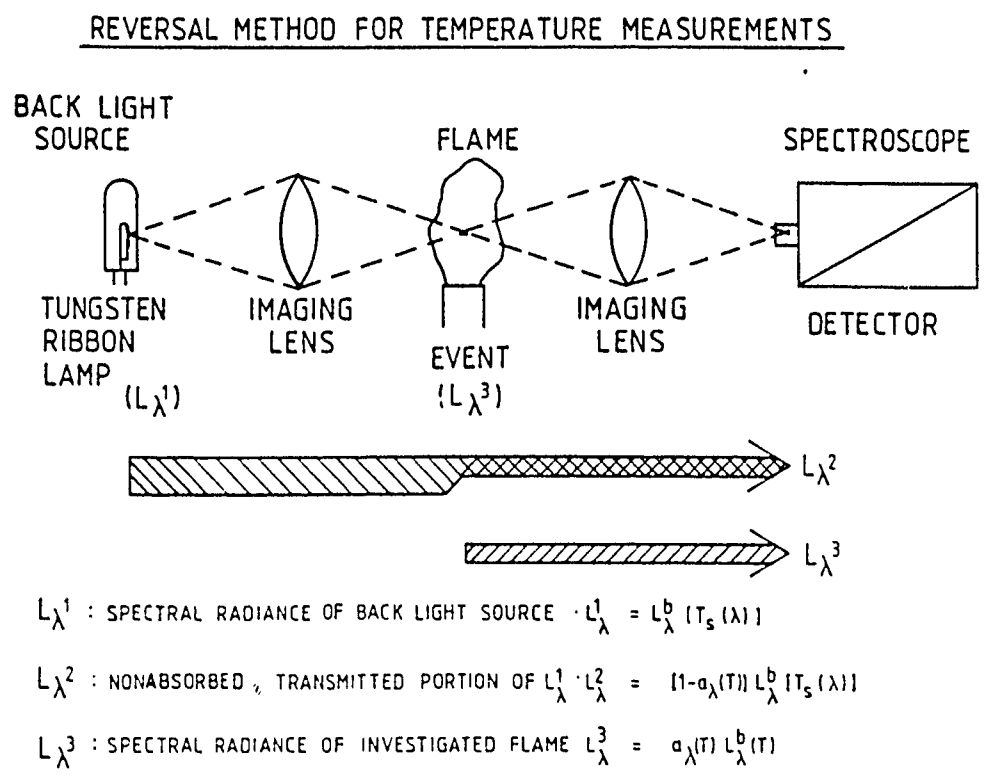

Fig. 19. Schematic of reversal method

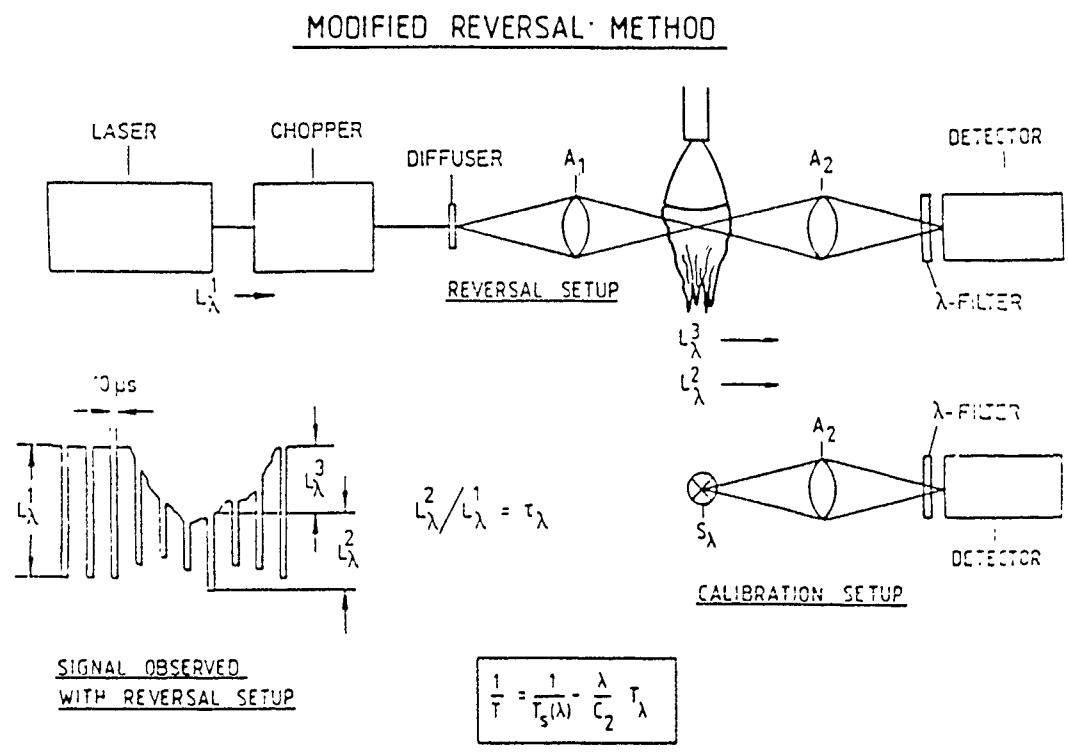

Fig. 20. Schematic of modified reversal method

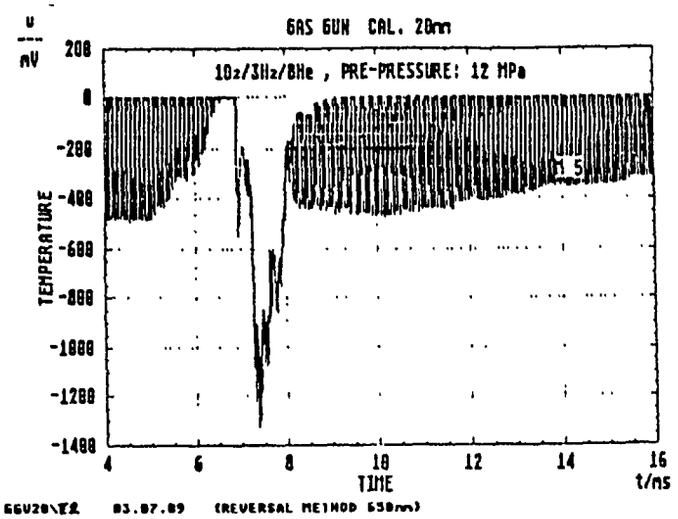

a) Emission/absorption versus time

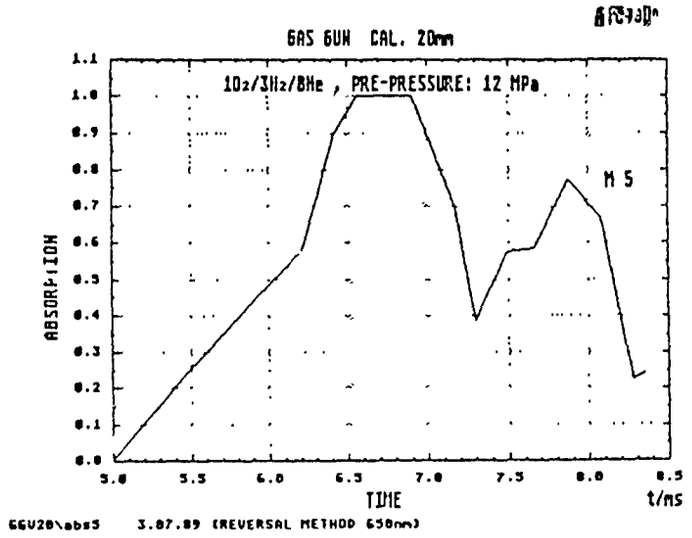

b) Absorption versus time

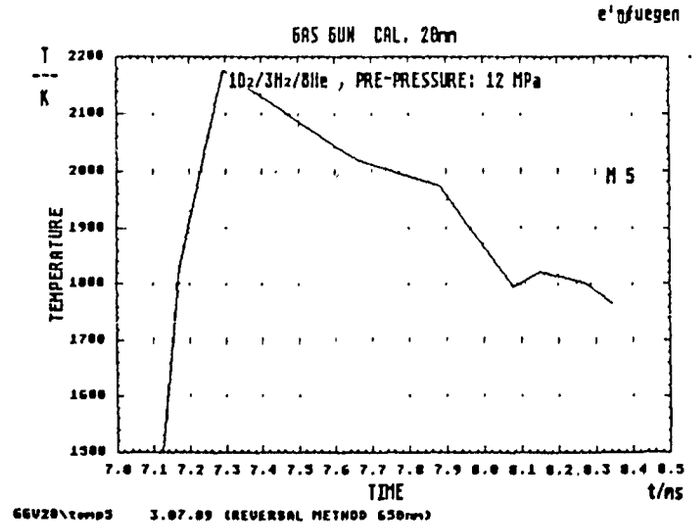

c) Temperature versus time

Fig. 21. Results obtained by applying the reversal method at location M5 (Gas mixture: (O_2 + 3 H_2 + 8 He); prepressure: 12 MPa)

A temperature with a maximum of T = 2180 K was measured in this gun discharge (Fig. 21c).

The above example taken with the gas mixture O_2/3 H_2/8 He demonstrates that temperature recordings are possible. A major drawback of the emission/absorption or modified reversal methods is, however, that only average values across the line of sight are obtained. A spatial or radial resolution of gas temperature would require Abel inversion methods or even the "onion peeling" method of optical tomography. Therefore, in parallel to the simulation experiments some work has been devoted to study these novel methods. The successfull application of emission/absorption spectroscopy with spatial resolution would be a breakthrough in interior ballistic research, because is should yield information on concentration profiles (absorption) and radial temperature distribution (emission/-absorption). Studies are under way using at first defined (stationary) gas flames (Hefner's candle) and then specially designed gas gun window setup. First results were obtained with Hefner's candle flames demonstrating the superiority of optical tomography to the Abel inversion method. This is the subject of a forthcoming report.

9. LASER DOPPLER VELOCIMETER

9.1 Apparatus

The apparatus used for measuring gas or particle velocity within the gun tube flow is a laser Doppler device based on a Michelson interferometer (Diehl/ISL method) which is described in detail in [27]. Basically, it measures the back or forward scattered light from flow-borne particles, either present as a natural component (dust) or seeded to the flow. Here, the flow is seeded with 1 g of TiO particles whose diameter is of the order of 0.1 - 0.3 μm. Therefore, the incident laser light is scattered by the moving particles which, due to their negligible lag, represent the flow velocity. The light scattered at the flow-borne particles is Doppler-shifted relative to the incident beam. A 45° polarizer splits the incoming signal equally into its vertical and horizontal components. A path difference Δl is induced as the beam passes the Michelson interferometer and a phase shifting pockels cell. The ratio $\Delta l/l$ is then kept constant via electronic

adjustment of the phase difference and the corresponding supply voltage is translated into a signal that is proportional to the gas (particle) velocity [27]. Figure 22 shows a color photograph of the Diehl/ISL velocimeter. Figure 23 presents a schematic of the measurement method. With this method there is, however, a substantial sensitivity of the signal to back-scattering of light from nearby walls and the rear of the projectile, which may degrade the velocity measurement [11,27].

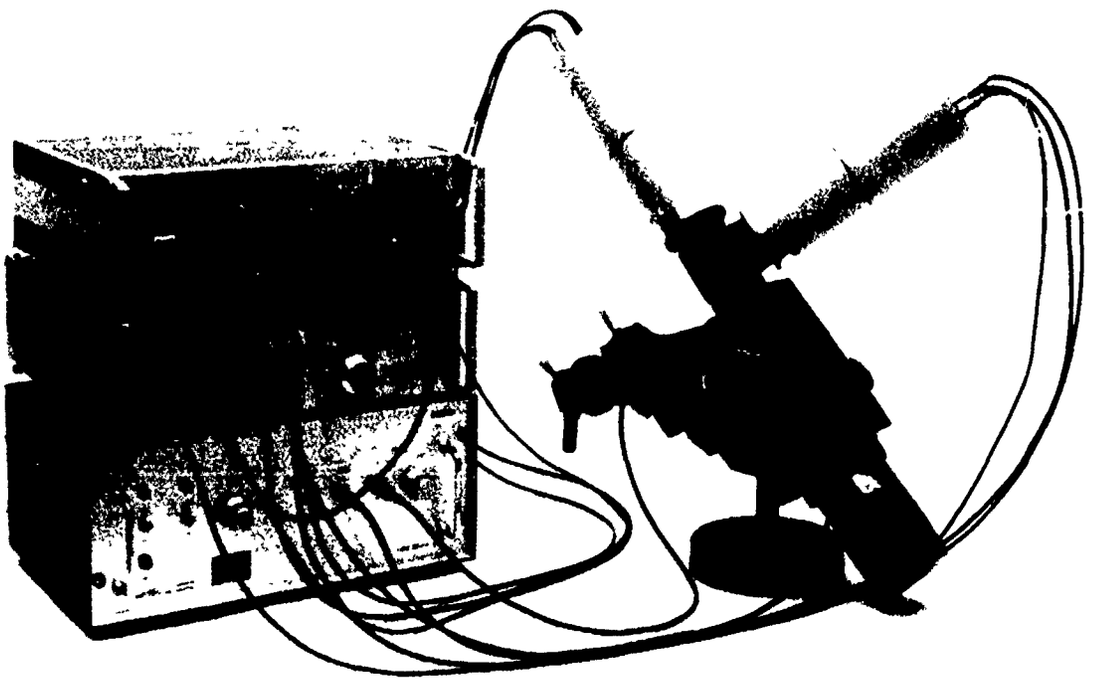

Fig. 22. Color photograph of the Diehl/ISL laser Doppler velocimeter

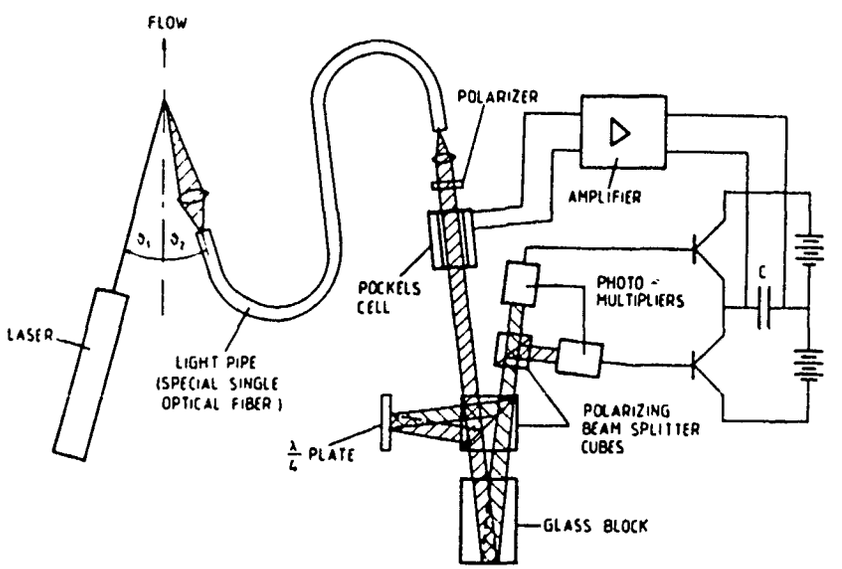

Fig. 23. Diehl/ISL laser Doppler velocimeter devised by Smeets [27] at the Franco-German Research Institute (ISL), Saint-Louis, France

9.2 Optical Windows

Initially, the scattered radiation from the moving particles was measured at 60° forward scattering angle with the entrance beam passing through a large sapphire window at a 30° angle to the barrel axis and the exit beam passing through a small 10 mm diameter window perpendicular to the barrel wall. There was no "light trap" for the unused intensity portion of the incident beam, see Figure 24. As it turned out in extensive testing, this optical setup displayed several critical disadvantages. Due to the considerable diameter (12 to 20 mm) the mechanical stability of the window against shock waves running behind the projectile was poor. Data acquisition was invariably interrupted by cracking of the window, an event that happened frequently. Further, the absence of a "light trap" led to high levels of scattered light from the walls, which was detected by the velocimeter and incorporated into the signal as a zero velocity component and thus degraded the velocity measurement. In addition, further tests showed that the beam geometry was strongly affected by the shot engendered low frequency contortions of the barrel even through their magnitude was rather low. Axial, vertical, and horizontal displacement of the barrel was encountered during a typical firing. In order to keep the beam geometry constant throughout the experiment, fiber optics were employed. Further, the optical window setup was improved by developing a new mounting principle which uses smaller window diameters and, significantly, an opening ("light trap") for the main beam to pass through and exit the gun tube thus minimizing stray light to overlap the velocity signal, see Figure 25.

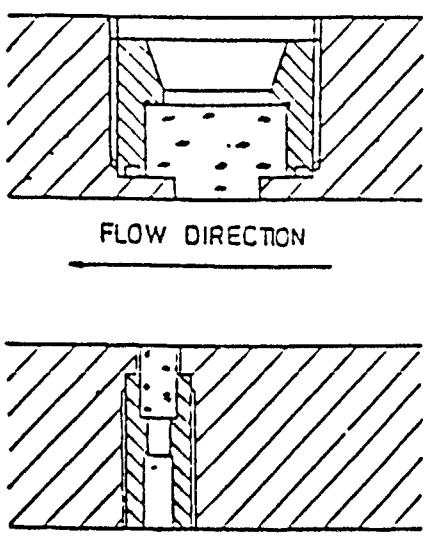

Fig. 24. Schematic of gun tube optical window arrangement and for laser Doppler velocimetry

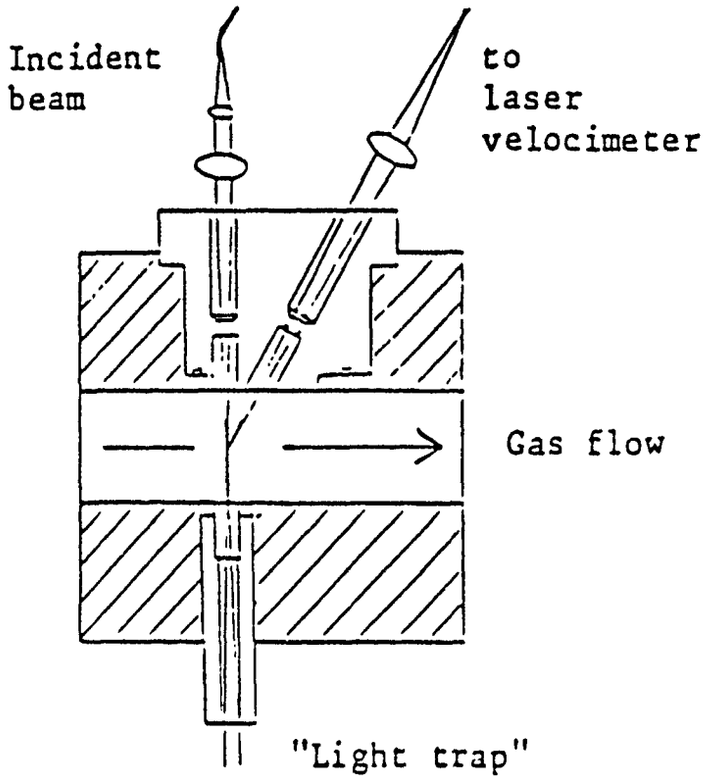

Fig. 25. Experimental window setup for velocity measurements using a "light trap"

The color photograph in Figure 26 shows the window setup together with the calibration device.

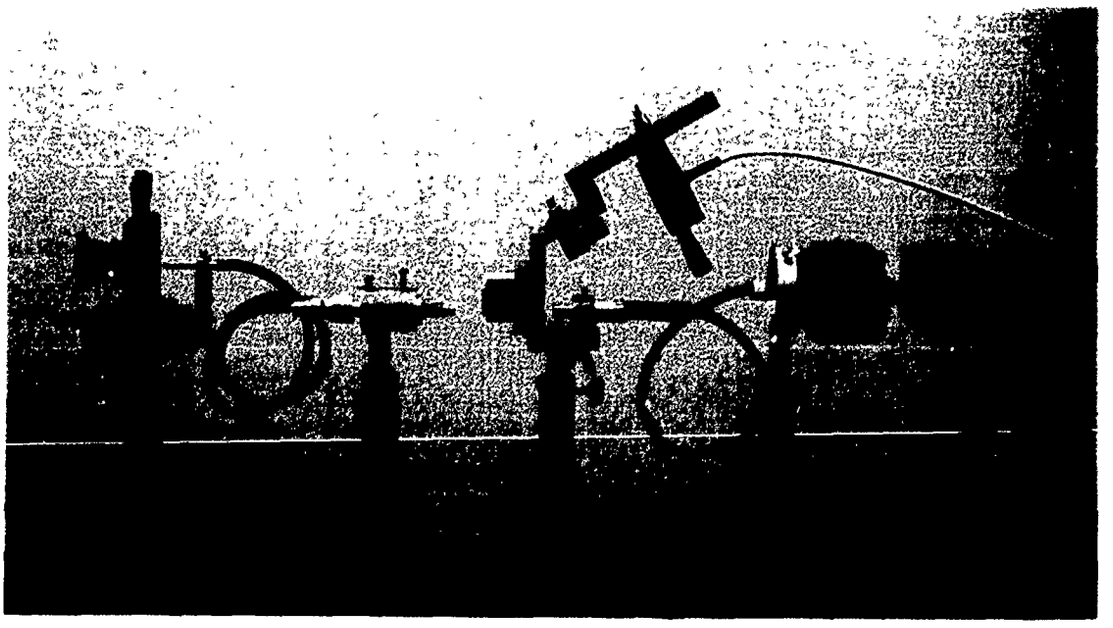

Fig. 26. Optical window and calibration setup

The optical window setup is calibrated by means of a laser or tungsten ribbon lamp and a photomultiplier as detector to measure the absorptance of the device. The setup mounted at the port M4 in the middle of the gas gun is shown in the photograph of Figure 27.

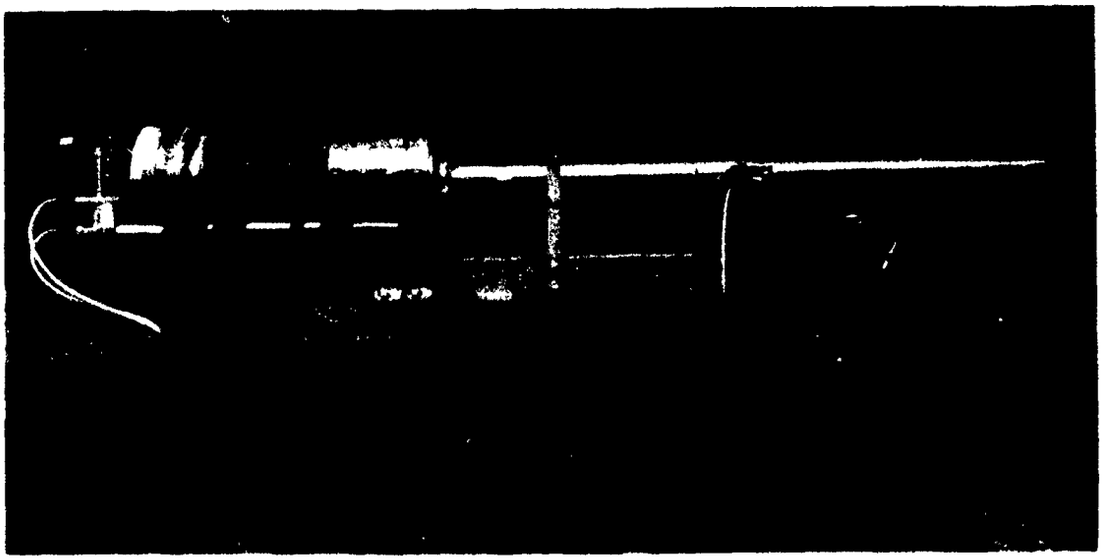

Fig. 27. Velocity measurement at location M4 of the 20-mm caliber gas gun tube

The novel setup permits measurements of back scattered and forward scattered light. In the beam configuration shown in Figure 24 the light is back scattered towards the velocimeter. It is also possible albeit less convenient to operate the window in the forward scattering mode, Figure 25. Since it has turned out in the first two tests that the back scattered light intensity is insufficient for operation of the velocimeter, the testing of the experimental setup for the forward scattering mode was used.

9.3 Radial Velocity Profiles

The radial gas velocity profiles were measured in the six lateral flow points y = 0 (flow axis), 5 mm, 7.5 mm, 8.5 mm, 9 mm, and 9.5 mm (0.5 mm distance from window), respectively (Figure 28). First results taken at location M5 in the gas gun tube when firing the "standard" gas mixture (O_2 + 3 H_2 + 8 He) at prepressures of p_l = 12 MPa are given in the following Figures 29 to 34. Here time zero (t = 0) is the time of projectile passage at the measurement location M5.

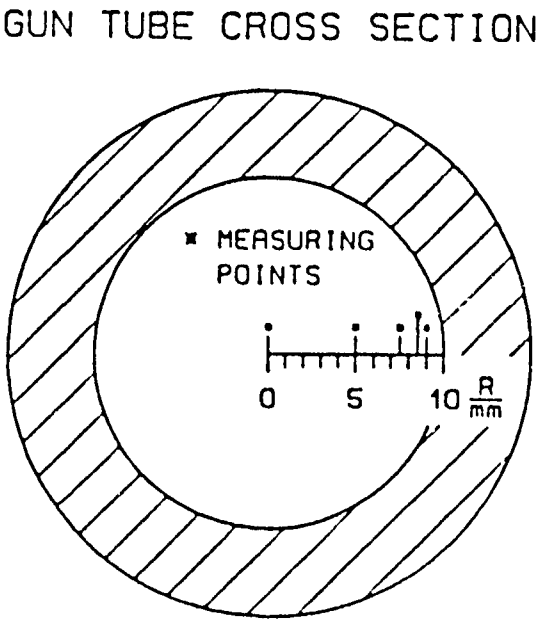

Fig. 28. Measuring points across the gun tube flow

Figure 29 shows the pressure curves recorded at locations M1 (gun chamber) and M6 (muzzle). The velocity curves for lateral positions R = 0, 5 mm, 7.5 mm, and 8.5 mm together with the pressure histories are shown in Figures 31 to 33. In the lateral flow layer, R = 5 mm, the velocity shows an increase after projectile passage and a further increase for times $t \geq 9$ ms. The launch of the projectile occurs at about 8.3 ms. In the outer gun tube flow layers (R = 7.5 mm and R = 8.5 mm) the velocity decreases for $t > 8$ ms (Figure 32) or shows a slight increase for $t > 9$ ms associated with layer pressure disturbances because of turbulence in the flow layers near the wall (Figure 33). The pressure in these single firings is approximately the same. Figure 34 shows two radial velocity profiles derived from these velocity versus time curves. They show the expected definite decrease towards the gun tube wall.

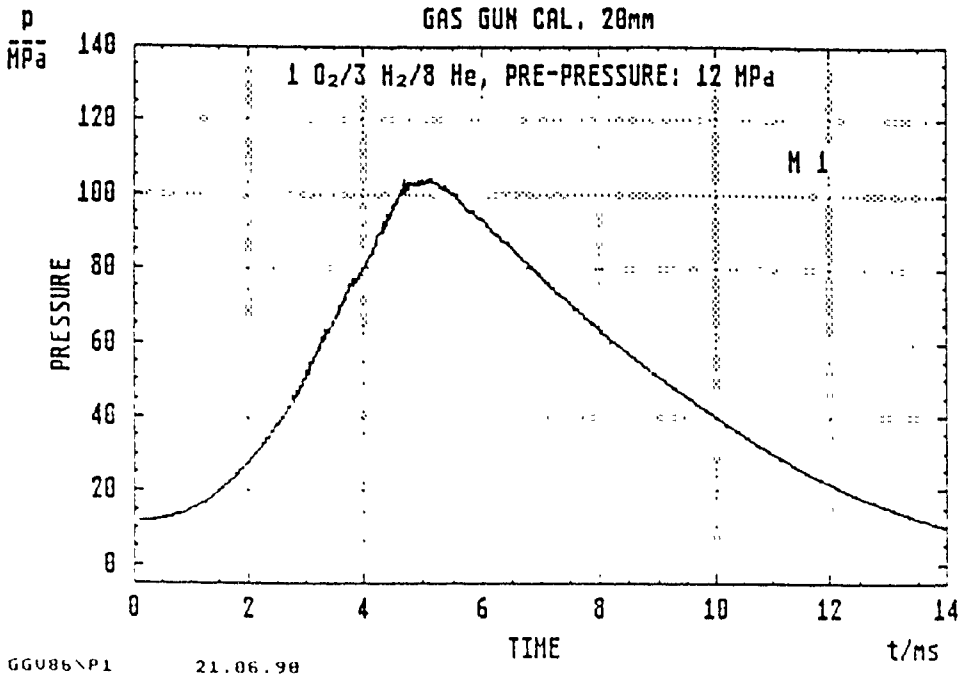

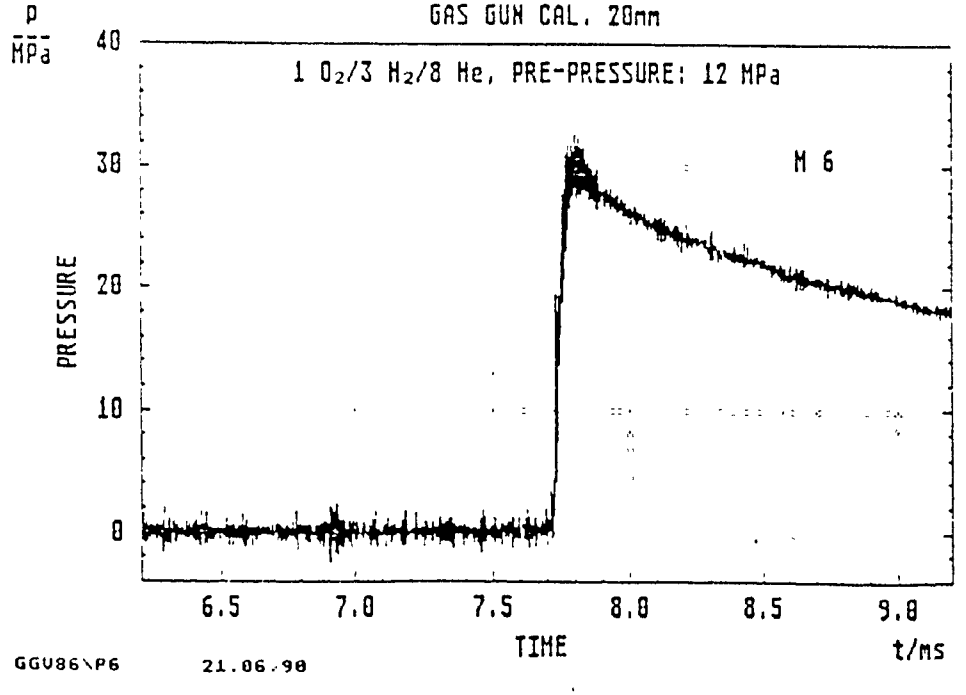

Fig. 29. Pressure vs time at M1 and M6
(Gas mixture: O_2 + 3 H_2 + 8 He; prepressure: 12 MPa)

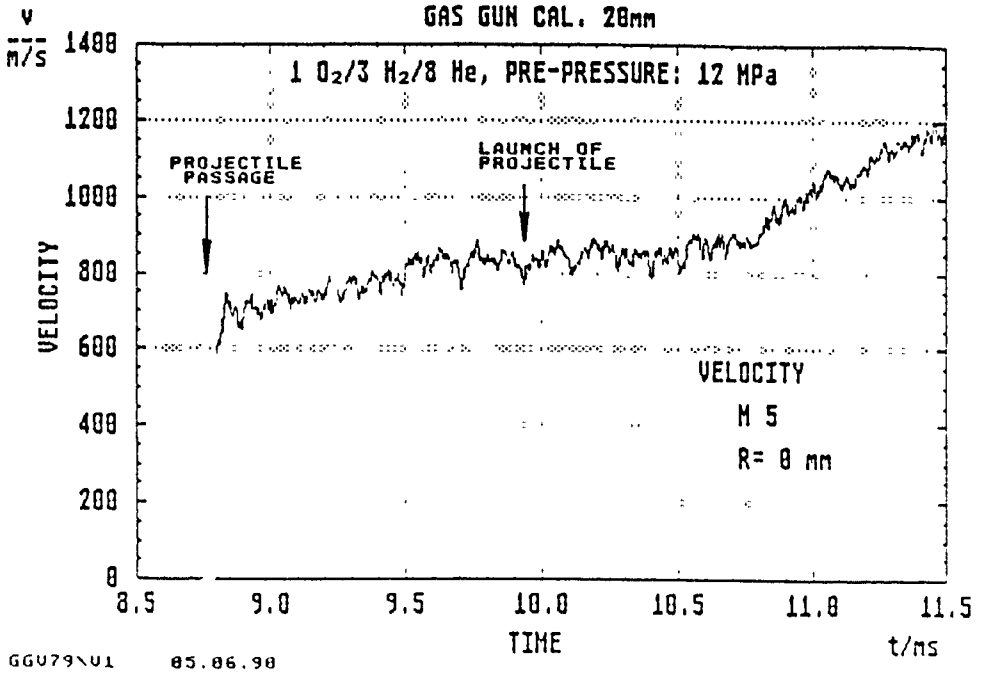

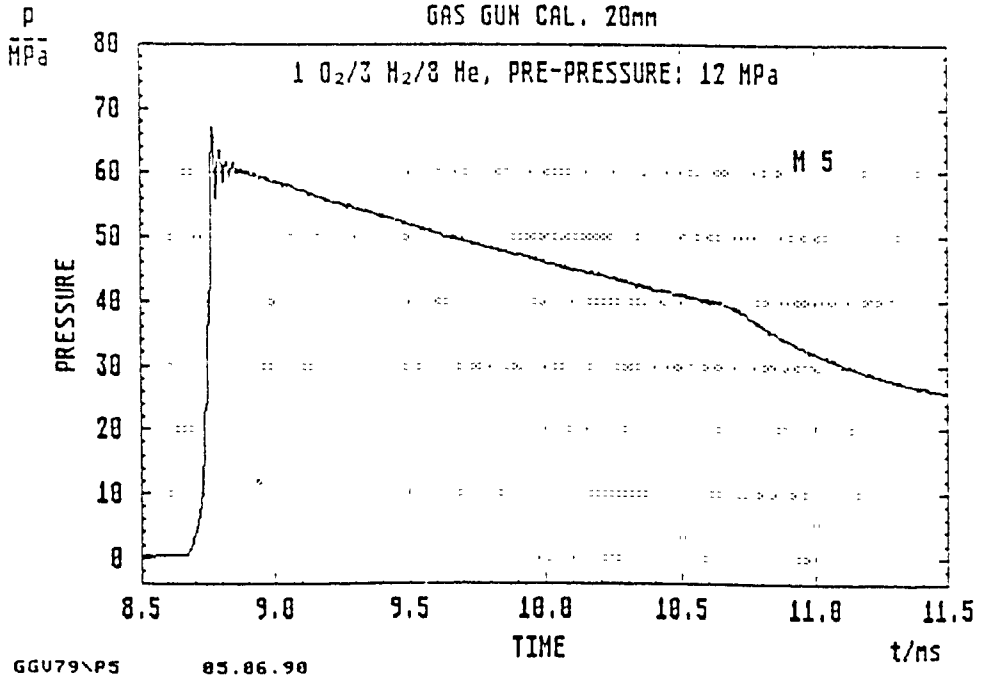

Fig. 30. Velocity at R = 0 (flow axis)and pressure vs time at location M5 (Gas mixture: O_2 + 3 H_2 + 8 He; prepressure: 12 MPa)

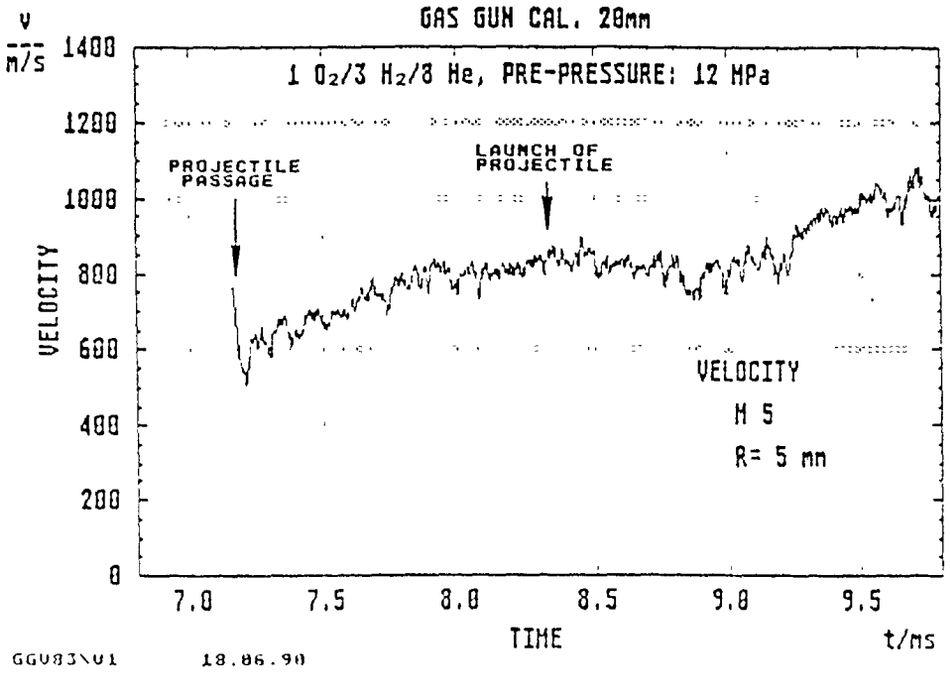

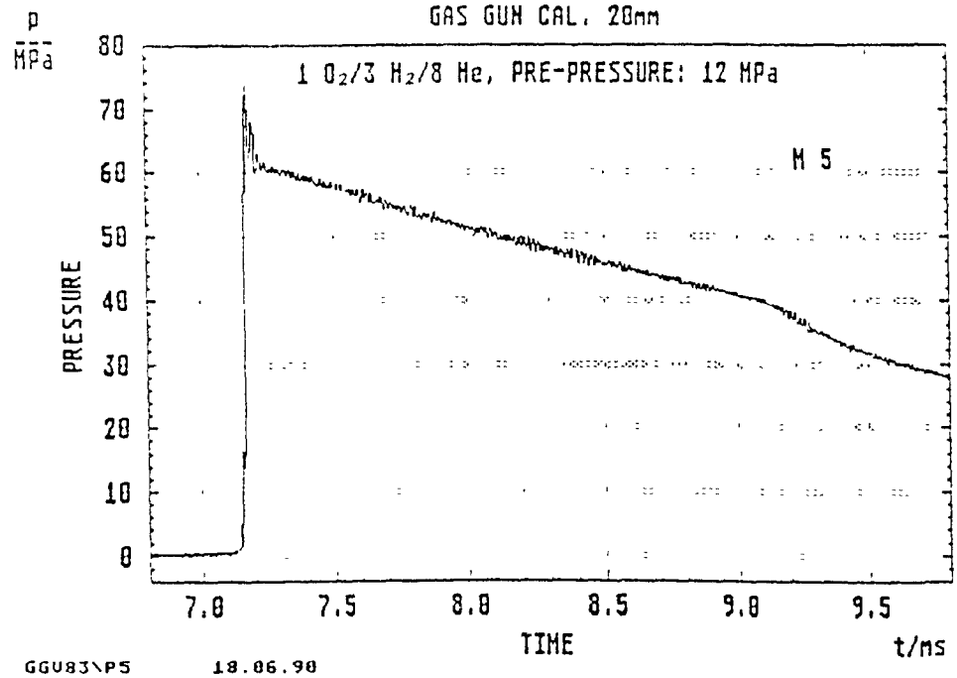

Fig. 31. Velocity at R = 5 mm and pressure at M5
(Gas mixture: O_2 + 3 H_2 + 8 He; prepressure: 12 MPa)

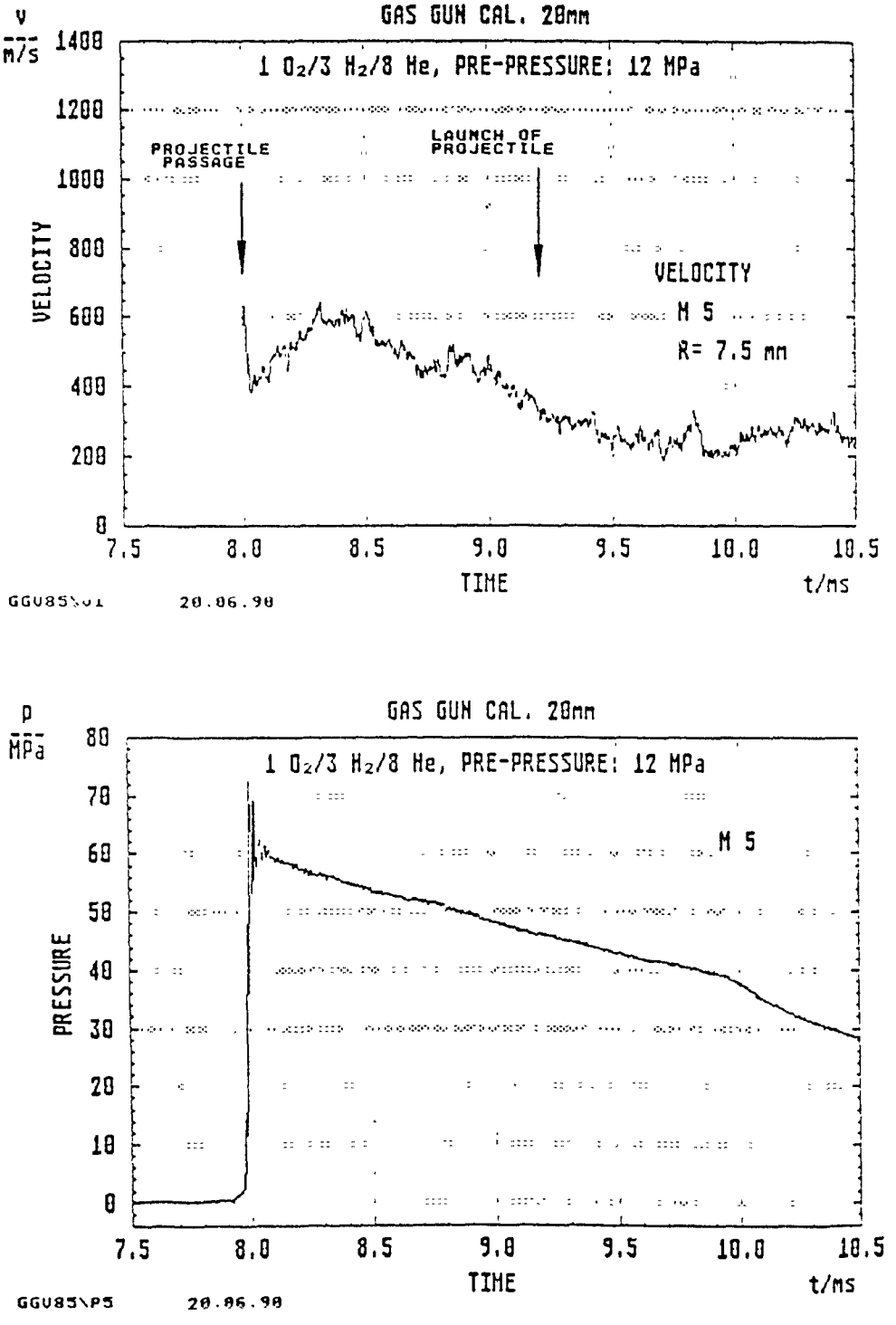

Fig. 32. Velocity at R = 7.5 mm and pressure at M5
(Gas mixture: O_2 + 3 H_2 + 8 He; prepressure: 12 MPa)

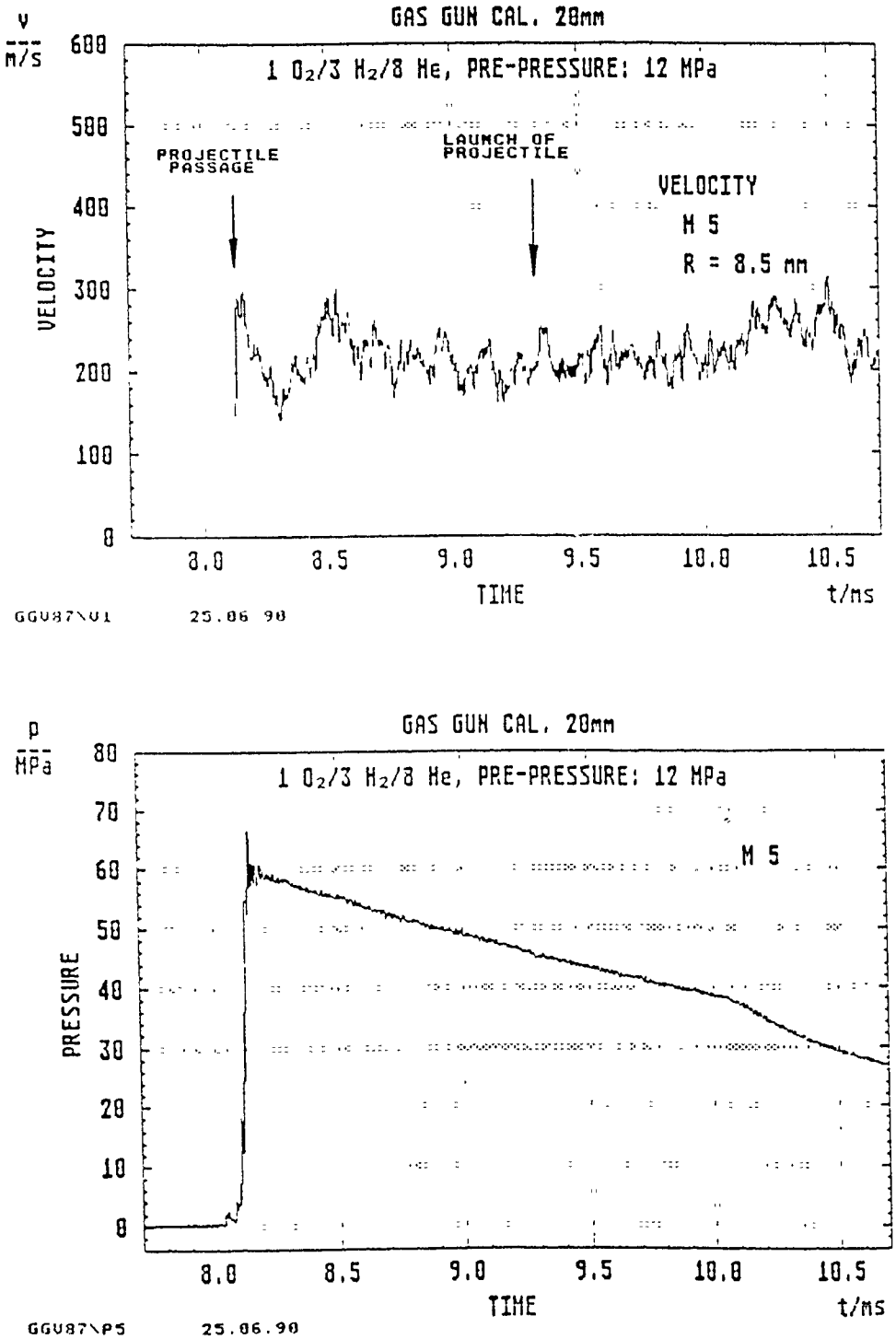

Fig. 33. Velocity at R = 8.5 mm and pressure at M5
(Gas mixture: O_2 + 3 H_2 + 8 He; prepressure: 12 MPa)

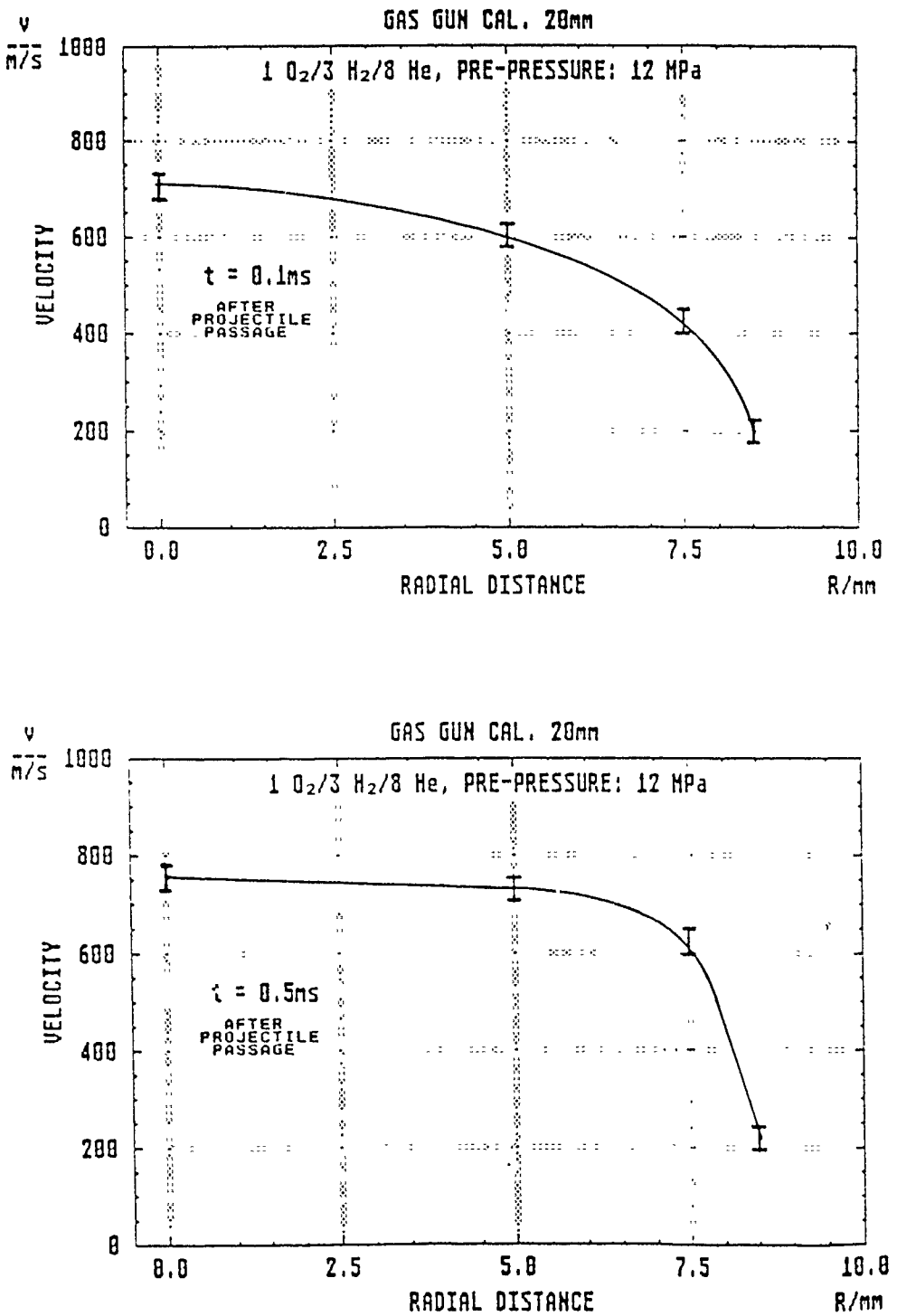

Fig. 34. Radial velocity profiles at times t = 0.1 ms and 0.5 ms after projectile passage

10. THERMOCOUPLE MEASUREMENTS

10.1 Description

A fast response (1 μs) surface thermocouple has been fitted to the bore surface at location M5A, which is about 200 mm from M5 towards the breech. This type of thermocouple is described in [28]. It is of 5 mm diameter and mounted flush with the bore surface.

10.2 Signal Recording

The signal is amplified using a gain of about 100 and recorded by the transient recorder. The measured gas temperature at the gas/wall interface is displayed in Figure 35. The gas mixture was (O_2 + 3 H_2 + 8 He) and the prepressure 12 MPa.

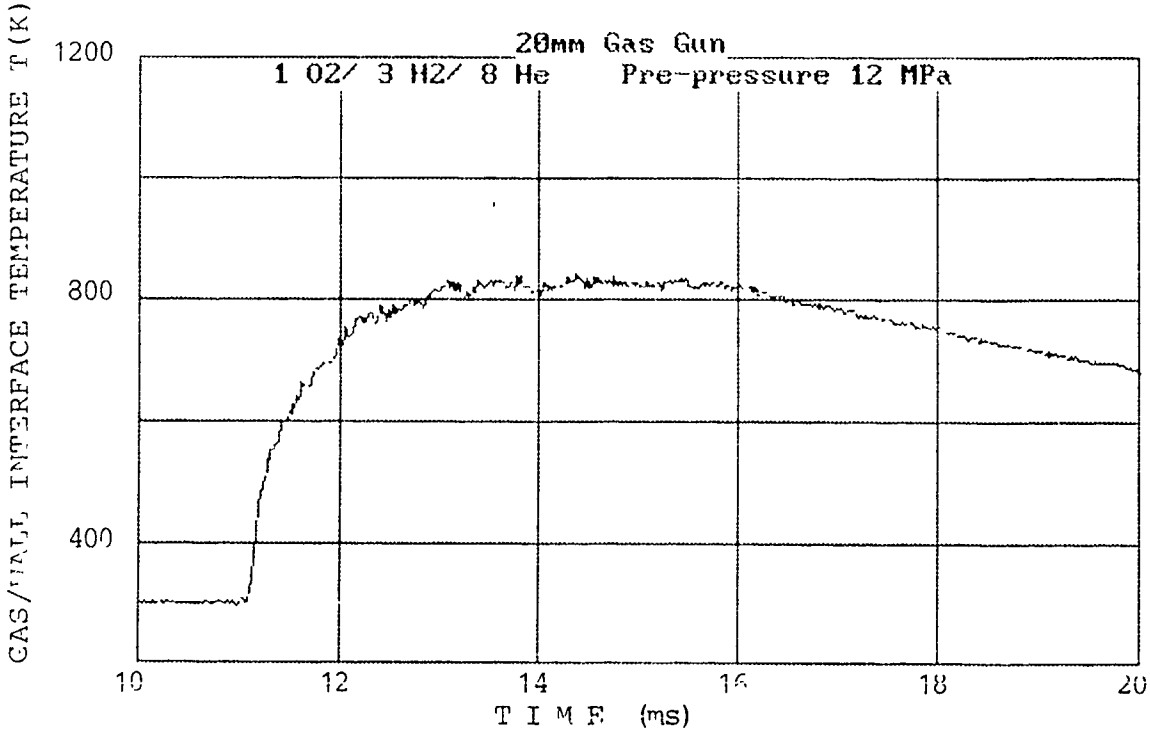

Fig. 35. Gas/wall interface temperature vs time at location M5A (Gas mixture: O_2 + 3 H_2 + 8 He; prepressure: 12 MPa)

The thermocouple temperature rises from an initial value of 298 K to a maximum value of about 840 K. The temperature starts to rise at 11 ms and reaches its maximum at about 14 ms. This signal may be processed to reveal the interface heat flux and interface heat transfer by using a numerical method described, for example, in reference 29. The interface heat flux is shown in Figure 36 and has a maximum value of about 200 MW/m^2, as the projectile passes the thermocouple, and it falls to about 60 MW/m^2 at projectile exit.

10.3 Heat Flux

The heat flux is a "noisy" curve because it is the differential of the temperature (Fourier's Law) and differentiation usually increases the signal noise level. It may be, however, that these fluctuations are real because the thermocouple's response time is much shorter than the oscillation period of the noise. These oscillations are most likely caused by boundary layer turbulence. The noise level is quite low before the projectile passes the thermocouple, is very high when heat flux is high and attenuates as the heat flux declines.

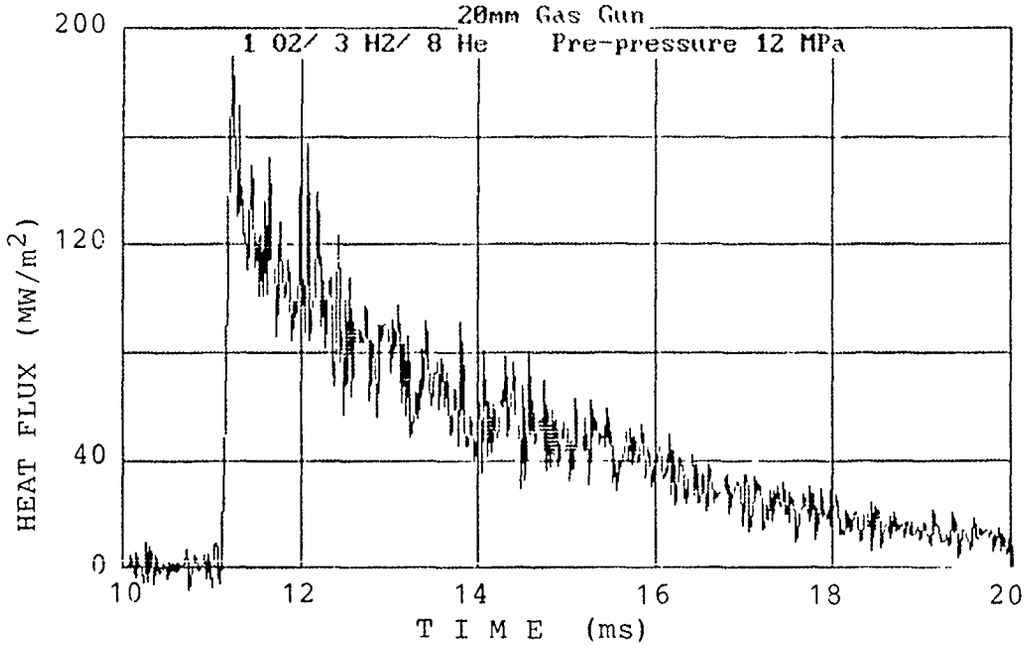

Fig. 36. Heat flux vs time
(Gas mixture: O_2 + 3 H_2 + 8 He; prepressure: 12 MPa)

10.4 Interface Heat Transfer

Integration of the interface heat flux with respect to time gives the interface heat transfer, Figure 37. This curve, being the result of an integration process, is smooth and relatively noise free. Rather less than 500 kJ/m^2 is transferred from the gas to the barrel at the thermocouple. In these calculations the thermal conductivity of the thermocouple is taken to be 24 W/m^{2}K and diffusivity is 7.3 x 10^{-6} m^2/s.

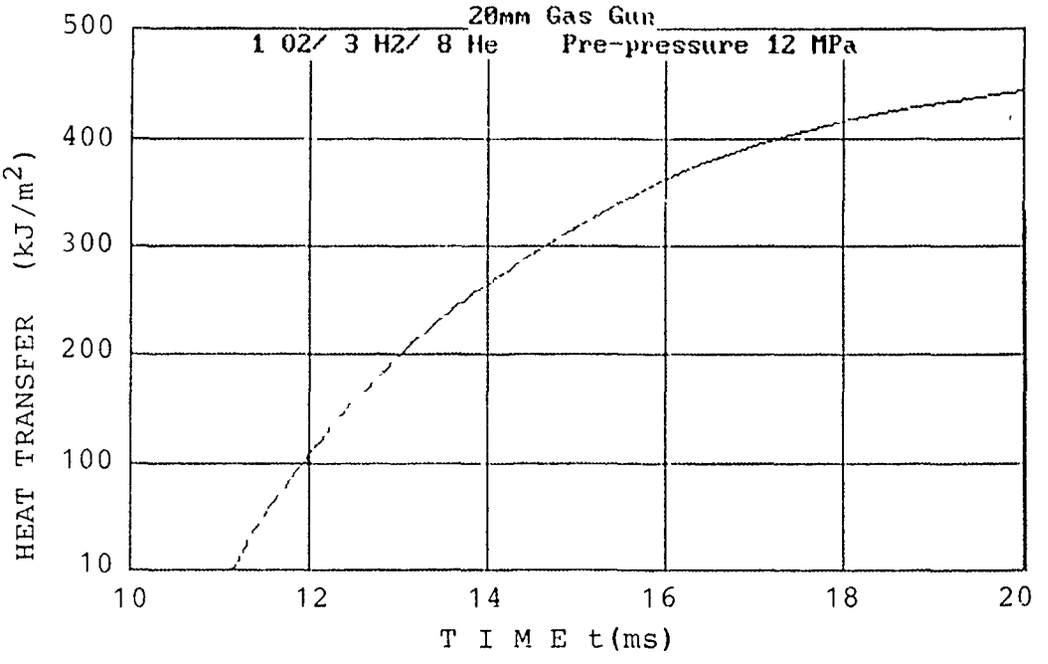

Fig. 37. Heat transfer vs time
(Gas mixture: O_2 + 3 H_2 + 8 He; prepressure: 12 MPa)

11. RADIAL TEMPERATURE AND VELOCITY PROFILES

11.1 Overview

Radial temperature and velocity profiles were measured with three different gas compositions. One composition was the "standard" gas mixture. The other two contained CO.

11.2 Recorded Data for the Gas Mixture (O_2 + 3 H_2 + 8 He)

Pressure recordings show that the location M5 is uncovered by the projectile at 11.5 ms; projectile exit is at 13.5 ms, see Figures 38 and 39.

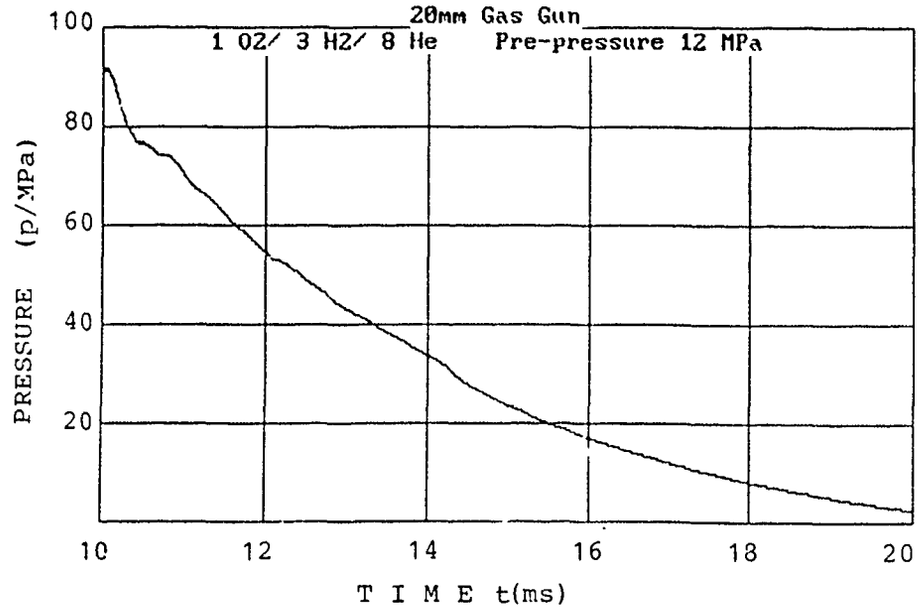

Fig. 38. Pressure vs time at location M4
(Gas mixture: O_2 + 3 H_2 + 8 He; prepressure: 12 MPa)

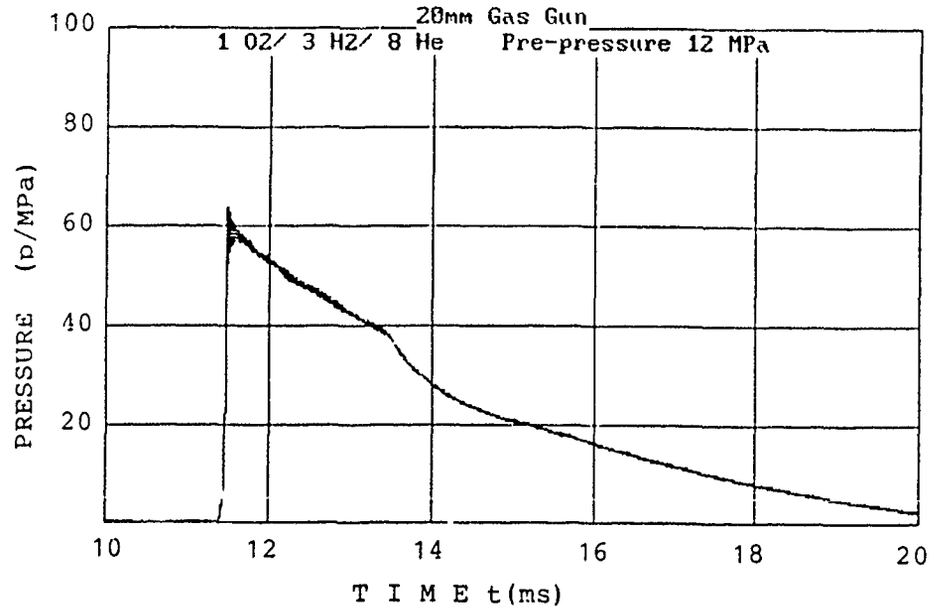

Fig. 39. Pressure vs time at location M5
(Gas mixture: O_2 + 3 H_2 + 8 He; prepressure: 12 MPa)

The radiation signal, Figure 40, is of the usual type and application of the approximate reversal method gives the average gas temperature, Figure 41. This gas temperature falls from about 1900 K immediately behind the projectile (11.5 ms) to about 1800 K at 12.3 ms when the projectile has travelled about 400 mm from the window. Such cool regions may be formed when gases expand (hot regions form when gases are compressed) and they have been measured and computed, in a simple reciprocating mechanism [29]. Low levels of heat transfer between the gas and the wall, i.e., low Nusselt numbers, have also been measured in guns immediately behind the shot [28], and this strongly suggests that the theoretical understanding of conditions behind the projectile are not correct. The usual ballistic codes do not reproduce this behavior.

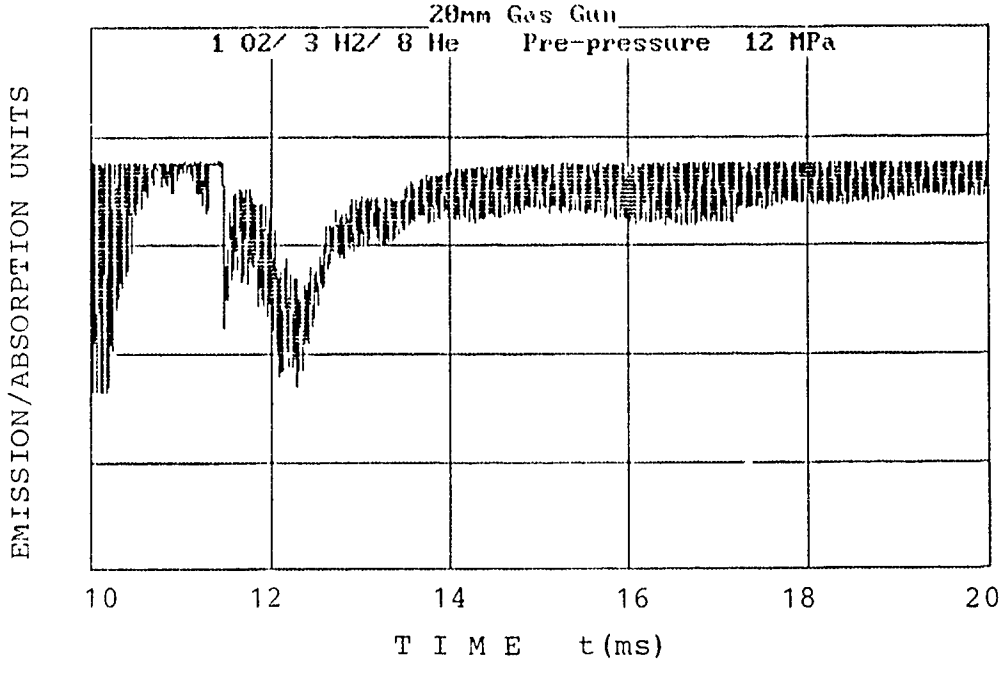

Fig. 40. Emission vs time at location M5
(Gas mixture: O_2 + 3 H_2 + 8 He; prepressure: 12 MPa)

To give some idea of the radial distribution of the data and the effect of the thermal boundary layer, Figures 42, 43 and 44 are prepared. This is done by assuming that the temperature distribution is similar to the velocity distribution; i.e., Reynold's analogy is valid and Prandtl number is unity. It is also assumed that the average gas temperature, Figure 41, is related to the local gas temperature at radius r by:

$$\bar{T}_a = \left[\frac{1}{R} \int_0^R T_a^n \, dr \right]^{1/n} . \qquad (8)$$

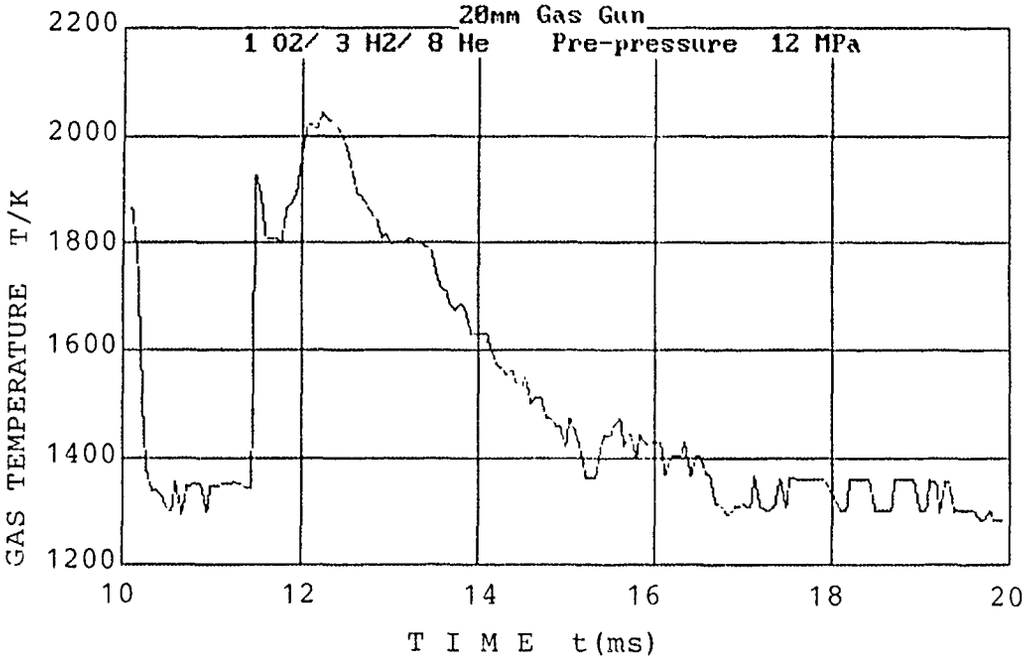

Fig. 41. Gas temperature vs time at location M5
(Gas mixture: O_2 + 3 H_2 + 8 He; prepressure: 12 MPa)

The arithmetic mean is given by n = 1, the root-mean-square by n = 2; in this analysis n = 4 is used. T_a is the temperature at any point between 0 and R.

Figures 42, 43, and 44 suggest that some care is needed in the interpretation of gas temperature and so it is desirable to measure the temperature distribution in the gas using, for example, the Abel inversion method.

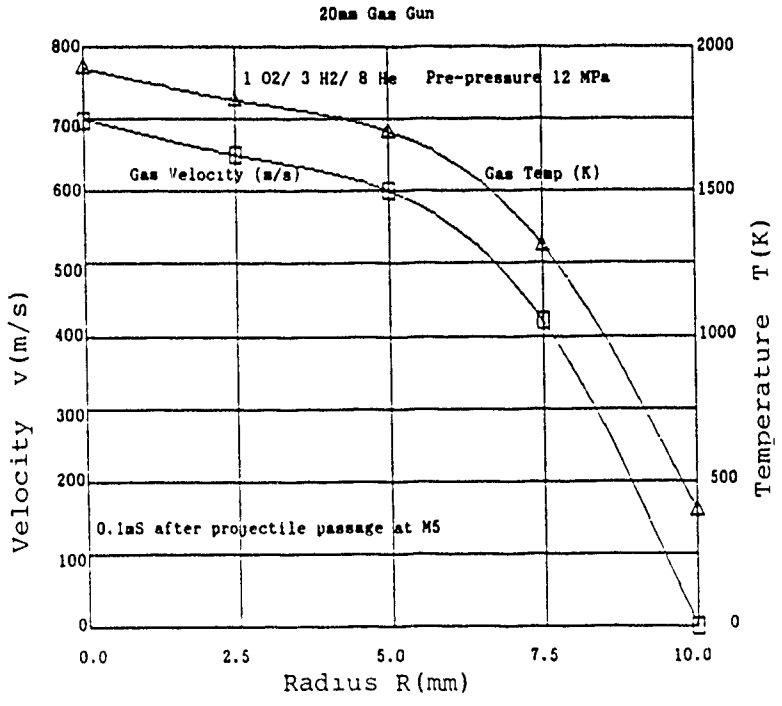

Fig. 42. Radial velocity and temperature profiles at M5 between gun tube flow axis (R = 0) and wall (R = 10 mm) at time t = 0.1 ms after the projectile passes M5
(Gas mixture: O_2 + 3 H_2 + 8 He; prepressure: 12 MPa)

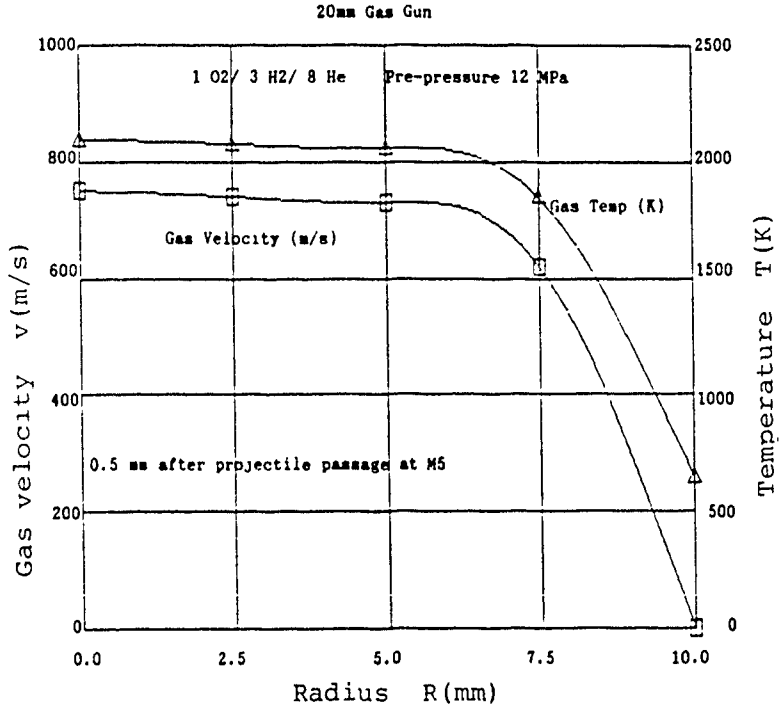

Fig. 43. Radial velocity and temperature profiles between gun tube flow axis (R = 0) and wall (R = 10 mm) at time t = 0.5 ms after the projectile passes M5
(Gas mixture: O_2 + 3 H_2 + 8 He; prepressure: 12 MPa)

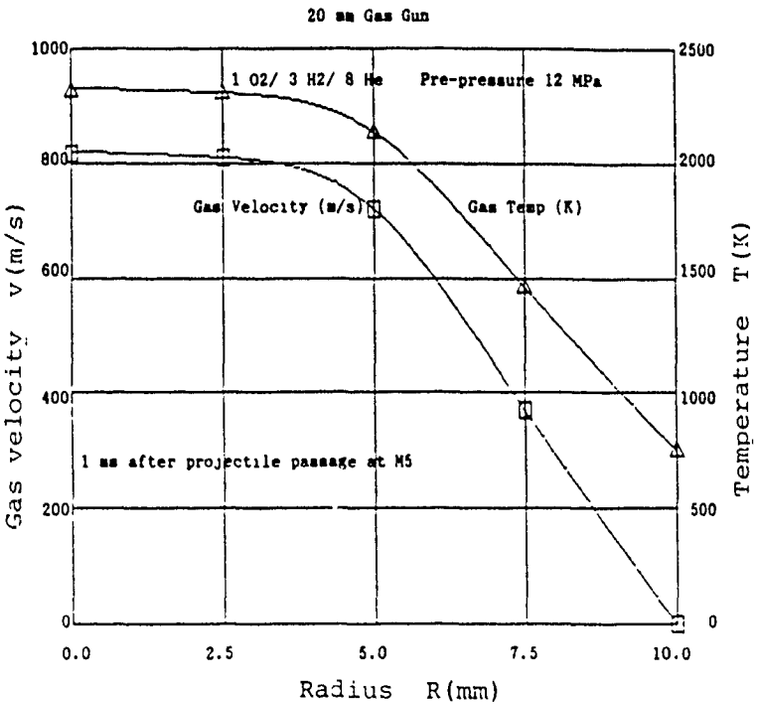

Fig. 44. Radial velocity and temperature profiles between gun tube flow axis (R = 0) and wall (R = 10 mm) at time t = 1.0 ms after the projectile passes M5
(Gas mixture: O_2 + 3 H_2 + 8 He; prepressure: 12 MPa)

A repeat of this trial, Figures 45 to 51 gives similar results. In particular, the gas temperature, Figure 47, again shows a low temperature region just behind the projectile. Gas temperatures, however, are somewhat higher than in the previous test. This higher gas temperature is also detected by the surface thermocouple, Figure 48, which recorded a temperature about 100 K higher than the previous test. In the repeated trial an alternative design of surface thermocouple was provided by the Franco-German Research Institute (ISL), Saint-Louis, France. This was placed opposite to the RMCS thermocouple at position M5A. Its output, in mV, is shown in Figure 49. The given calibration is about 50 K per mV so the maximum temperature is about 700 K, i.e., about 240 K lower than the RMCS thermocouple. Also, it is evident that the noise level of the ISL thermocouple is higher and the response time longer than the RMCS thermocouple. The ISL and RMCS thermocouples were calibrated at the RMCS and the ISL thermocouple proved to be faulty and produced inconsistent results varying from 40 K/mV to 55 K/mV. Apparently, the thermocouple wires are not properly insulated from each other and touch at places other than the hot junction. It seems best to disregard the magnitude of the ISL thermocouple signals although the transient response seems quite good and is comparable to the RMCS thermocouple.

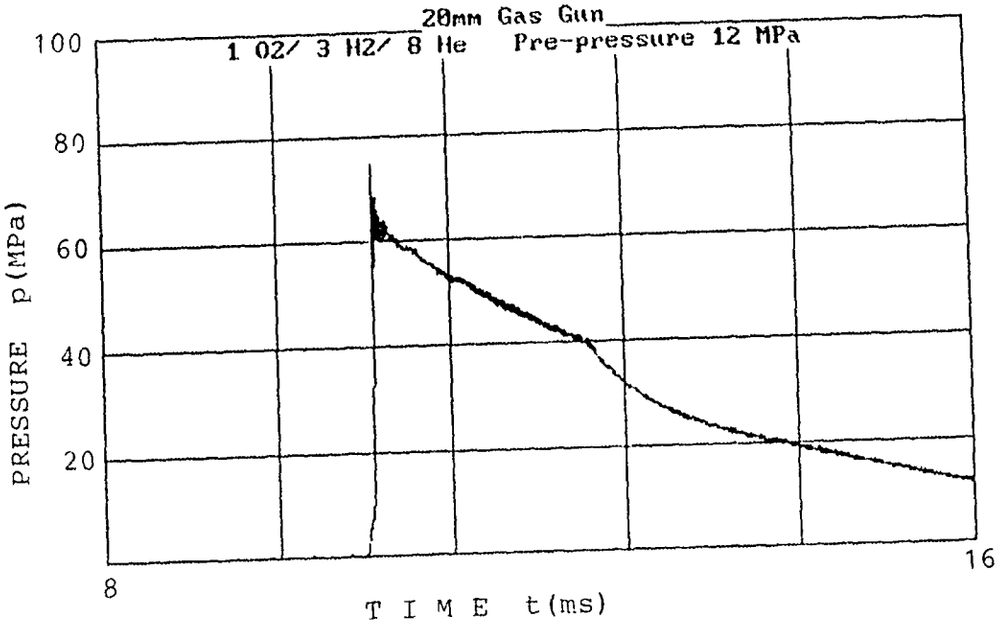

Fig. 45. Pressure vs time at location M5
(Gas mixture: O_2 + 3 H_2 + 8 He; prepressure 12 MPa)

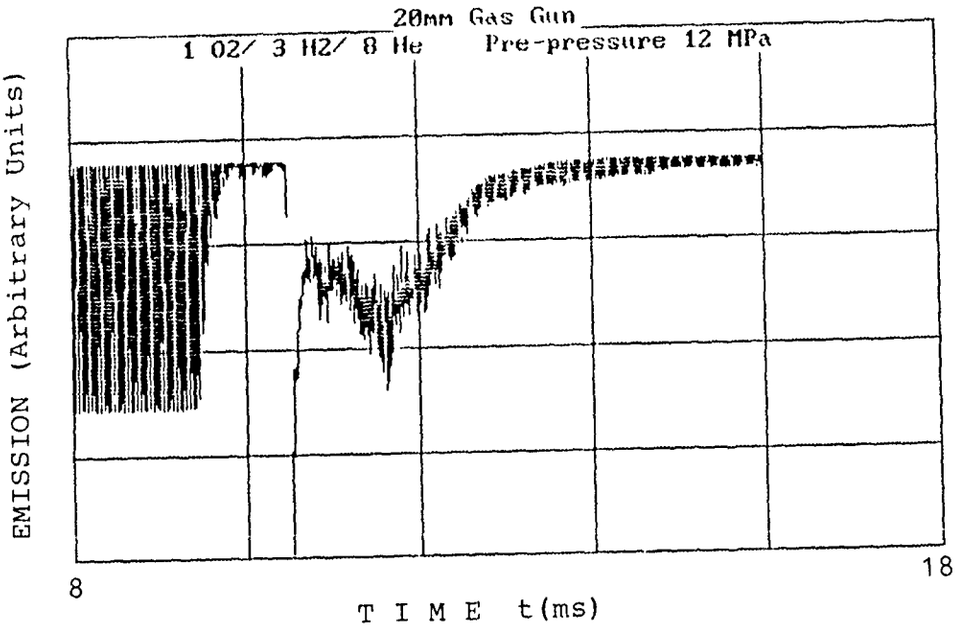

Fig. 46. Emission vs time at location M5
(Gas mixture: O_2 + 3 H_2 + 8 He; prepressure 12 MPa)

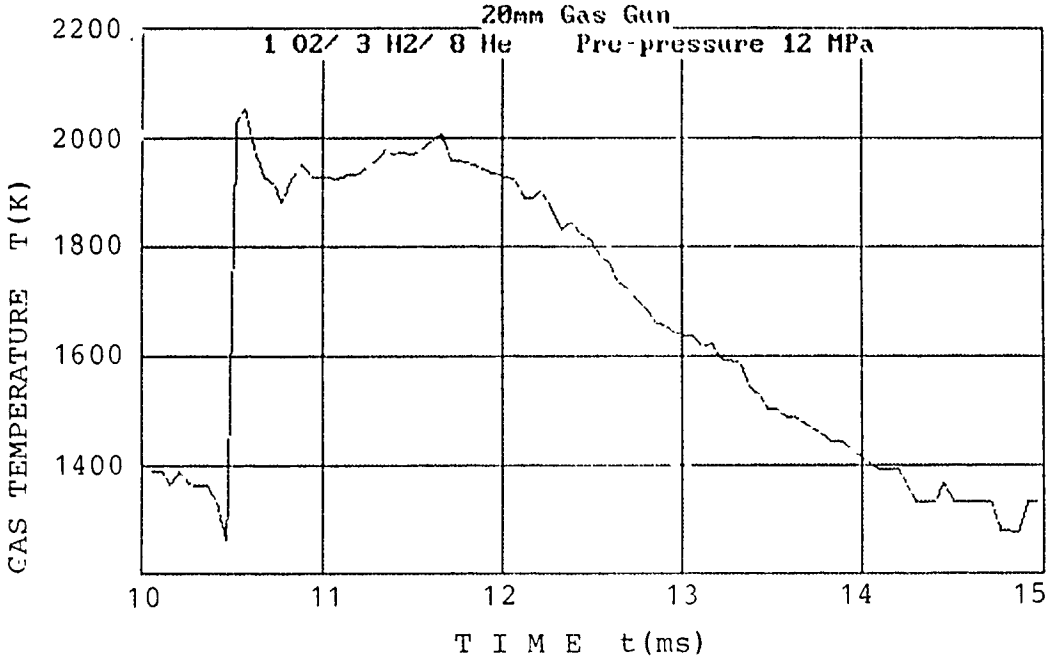

Fig. 47. Gas temperature vs time at location M5
(Gas mixture: O_2 + 3 H_2 + 8 He; prepressure 12 MPa)

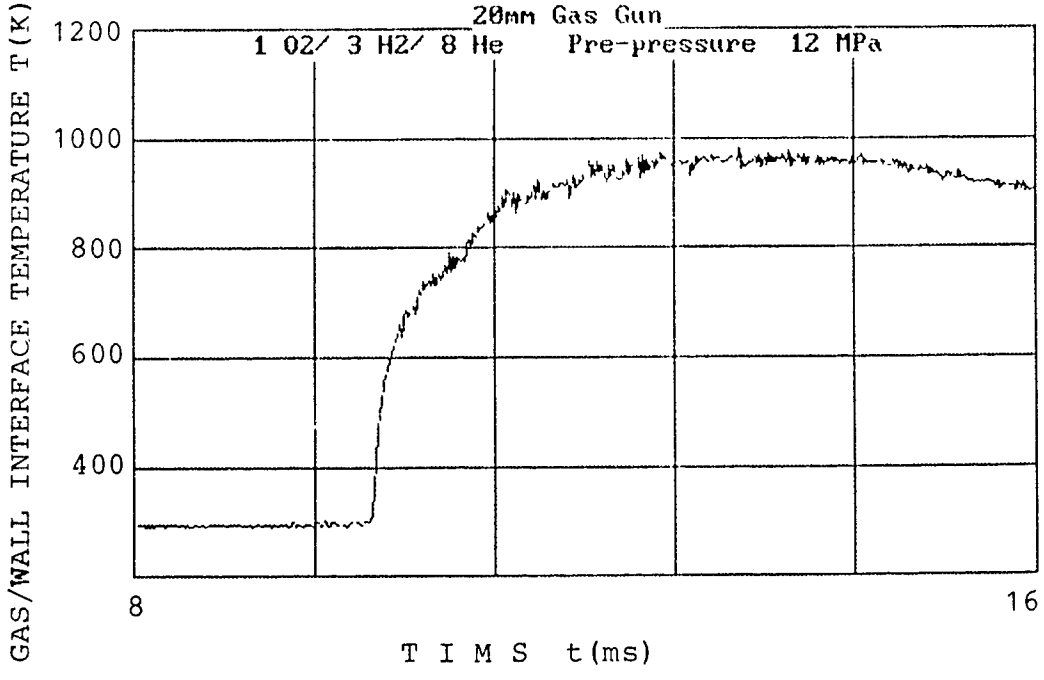

Fig. 48. Gas/wall interface temperature vs time at location M5A
(Gas mixture: O_2 + 3 H_2 + 8 He; prepressure 12 MPa)

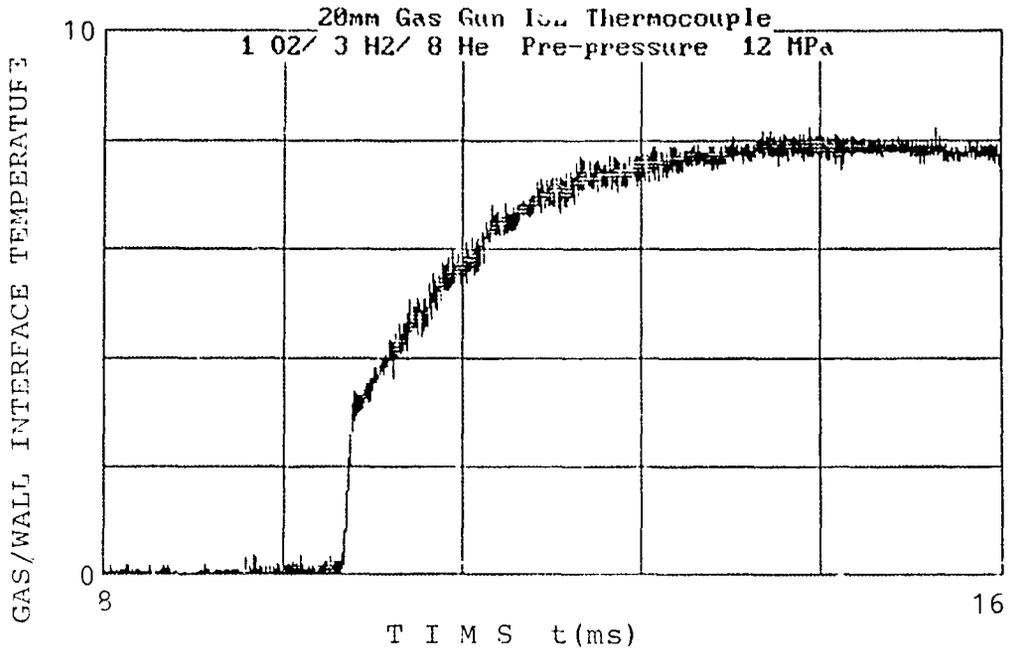

Fig. 49. Data taken with ISL thermocouple (not converted)

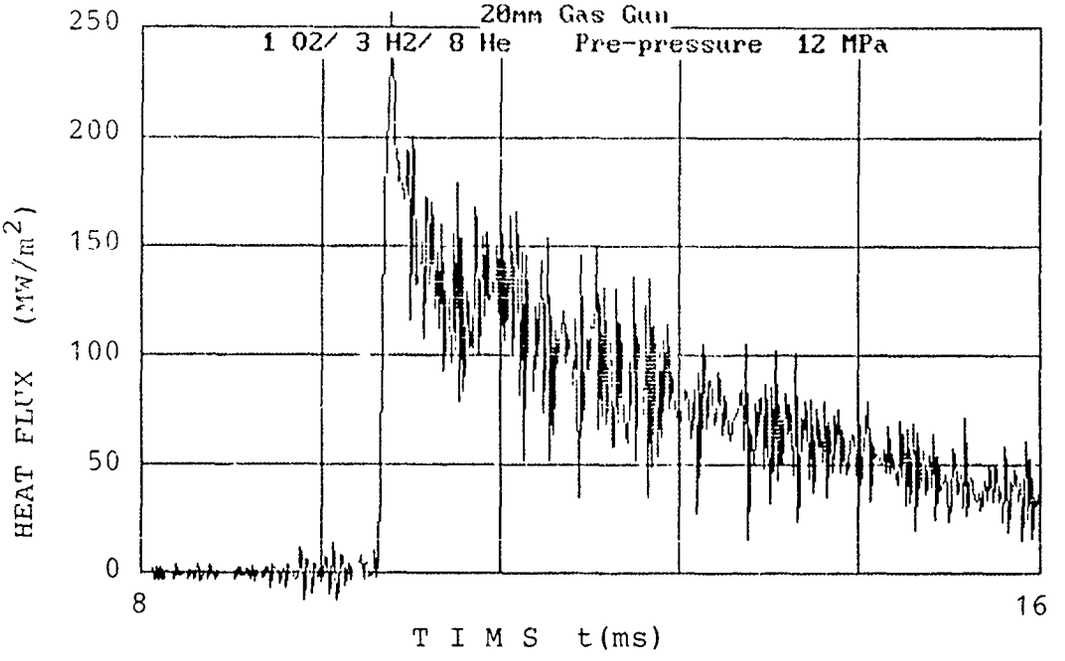

Fig. 50. Heat flux vs time at location M5A
(Gas mixture: O_2 + 3 H_2 + 8 He; prepressure 12 MPa)

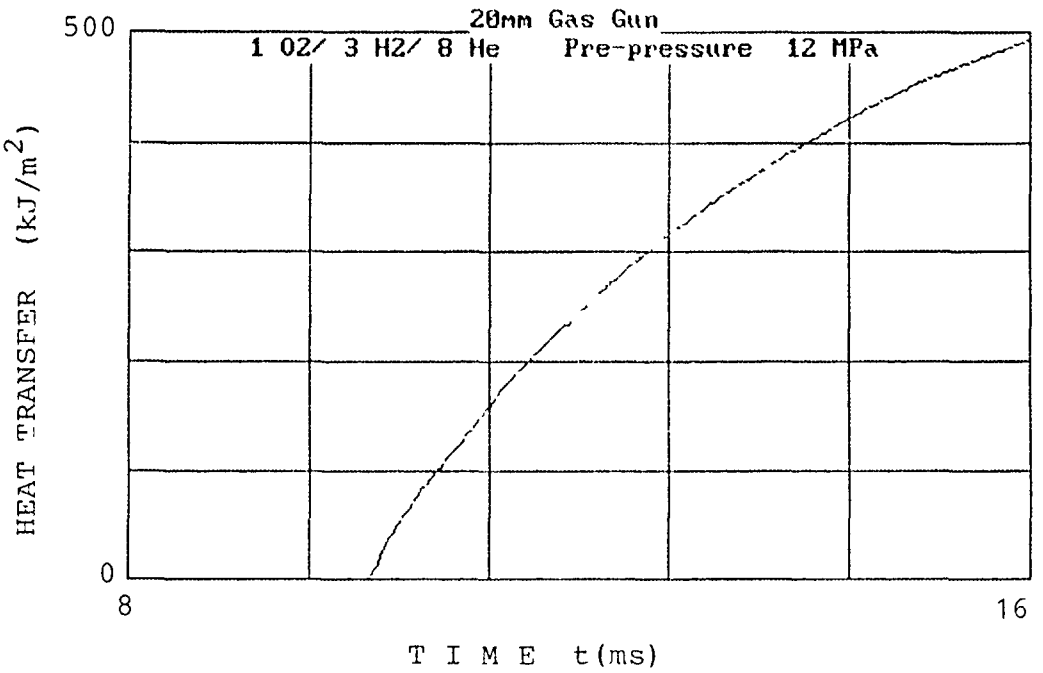

Fig. 51. Heat transfer vs time at location M5A
(Gas mixture: O_2 + 3 H_2 + 8 He; prepressure 12 MPa)

11.3 Recorded Data for the Gas Mixture 0.6 O_2 + 1.5 H_2 + 4 He + 0.3 CO

A series of tests have further been made using small amounts of CO in the reactant mixture. In one tet, Figures 52 to 58, the prepressure was only 6.4 MPa and the partial pressure of CO was 0.3 MPa. This resulted in a good combustion without oscillation, Figure 52. The gas temperature, Figure 54, is lower than in the two previous trials and reaches a maximum value of only 1800 K. However, the gas temperature still shows a cool region behind the projectile. The interface temperature is also lower than in the previous tests and attains only 760 K with correspondingly lower heat flux and heat transfer. The ISL thermocouple again records temperatures about 180 K lower than the RMCS thermocouple.

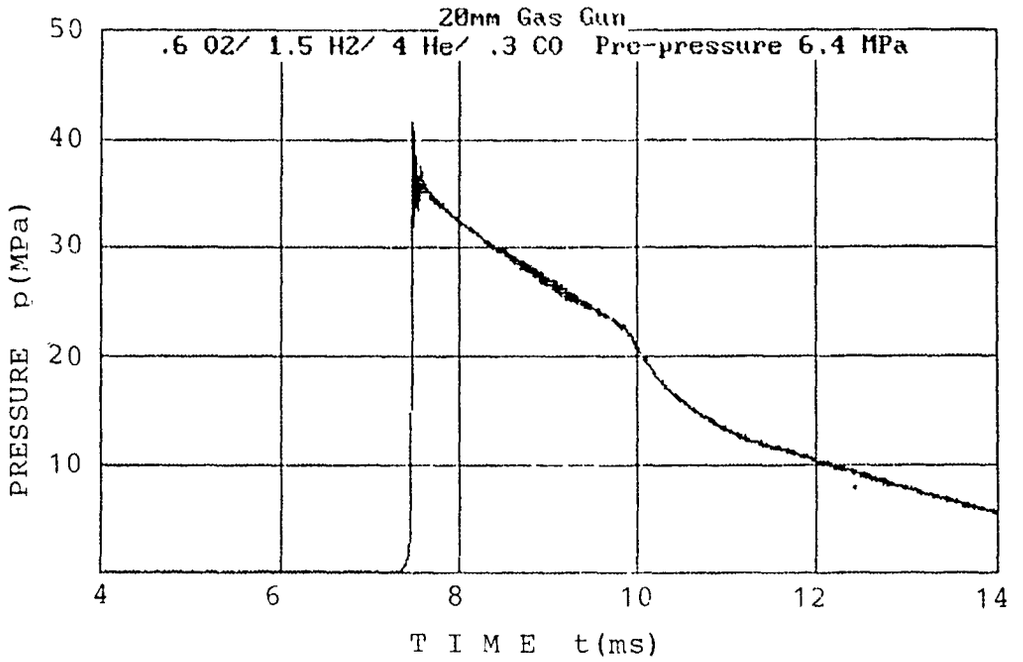

Fig. 52. Pressure vs time at location M5
(Gas mixture: 0.6 O_2 + 1.5 H_2 + 4 He + 0.3 CO;
prepressure: 6.4 MPa)

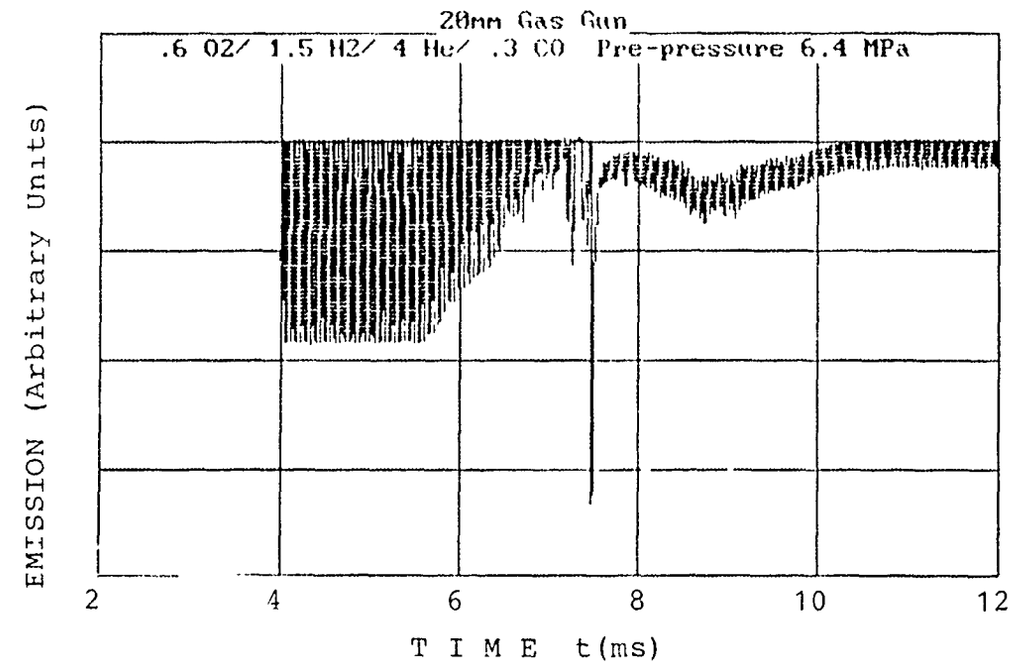

Fig. 53. Emission vs time at location M5
(Gas mixture: 0.6 O_2 + 1.5 H_2 + 4 He + 0.3 CO;
prepressure: 6.4 MPa)

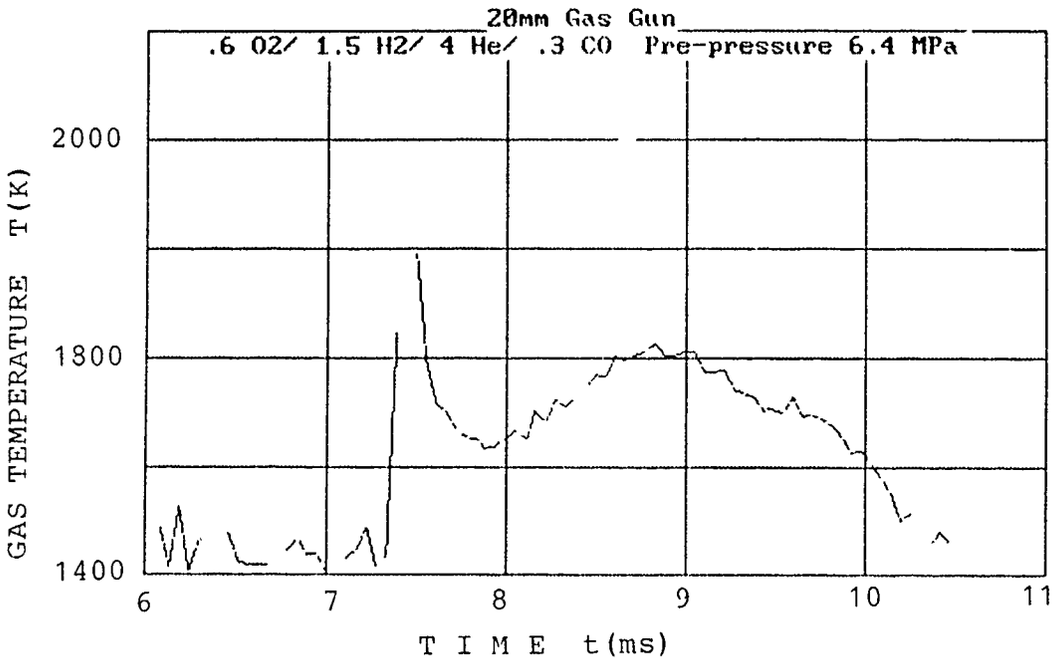

Fig. 54. Gas temperature vs time at location M5 (Gas mixture: 0.6 O_2 + 1.5 H_2 + 4 He + 0.3 CO; prepressure: 6.4 MPa)

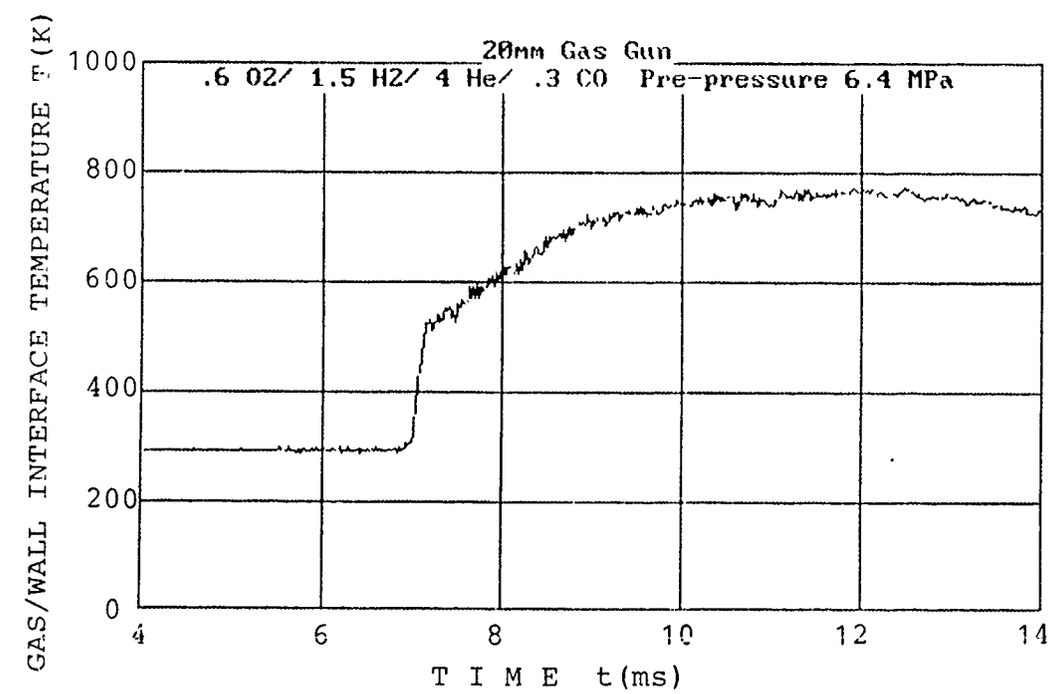

Fig. 55. Gas/wall interface temperature at location M5A (Gas mixture: 0.6 O_2 + 1.5 H_2 + 4 He + 0.3 CO; prepressure: 6.4 MPa)

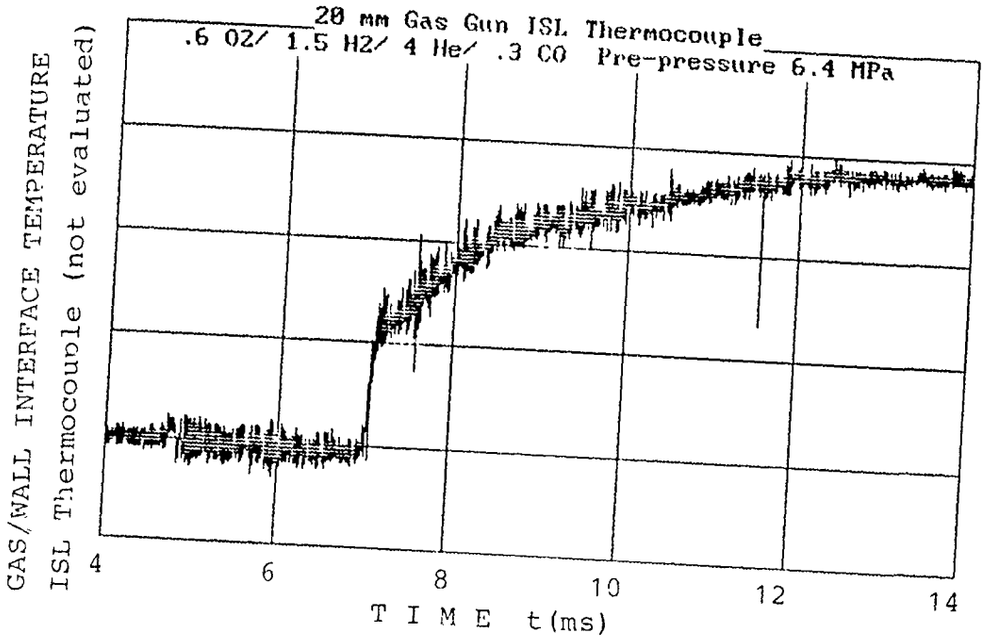

Fig. 56. ISL thermocouple readings at location M5A (not evaluated)
(Gas mixture: 0.6 O_2 + 1.5 H_2 + 4 He + 0.3 CO;
prepressure: 6.4 MPa)

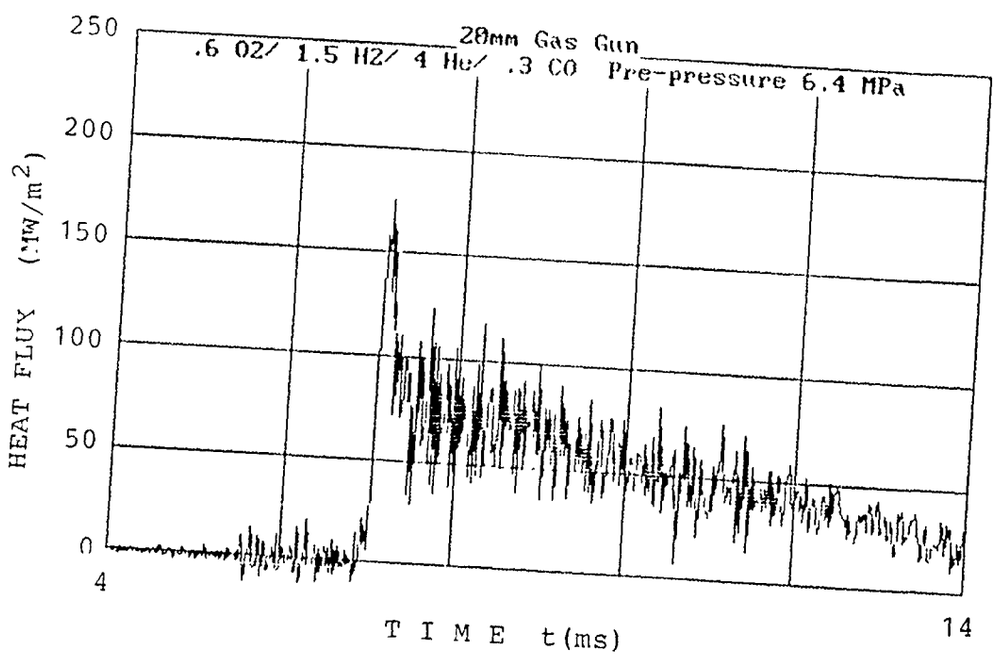

Fig. 57. Heat flux vs time at location M5A
(Gas mixture: 0.6 O_2 + 1.5 H_2 + 4 He + 0.3 CO;
prepressure: 6.4 MPa)

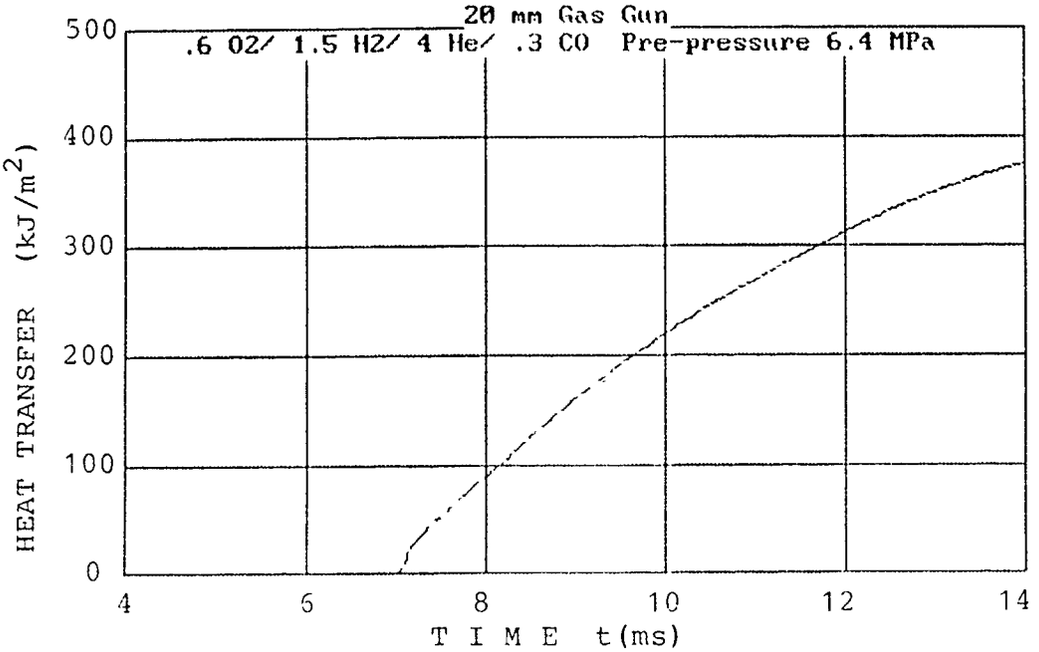

Fig. 58. Heat transfer vs time at location M5A
(Gas mixture: 0.6 O_2 + 1.5 H_2 + 4 He + 0.3 CO;
prepressure: 6.4 MPa)

Figures 59 to 63 show velocity data obtained with the gas mixture containing 0.6 O_2 + 1.5 H_2 + 4 He + 0.3 CO. The prepressure was 6.4 MPa. The velocity distribution compares with the previous firings.

These gas velocity measurements were made at window M5 using a mixture containing CO (.6 O_2/1.5 H_2/4 He/.3 CO). The velocity histories at radii of 0, 7.5, and 8.5 mm are plotted in Figures 59 to 61. A notable feature of these results is the acceleration of the gas that occurs after the shot leaves the barrel. This is because the unrestrained gas velocity at the muzzle is sonic and for a light gas mixture at a temperature of about 2000 K this is about 2400 m/s. As window M5 is about 2/3 along the barrel from the breech, then the velocity at M5 should increase to a maximum of about 1600 m/s. The measured velocities do not reach this value but they do accelerate from about 600 m/s at projectile exit (1.5 ms) to about 1050 m/s at about 4.0 ms.

The radial velocity distributions for this mixture are plotted in Figure 62 and clearly illustrate the growth in the boundary layer thickness with time. From these velocity distributions the distribution of gas temperature may be estimated, as described above. The estimated temperature distributions are shown in Figure 63. These estimates are based on an assumed Prandtl number of unity. The Prandtl number of the gas mixture is less than unity and so the termal boundary layer will be thicker than that shown in Figure 63. These data are no more than a useful first estimate of the temperature distributions to be expected but they do indicate a rather thick boundary layer and the need for more direct and accurate measurements using Abel inversion or computer aided tomography, a method that is currently being developed at the Ernst-Mach-Institut.

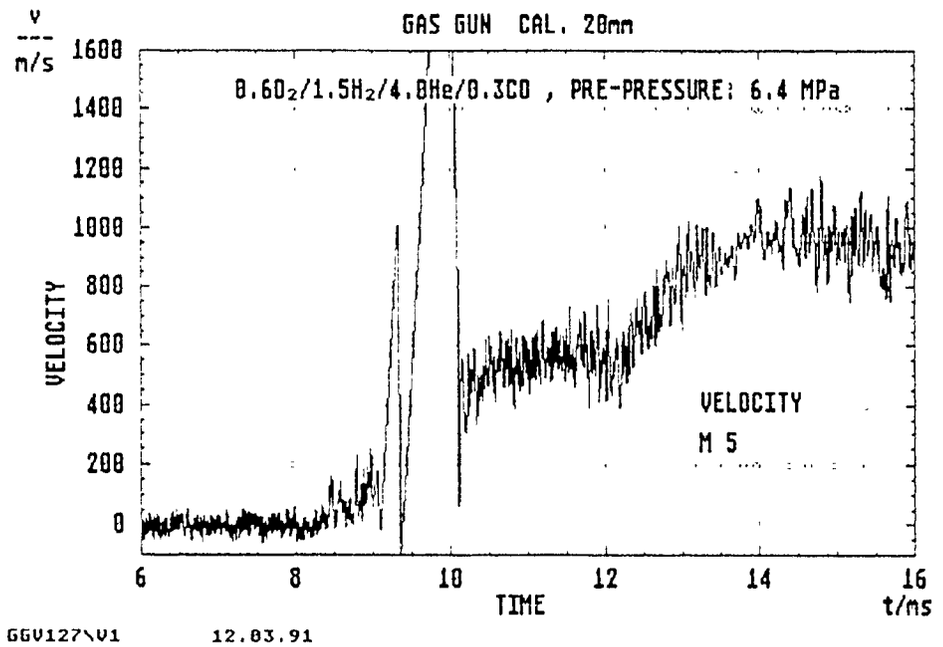

Fig. 59. Velocity vs time at location M5 and R = 0
(Gas mixture: 0.6 O_2 + 1.5 H_2 + 4 He + 0.3 CO;
prepressure: 6.4 MPa)

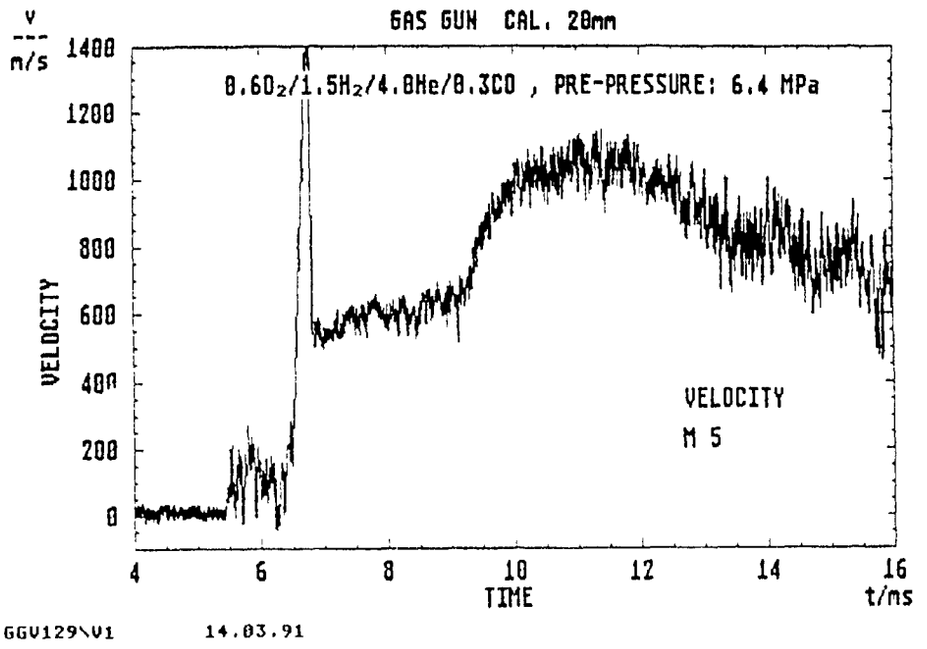

Fig. 60. Velocity vs time at location M5 and R = 7.5 mm (Gas mixture: 0.6 O_2 + 1.5 H_2 + 4 He + 0.3 CO; prepressure: 6.4 MPa)

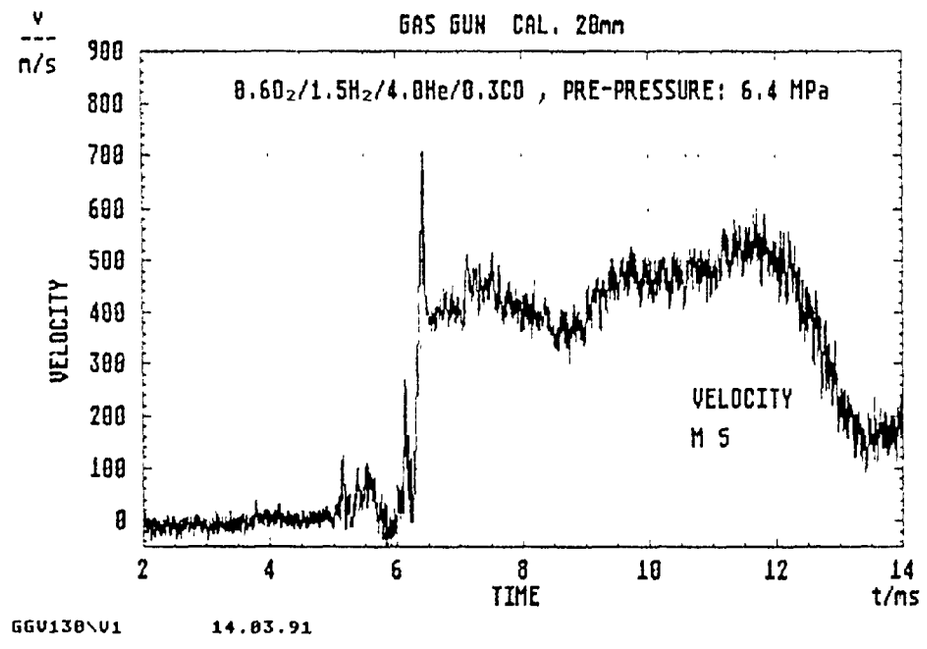

Fig. 61. Velocity vs time at location M5 and R = 8.5 mm (Gas mixture: 0.6 O_2 + 1.5 H_2 + 4 He + 0.3 CO; prepressure: 6.4 MPa)

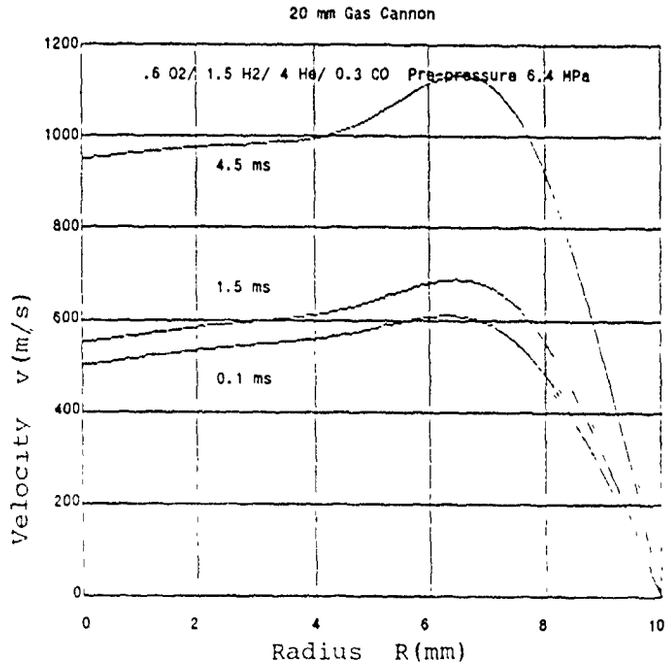

Fig. 62. Radial velocity profiles at times t = 0.1 ms, 1.5 ms, and 4.5 ms at location M5
(Gas mixture: 0.6 O_2 + 1.5 H_2 + 4 He + 0.3 CO;
prepressure: 6.4 MPa)

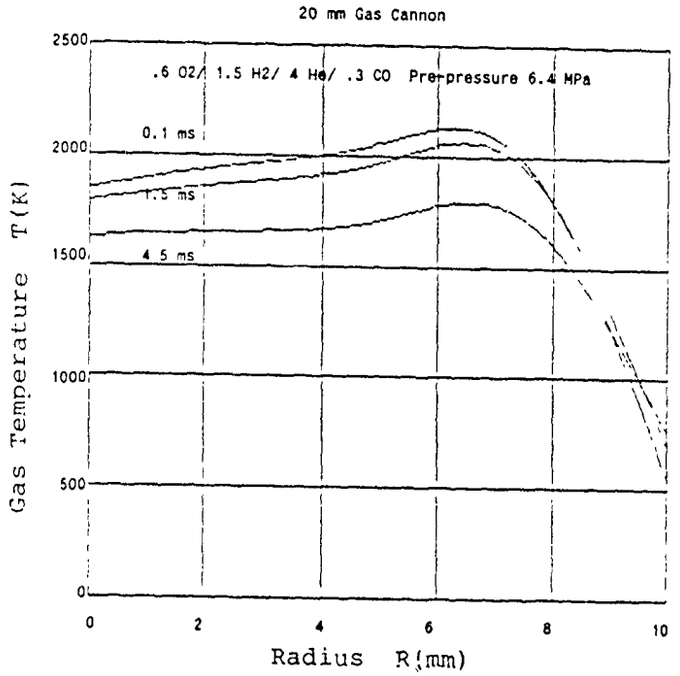

Fig. 63. Radial gas veocity profiles at times t = 0.1 ms, 1.5 ms, and 4.5 ms at location M5
(Gas mixture: 0.6 O_2 + 1.5 H_2 + 4 He + 0.3 CO;
prepressure: 6.4 MPa)

11.4 Recorded Data for the Gas Mixture 0.6 O_2 + 1.5 H_2 + 4 He + 0.6 CO (Prepressure: 5.6 MPa)

In a further test the CO was increased to a partial pressure of 0.6 MPa and the other constituents were also changed to give a prepressure of 5.6 MPa. This test produced very noisy signals, even the pressure measurement, Figure 64 exhibits considerable noise. The gas radiation signal, Figure 65, is not well defined and overloads the amplifiers. However, where the signal may be processed, Figure 66, the gas temperature is very high, up to 2400 K, and does not show the usual cool region behind the projectile. The interface temperature is also very high at 980 K, Figure 67. The interface temperature recorded by the ISL thermocouple has a maximum value of only about 570 K and is particularly noisy, Figure 68. The heat flux and heat transfer are illustrated in Figures 69 and 70.

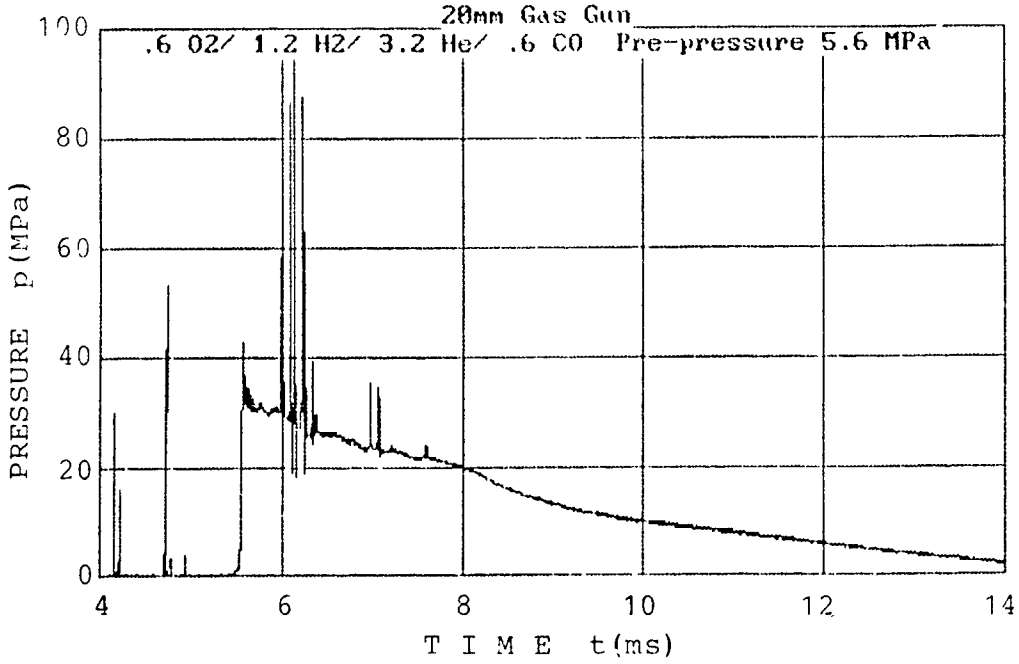

Fig. 64. Pressure vs time at location M5
(Gas mixture: 0.6 O_2 + 1.2 H_2 + 3.2 He + 0.6 CO;
prepressure: 5.6 MPa)

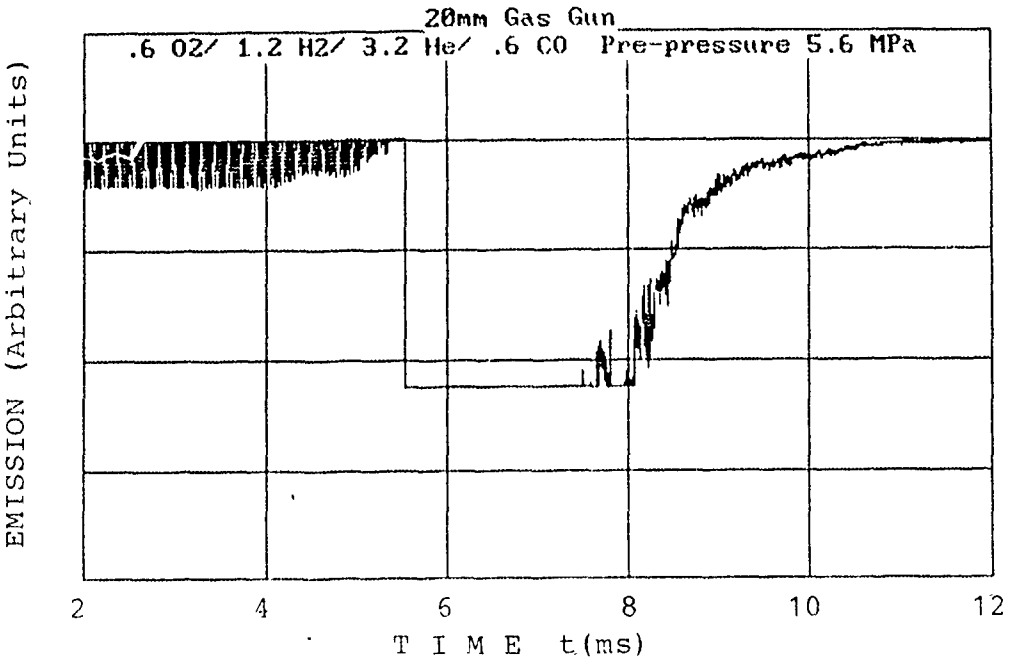

Fig. 65. Emission vs time at location M5
(Gas mixture: 0.6 O_2 + 1.2 H_2 + 3.2 He + 0.6 CO;
prepressure: 5.6 MPa)

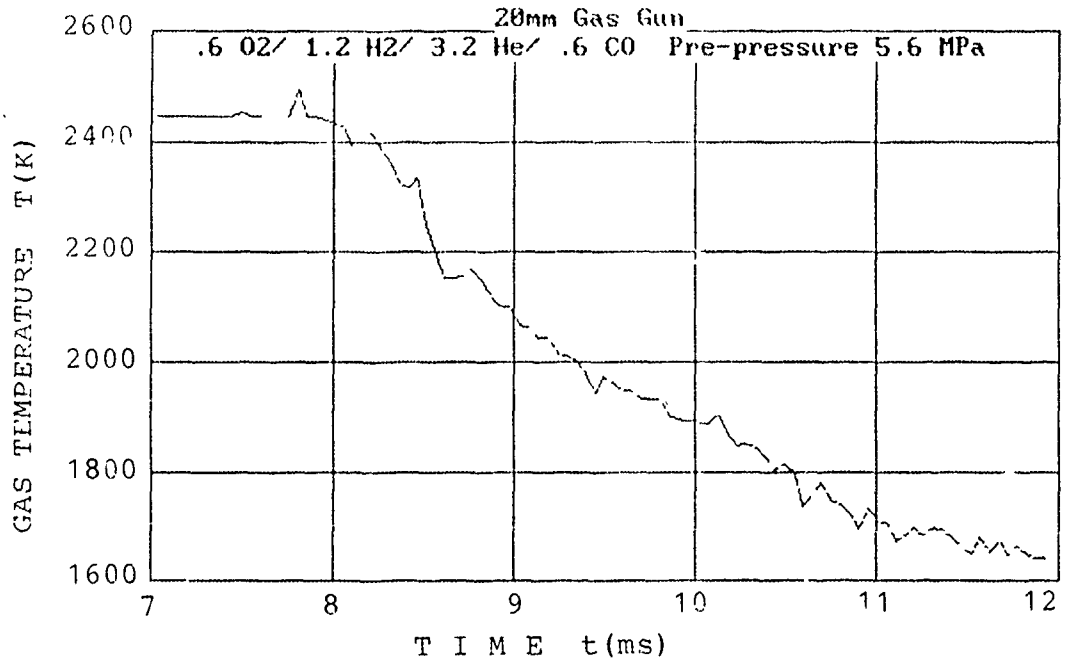

Fig. 66. Gas temperature vs time at location M5
(Gas mixture: 0.6 O_2 + 1.2 H_2 + 3.2 He + 0.6 CO;
prepressure: 5.6 MPa)

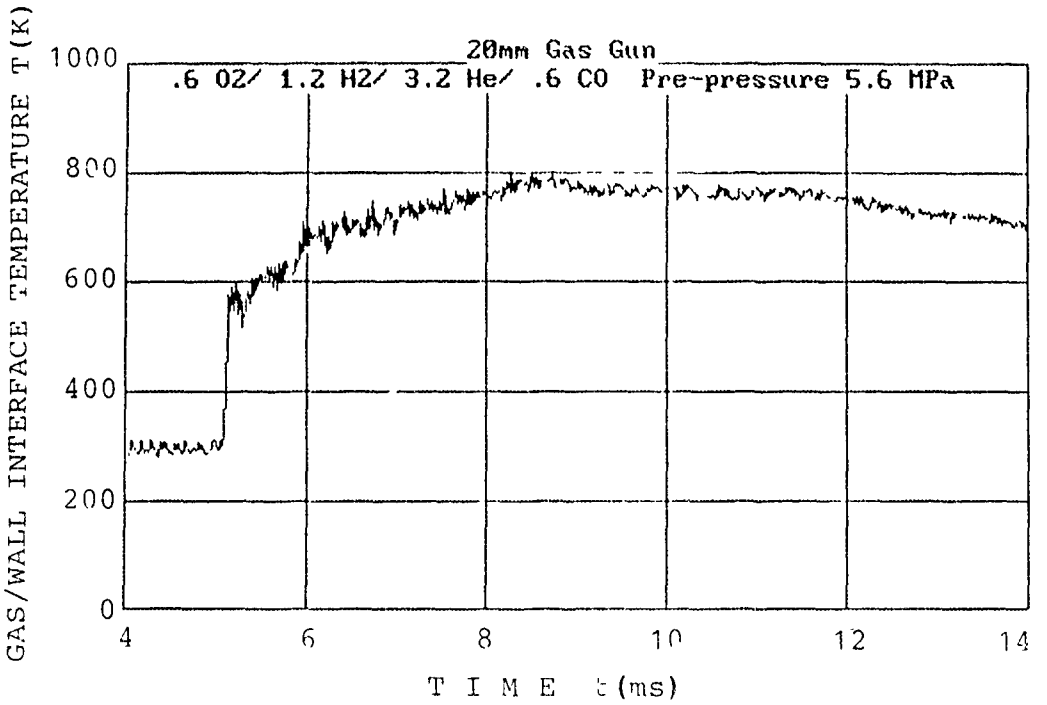

Fig. 67. Gas/wall interface temperature vs time at location M5A (Gas mixture: 0.6 O_2 + 1.2 H_2 + 3.2 He + 0.6 CO, prepressure: 5.6 MPa)

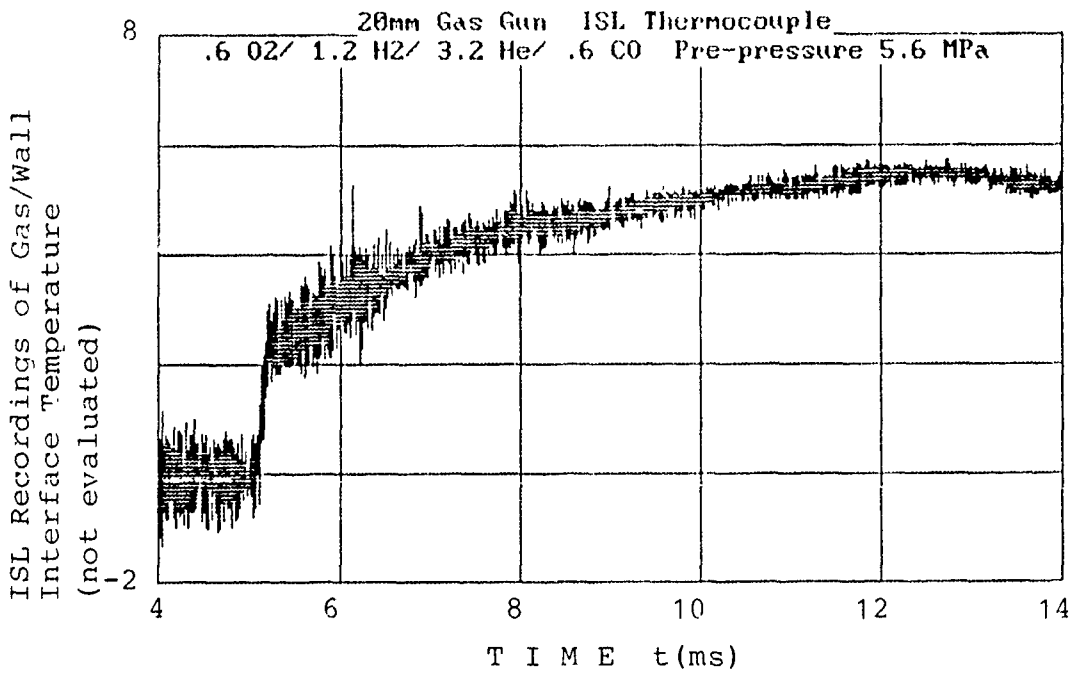

Fig. 68. ISL thermocouple recordings (not evaluated)

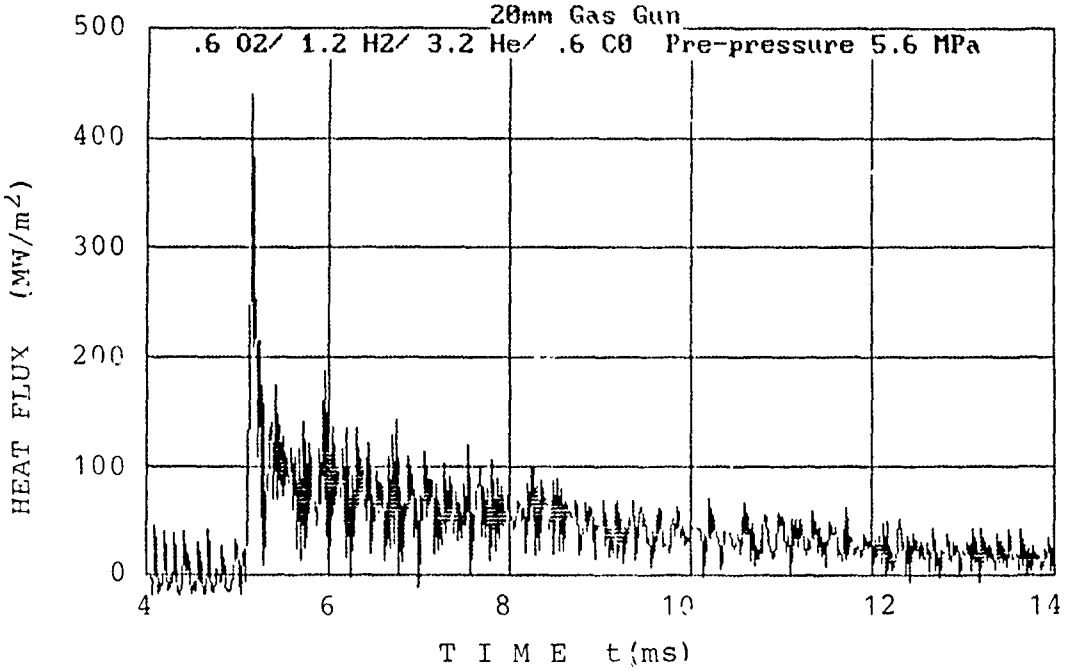

Fig. 69. Heat flux vs time at location M5A
(Gas mixture: 0.6 O_2 + 1.2 H_2 + 3.2 He + 0.6 CO;
prepressure: 5.6 MPa)

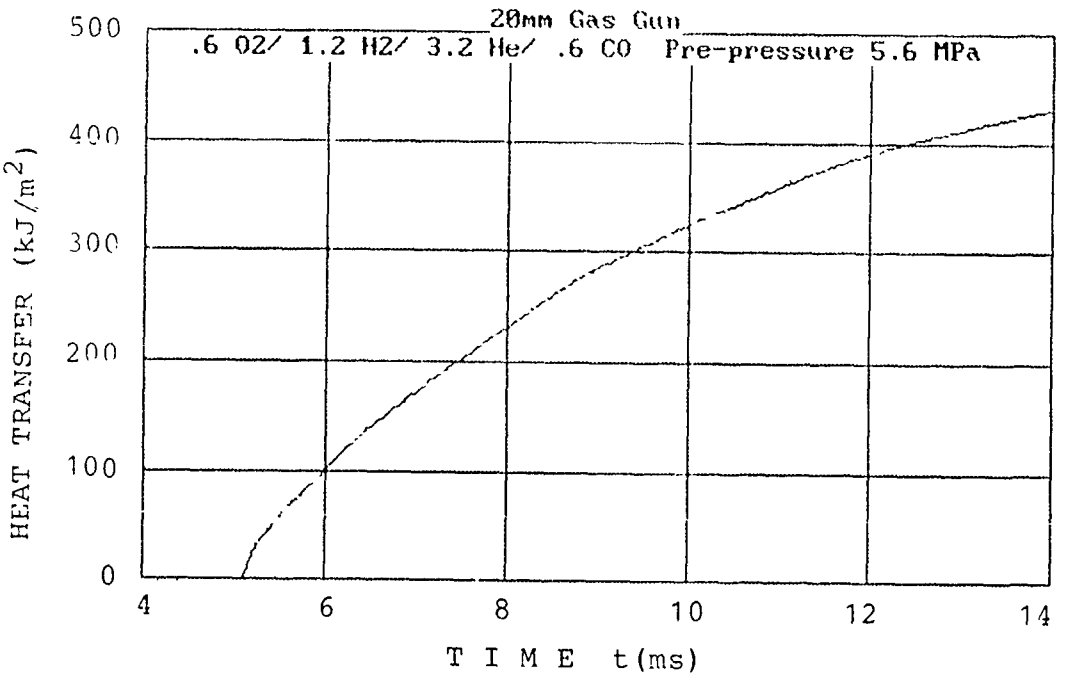

Fig. 70. Heat transfer vs time at location M5A
(Gas mixture: 0.6 O_2 + 1.2 H_2 + 3.2 He + 0.6 CO;
prepressure: 5.6 MPa)

Figure 71 shows the correlation between maximum interface temperature and the heat transfer to the wall. Strictly, the maximum heat transfer should be plotted but as the signal records did not extend to this point the heat transfer after 6 ms has been used. It has been shown [28] that these quantities are related by:

$$T_{max} = T_{initial} + \frac{1.082\ H}{\sqrt{\pi k \rho c_v t_0}} \qquad (9)$$

where k is thermal conductivity, ρ is density and c_v is specific heat of the thermocouple. The value of the time constant at the commencement of rifling, t_0, is usually equal to the time taken for the pressure to rise from 10 % to 90 % its maximum value. In this case the time constant is about 2.4 ms, which is reasonable.

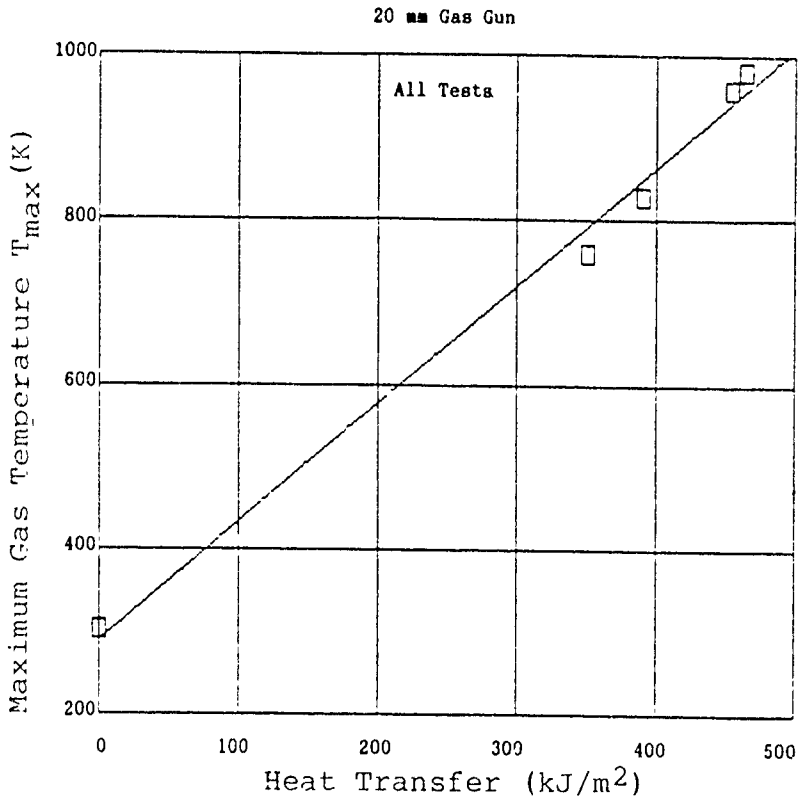

Fig. 71. T_{max} vs heat transfer after 6 ms

12. SUMMARY

In summary the data measured and presented provide first radial velocity and temperature profiles in reacting single-phase and two-phase flows. Obviously, boundary layer thicknesses are much greater than usually predicted by theory. This large boundary is attributed to the formation of turbulence at the wall which diffuses much faster in direction to the flow axis than current theory suggests. More experimental and theoretical work is required to solve this problem. A way to obtain improved radial resolution is the multi-scanning approach such as Abel inversion or tomography as being developed at EMI.

13. ACKNOWLEDGEMENT

The research work conducted has been made possible through the support and sponsorship of the German Ministry of Defence and the U. S. Government through its U. S. Army Ballistic Research Laboratory and the European Research Office of the U. S. Army. I thank Dr. T. Minor of the BRL, Dr. R. Reichenbach of USARDSG (UK), and Dr. G.-A. Schröder of the Ernst-Mach-Institut for their support. Also, I would like to extend my thanks to Mr. O. Wieland of EMI who carried out substantial amounts of experimental work and to Mrs. E. Messner of EMI for typing and arranging the manuscript. Further, I wish to express my gratitude to Dr. B. Lawton of the Royal Military College of Science, Shrivenham, UK, who is currently with EMI and transferred his technology for measuring temperature at the wall by using fast responding thermocouples to EMI. He also assisted in evaluating heat transfer and the radial temperature profiles.

14. REFERENCES

[1] G. Klingenberg and N. E. Banks

Review of Interior Ballistic Research: State-of-the-Art of Computational and Experimental Efforts

Proceedings of the 6th International Symposium on Ballistics, Orlando, Florida, USA, October 1981

[2] F. Seiler

Experimental Simulation of Flow Inside a Gun Barrel

Proceedings of the 7th International Symposium on Ballistics, The Hague, The Netherlands, April 1983

[3] H. Mach, U. Werner, A. Eichhorn, and H. Masur

Simulating the Flow Inside a Gun Barrel

Franco-German Research Institute, Saint-Louis, France, ISL Report No. R 122/82, 1982

[4] G. Klingenberg, E. Schmolinske, H. Mach, and F. Seiler

Flow Simulation Experiments in Ballistics

Journal of Ballistics, Vol. 8, No. 4, November 1985, pp. 2085-2117

[5] A. F. Bicen, L. Khezzar, and J. H. Whitelaw

Subsonic Single-Phase Flow in a Gun Simulator

AIAA Journal, Vol. 25, 1988, pp. 47-51

[6] J. Garloff and R. Heiser

A Contribution to the Turbulence of Interior Ballistic Flows

AIAA/ASME/SAE/ASEE 25th Joint Propulsion Conference, Monterey, California, USA, July 1989; AIAA Paper No. 89-2557

[7] G. Klingenberg

Gas Velocity Measurements Inside the Bore of a Gun

Proceedings of the 12th International Symposium on Ballistics, San Antonio, Texas, USA, October 1990

[8] G. Klingenberg and H. Rockstroh

Single-Stage Gas Gun Experiments

Proceedings of the 11th International Symposium on Ballistics, Brussels, Belgium, May 1989

[9] G. Klingenberg, J. M. Heimerl, and E. Schmolinske

Simulation Experiments -- Gas Gun Simulator

Proceedings of the 9th International Symposium on Ballistics, Shrivenham, England, April 1986

[10] G. Klingenberg

Investigation of Highly Pressurized Two-Phase, Reacting Flow

Final Technical Report under Contract DAJA 45-84-C-0013 to the U.S. Army Research, Development and Standardization Group (UK), London, England, April 1987

[11] G. Klingenberg and J. M. Heimerl

Gun Muzzle Blast and Flash

Progress in Aeronautics and Astronautics, Washington, DC, April/May 1991

[12] M. Summerfield

An Overview of Some Scientific Problems in the Interior Ballistics of Guns

AGARD Conference Proceedings No. 392: "Interior Ballistics of Guns", Propulsion and Energetics Panel 66th (B) Specialists Meeting, Florence, Italy, September 1985

[13] G. Klingenberg

Survey of Ballistic Flow Studies

Journal of Ballistics, Vol. 10, No. 4, October 1990, pp. 2680-2731

[14] M. E. Lord

Performance of a 40-mm Combustion Heated Light Gas Gun Launcher

Arnold Engineering Center, Inc., Report, October 1960

[15] M. E. Wilkins and R. J. Carros

Combustion Tests of Oxygen-Hydrogen-Helium Mixtures at Loading Pressures up to 8,000 Pounds per Square Inch

NASA Technical Note, NASA-TN-D-1892, October 1963

[16] J. M. Heimerl

A Comparison of Thermodynamic Calculations of the BLAKE- and the ICT-Code (A Translation)

Fraunhofer-Institut für Kurzzeitdynamik, Weil am Rhein, Germany, EMI-AFB Report No. T 4/86, April 1986

[17] G. Klingenberg and J. M. Heimerl

Simulation Experiments on Reacting Muzzle Flows

Fraunhofer-Institut für Kurzzeitdynamik, Weil am Rhein, Germany, EMI-AFB Report No. 9/86, December 1986

[18] K. Kuo

Fundamentals of Solid Propellant Combustion

Volume 90, Progress in Astronautics and Aeronautics, AIAA. Washington, DC, 1984

[19] L. Stiefel

Gun Propulsion Technology

Volume 109, Progress in Astronautics and Aeronautics, AIAA, Washington, DC, 1984

[20] G. Klingenberg and H. Mach

Experimental Study of Non-Steady Phenomena Associated with the Combustion of Solid Gun Propellants

Proceedings of the 16th Symposium (International) on Combustion, The Combustion Institute, Pittsburgh, Pennsylvania, USA, 1976, pp. 1193-1200

[21] G. Klingenberg

Temperature History of the Interior Ballistic Flow of a 20-mm Caliber Cannon

Journal of Ballistics, Vol. 8, No. 2, August 1985, pp. 1896-2008

[22] G. Klingenberg, J. D. Knapton, C. Watson, and I. C. Stobie

Liquid Gun Propellant Studies: Closed Bomb and Gun Experiments

Proceedings of the 10th International Symposium on Ballistics, San Diego, CA, USA, October 1987

[23] G. Klingenberg

Invasive Spectroscopic Technique for Measuring Temperature in Highly Pressurized Combustion Chambers

Journal Optical Engineering,Vol. 24, No. 4, July/August 1985, pp. 692-696

[24] G. Klingenberg and H. Rockstroh

Application of High Speed Infrared Emission Spectroscopy in Reacting Flows

Proceedings of the 19th International Congress on High Speed Photography and Photonics, Cambridge, UK, September 1990

[25] J. Warnatz and U. Maas

Simulation von Zündung und Verbrennung

Nachr. Chem. Techn. Lab., Vol. 37, No. 12, Dezember 1989, pp. 1262-1270

[26] M. E. Gersh, J. S. Draper, J. C. Wormhoudt, J. B. Elgin, C. E. Kolb, D. C. Robertson, L.S. Bernstein, and A. C. Victor (Techn. Coordinator)

Rocket Exhaust Plums Technology, Chapter 3: Rocket Exhaust Plume Radiation

Chemical Propulsion Information Agency, CPIA Publication 263, May 1980

[27] G. Smeets and A. George

Instantaneous Laser Doppler Velocimeter Using a Fast Wavelength Tracking Michelson

Journal Review Scientific Instruments, Vol. 49, No. 11, November 1978, pp. 1589-1596

[28] B. Lawton

Measurement of Instantaneous Nusselt Number - Reynolds Number Relationship in Gun Barrels

Proceedings of the 12th International Symposium on Ballistics, San Antonio, Texas, USA, November 1990

[29] B. Lawton

Effect of Compression and Expansion of Instantaneous Heat Transfer in Reciprocating Internal Combustion Engines

Proceedings Instn. Mech. Engs., Vol. 201, No. A3, 1987, pp 175-186